PRODUCTION OF FLUORINE IN A PROTON EXCHANGE MEMBRANE REACTOR

By

ROBERT LOWREY

A DISSERTATION PRESENTED TO THE GRADUATE SCHOOL
OF THE UNIVERSITY OF FLORIDA IN PARTIAL FULFILLMENT
OF THE REQUIREMENTS FOR THE DEGREE OF
DOCTOR OF PHILOSOPHY

UNIVERSITY OF FLORIDA

2003

ACKNOWLEDGMENTS

DuPont Central Research and Development funded the work described in this manuscript. Experimental work was performed at DuPont Experimental Station in Wilmington, Delaware and at DuPont Chambers Works in Deepwater, New Jersey. A contract was made between DuPont Central Research and Development and University of Florida establishing a grant for collaborative research. In accordance with this contract I worked full time at DuPont Experimental Station as a graduate research fellow from January 1997 through December 1999.

Dr. Marc Doyle of DuPont Central Research and Development was the senior engineer for this project. Dr. Doyle supervised my work, assisted in some laboratory operations, and in general was a tremendous mentor. Several other DuPont personnel contributed to our effort. Bill Stevens trained me for handling hydrogen fluoride, consulted for process hazard assessment, and assisted in some laboratory operations. Marlin Ridley assisted in construction of the electrolysis system. Dr. Mario Nappa consulted for development of methods employed in quantitative analysis of fluorine. Bob VanNess assisted with calibration of fluorine analytical scrubbers. Dr. Raj Ragendran and Wendell Hall fabricated some of the membrane-electrode-assemblies employed in experiments. Dr. Jeremy Blanks consulted on use of gas chromatography and mass spectrometry and assisted with interpretation of data. Eric Thrasher consulted on design, directed construction, and supervised operation of the pressure vessel employed in

experiments at Chambers Works. Dr. Bertrum Diemer consulted on thermochemical assessment of the KF-HF molten salt system.

Dr. Timothy J. Anderson, my academic advisor, arranged the contract with DuPont. He also consulted on thermochemical assessment of the KF-HF molten salt system, reviewed our academic publications, and helped shape the direction of our research through informal communications and on-site visits. Dr. Anderson has provided his students with opportunities well beyond the scope of a typical University research program.

TABLE OF CONTENTS

		page
ACKNOWLEDGMENTS		ii
LIST OF TABLES		vi
LIST OF FIGURES		vii
ABSTRACT		x
CHAPTER		
1	INTRODUCTION	1
	Fluorine Production	2
	DuPont HCl Recycle Process	7
	Proton Exchange Membrane Reactors	12
	Proton Transport in Nafion® Membranes	13
2	RESEARCH PROGRAM	16
	Overview	16
	Thermochemical Assessment and Conductivity Measurement	17
	Catalyst Screening	18
	Reactor Performance Evaluation	20
	Gas Phase Coreactants	22
3	PROCESS DESIGN	24
	Overview	24
	Process Hazards Assessment	25
	Electrolysis Reactor Design	27
	Fluid Flow and Product Separation Systems	32
	Process Operation	37
	Process Control and Data Acquisition	49
	Material and Energy Balances	50
	Pressure Vessel and Conductivity Cell Design	55

page

4 DIRECT OXIDATION OF ANHYDROUS HF GAS 58

Introduction 58
Experimental 59
Results and Discussion 62
Aqueous Operation - Deionized Water Catholyte 62
Anhydrous Operation - AHF Gas Catholyte 67
Anhydrous Operation - KF·xHF Molten Salt Catholyte 75
Interpretation of Impedance Spectra 81
Conclusions 84

5 ELECTROLYSIS OF KF·xHF MOLTEN SALT 89

Introduction 89
Experimental 90
Results and Discussion 92
Operation with a Porous Membrane Separator 92
Operation with a Nafion® Membrane Separator 101
Operation with Teflon® AF Solution Catalyst Binder 106
Operation with a Bare Platinum Mesh Anode 109
Conclusions 114

6 THERMOCHEMICAL ASSESSMENT OF THE
BINARY KF-HF MOLTEN SALT SYSTEM 115

Introduction 115
Experimental Methods 117
Results 119
Discussion 119
Binary Solution Theory 121
Vapor-Liquid Equilibrium 123
Solid-Liquid Equilibrium 125
Pure Component Properties 127
Binary Solution Model for HF - KHF_2 131

REFERENCE LIST 146

BIOGRAPHICAL SKETCH 150

LIST OF TABLES

Table		page
3-1.	PEM Reactor Components	29
3-2.	Experimental Methods and Devices	50
4-1.	Bulk Impedance of PEM Reactors Following Pre-electrolysis	69
4-2.	Equivalent Circuit Elements Fit to PEM Reactor Impedance Spectra	85
5-1.	Coulometric Efficiency for Fluorine Production in Selected Cells	107
6-1.	Loading Requirements for KF in 365 grams HF	117
6-2.	Total Free Energy and Free Energy of Fusion for Stoichiometric Solids Relative to Pure Component Liquids	137
6-3.	Standard Heat of Formation, Standard Entropy, and Heat Capacity for Intermediate Compounds KF·nHF	139

LIST OF FIGURES

Figure		page
1-1.	HCl PEM Reactor Electrolytic Process	10
1-2.	HCl Recycle Plant Process Flow Diagram	11
3-1.	Expanded View of the Laboratory Scale PEM Reactor	28
3-2.	General Laboratory Process Flow Diagram	33
3-3.	Process Flow Diagram for Mode I Operation	40
3-4.	PEM Reactor Reactor Flow Diagram for Mode I Operation	41
3-5.	Process Flow Diagram for Mode II Operation	42
3-6.	PEM Reactor Reactor Flow Diagram for Mode II Operation	43
3-7.	Process Flow Diagram for Mode III Operation	44
3-8.	PEM Reactor Reactor Flow Diagram for Mode III Operation	45
3-9.	Process Flow Diagram for Mode IV Operation	46
3-10.	PEM Reactor Reactor Flow Diagram for Mode IV Operation	47
3-11.	Schematic of Pressure Vessel with Conductivity Cell	56
3-12.	Process Flow Diagram for Pressure Vessel System	57
4-1.	Steady State Current-Voltage Data for Mode I Operation with Various Anode Current Collector Materials	66
4-2.	Steady-State Current-Voltage Data for Mode I Operation with Various Anode Feed Streams	68
4-3.	Comparison of Bulk Impedance Before and After Mode II Operation	71
4-4.	Bulk Impedance Arrhenius Plot: Mode II Operation Start-up	72

Figure page
4-5. Cyclic Voltammograms from Mode II Operation 73

4-6. Current-Voltage Curves: Mode II Operation with Varied Catalysts 74

4-7. Anode Half-cell Open-circuit Impedance Response for a Cell with a Platinum Black MEA: Mode III Operation 78

4-8. Linear Current Sweep Data: Mode III Operation 79

4-9. Open-circuit Potential Decay Following Mode III Operation at 6.0 V 80

4-10. Impedance Model Circuit Diagrams 86

4-11. Open-circuit Impedance Spectra Model Simulations 87

4-12. Biased Potential Impedance Spectra Model Simulations 88

5-1. Cyclic Voltammograms from a Cell with a Porous Teflon Separator 94

5-2. Potentiostatic Operation of a Cell with a Porous Teflon Separator 95

5-3. Galvanostatic Operation of a Cell with a Porous Teflon Separator 97

5-4. Effect of Changing Anode Feed from HF to N_2 during Operation of a Cell with a Porous Teflon Separator 100

5-5. Comparison of Current-Voltage Curves for ELAT and MEA Cells 102

5-6. Galvanostatic Operation of a Cell with Platinum Black MEA 104

5-7. Comparison of Curent-Voltage Curves from Cells with Platinum Black MEA Employing Teflon® AF Solution and Nafion® Solution Catalyst Binder 108

5-8. Cyclic Voltammogram from a Cell with a Platinum Mesh Electrode: Potential Range -0.5 V to +1.5 V vs Pt/PtF_2 111

5-9. Cyclic Voltammogram from a Cell with Platinum Mesh Electrode: Potential Range +1.5 V to +3.5 V vs Pt/PtF_2 112

5-10. Comparison of Curent Voltage Data for Cells with ELAT, MEA and Platinum Mesh Electrodes 113

Figure page

6-1. Vapor Pressure Measurements for Dilute Solutions of KF in Anhydrous HF 120

6-2. Partial Molar Excess Free Energy of HF in the Liquid Phase Derived from Published Vapor Pressure Data 132

6-3. Temperature-Composition Phase Diagram for HF-KHF_2 142

6-4 Modified Temperature-Composition Phase Diagram for HF-KHF_2 143

6-5. Partial Pressure of HF as a Function of Temperature and Composition Near the Liquidus 144

6-6. Partial Pressure of HF as a Function of Temperature and Composition Away from the Liquidus 144

Abstract of Dissertation Presented to the Graduate School
of the University of Florida in Partial Fulfillment of the
Requirements for the Degree of Doctor of Philosophy

PRODUCTION OF FLUORINE IN A
PROTON EXCHANGE MEMBRANE REACTOR

By

Robert Lowrey

May 2003

Chair: Timothy J. Anderson
Major Department: Chemical Engineering

A unit operations laboratory was constructed at DuPont Central Research and Development for the purpose of investigating production of fluorine in a proton exchange membrane (PEM) reactor. Electrolytic processes to convert hydrogen fluoride to fluorine at moderate temperatures (0 to 100°C) using polymer-membrane-based electrochemical cells with flow-through gas diffusion electrodes were studied. Four different modes of operation were employed. An aqueous mode consisted of anhydrous HF (AHF) gas fed to the anode of the cell and deionized water fed to the cathode. Three anhydrous modes consisted of different permutations of either AHF gas or a liquid solution of KF dissolved in AHF fed to each side of the cell. Various operating conditions and cell designs were examined in an attempt to attain stable and high current density operation at low to moderate voltages. Platinum, nickel, ruthenium dioxide, and carbon were each evaluated as catalysts with loading ranging from 0.1 to 20 mg/cm^2. The primary membrane

separator used in this work was the Nafion® perfluorinated ionomeric membrane, either in acid or K^+ ionic form. Porous PTFE and polyolefinic membrane separators were also tested.

It was not possible to generate fluorine when operating with water present in the cell. High current densities for oxygen evolution were observed and extensive corrosion occurred for all anode cell materials except platinum. In the two anhydrous modes of operation with AHF gas purging the anode, low current densities for fluorine production and unstable cell behavior were observed. The limiting process was shown to be membrane specific by substitution of porous PTFE and polyolefinic membranes in place of the Nafion® membrane. These latter porous-membrane-based cells produced fluorine at rates up to 250 mA/cm^2 at voltages of 5 to 6 V. The third anhydrous operating mode, in which stagnant liquid KF-HF solution flooded both sides of the cell, generated fluorine at rates up to 400 mA/cm^2 at voltages of 5 to 10 V. This process was unstable with substantial corrosion of all cell materials except platinum.

A thermochemical assessment of the binary system KF-HF was performed for the purpose of evaluating vapor-liquid equilibrium measurements obtained at DuPont Chambers Works. A sub-regular solution model was fit to both literature data and new experimental data. The model compared favorably to most of the new data. Inconsistencies were attributed to measurements taken at non-equilibrium conditions.

CHAPTER 1
INTRODUCTION

The conversion of hydrogen fluoride to fluorine is an important industrial process that presents immense technological challenges. Fluorine is used in several processes including uranium refining, direct fluorination reactions, and electronic gas syntheses. Fluorine is produced industrially by only a single process: bulk electrolysis of KF·xHF molten salt ($1<x<4$).[1-5] The operating temperature is typically 85 to 100°C and the melt composition is held in the range of 38 to 42 wt.% KF.[1] Materials of construction for a typical electrolysis reactor consist of a steel vessel, a monel diaphragm, a monel counter electrode, and a carbon anode. The lifetime of a fluorine cell is limited by corrosion of the carbon anode and by corrosion of other components such as the electrode-current collector connections.

We pursued an alternative route to fluorine generation attempting to directly oxidize gas-phase anhydrous HF in a proton exchange membrane (PEM) reactor. This process is similar in concept to the anhydrous HCl process that utilizes a PEM reactor to electrolyze anhydrous HCl forming chlorine and hydrogen gas.[6] The advantages of the PEM reactor realized in the HCl recycle process were higher current densities or production rates per unit cell cost, lower operating voltages due to the reduction in the interelectrode gap distance, and better product gas separations leading to improved safety.

HF electrolysis presents a new challenge as compared with HCl electrolysis in that the thermodynamic potential for fluorine evolution is about 1.8 V more positive than the potential for chlorine evolution. Materials of construction for the HF PEM reactor must be stable to higher voltages than materials used in an HCl PEM reactor. In aqueous media such as the water-swollen Nafion® membrane used in the HCl process, there is an inherent oxidative stability limit due to the oxygen evolution reaction. Oxidation of water to form oxygen occurs well below the fluorine evolution potential (1.23 V versus 2.83 V vs. H^+/H_2). Fluorine also reacts chemically with water to form oxygen difluoride.

If water is removed from a Nafion® membrane, its ionic conductivity approaches zero. Fortunately, Nafion® membranes conduct ions when swollen with a variety of nonaqueous solvents.[7] The challenge is to find a solvent that does not oxidize at high voltages (up to 20 volts) and is stable in the presence of fluorine. The first logical choice would be to look at the industrial process that uses liquid KF-HF mixtures. Anhydrous HF itself may even be a suitable candidate because it is a dipolar liquid under ambient conditions.

Fluorine Production

Elemental fluorine gas is a powerful oxidant. Its primary industrial use is in production of uranium hexafluoride, sulfur hexafluoride and syntheses of fluorinated products (refrigerants, fluoropolymers, etc.). Fluorine is produced commercially by electrolysis of KF·xHF molten salt.[1-5] Fluorine currently costs between $30-60/lb. in cylinder quantities. This cost reflects stringent material demands and to some extent large power consumption (~10 kW/m^2). The corrosivity of HF-based electrolytes limits the materials that can be used as electrodes. In the past, consumable carbon anodes have

been used in industrial electrolysis cells to evolve fluorine. Side reactions produced fluorocarbon compounds that were difficult to separate. Nonconsumable anodes, such as the DSA® (dimensionally stable anode) widely used in chlorine production, have not been successful in the fluorine industry. A viable catalyst for industrial fluorine production has not been developed. To date, nongraphitized carbon is still the material of choice for the anode. Technology has advanced to minimize corrosion and polarization such that the reaction takes place on a fairly inert carbon surface; however the anode is still the primary consumable material in modern fluorine reactors.

To fully appreciate the selection of materials and operating conditions for modern fluorine reactors it is helpful to review the history of fluorine production. Several review articles have been published that provide insightful accounts of the history of elemental fluorine and fluorine reactors.[1,2,4,8] Fluorine is the 19th most abundant element in the crust of the earth. It is found primarily in the form of the mineral fluorite (calcium fluoride). Fluorite has been used as a liquifier in the smelting of iron ore since the early 1500s.[1,9]

A German glass worker named Schwanhardt is credited with discovery of hydrogen fluoride in the year 1670.[1,9] He discovered the acid when his glasses clouded up due to etching by a gas (hydrogen fluoride) that evolved after he poured sulfuric acid over fluorite. He used this etching gas to his advantage by patterning glass with wax and etching in the acid vapor to produce etched glass windows and ornaments. At the time the element fluorine was not known to exist. Scientists of this era attributed the acidic properties of this vapor to oxygen since all known acids at the time contained oxygen (with exception of hydrochloric acid which was also mistakenly assumed to contain

oxygen). Several decades later (early 1700s) scientists confirmed the existence of the element chlorine and by extension the fact that acids need not contain oxygen as in hydrochloric acid.[9]

In 1771 a German chemist named Scheele prepared crude hydrofluoric acid and named it fluoric acid as it was derived from the mineral fluorspar.[1,9] It was another forty years (1812) before scientists agreed on the existence of the element fluorine. The delay was in large part due to the fact that no one could isolate elemental fluorine. By this time the periodic table was much better established. The properties of several fluorine containing compounds were similar to the properties of chlorine containing compounds. It was agreed that a new element must exist in the same family of substances as chlorine and this element was thus labeled fluorine.[9] It would be still another 75 years before elemental fluorine gas was isolated.

Edward Fremy was the first scientist to produce fluorine.[1,9] He developed a method for preparing pure anhydrous hydrogen fluoride by thermal decomposition of potassium hydrogen difluoride salt (Fremy salt). He found that high-purity liquid hydrogen fluoride had very poor ionic conductivity. Addition of a small amount of water resulted in high conductivity until the water was exhausted by electrolysis. Addition of potassium fluoride resulted in high conductivity that could be sustained with evolution of gas at both the positive and negative electrodes. He was unable to collect the gas that evolved at the positive terminal as it reacted with the cork fittings in his electrolysis cell.[9,10]

Fremy's work was continued several decades later by one of his former students, Henry Moissan, who found suitable materials for isolation of elemental fluorine. Moissan

is credited as the first scientist to isolate elemental fluorine.[1,4,9,10] The electrolytic cell and fluorine collection apparatus employed by Moissan was carefully crafted with platinum electrodes, a copper vessel, and natural rubber fittings.[11] The electrolyte consisted of Fremy salt (potassium hydrogen difluoride) dissolved in liquid anhydrous hydrogen fluoride cooled below room temperature.[1,4,9,10,11]

All early work with fluorine (1886-1919) used variations on Moissan's fluorine cell.[1] Research was slowed by the complicated nature of purification of anhydrous hydrogen fluoride and the fact that the extremely hazardous nature of hydrogen fluoride and fluorine was not fully appreciated. Fluorine chemist Otto Ruff noted in the introduction to his textbook *Die Chemie des Fluors* that several of his collegues in the field had suffered severe injuries and one, Francais Louyet, had been killed due to fluoride poisoning.[12] Also the expense associated with replacing corroded platinum anodes was quite prohibitive relegating study of fluorine to well-funded institutions and government laboratories.[1]

The predecessor to the modern fluorine reactor was developed in Germany by Argo and coworkers in 1919.[13,14] They developed a high temperature electrolyzer using molten potassium hydrogen difluoride (m.p. 239°C) as the electrolyte and a graphite anode. This cell was practical in the sense that the complication of preparing anhydrous hydrogen fluoride was avoided and platinum was not required. However the melting point of the electrolyte had a tendency to increase as hydrogen fluoride was consumed resulting in anodic polarization after a short period of operation.[13] The electrolyte needed to be replenished on a semi-regular basis. These complications forced Argo's team to abandon the pursuit of fluorine and chlorine trifluoride as incendiary agents.[1] During the

period between 1919 and 1944, most fluorine-related research and patents employed electrolyzers of the high temperature type.[1,15]

In 1934 George Cady published a fairly comprehensive thermochemical assessment of the binary system HF-KF.[16] This was followed by a subsequent report describing optimization of melt composition for fluorine electrolyzers.[17] His work demonstrated that the most logical electrolyte composition to operate a fluorine cell was at the eutectic concentration KF·2HF (41 wt.% HF, m.p. 72C). The rationale is that this eutectic has an adequately low vapor pressure of hydrogen fluoride (18 mm Hg), a convenient operating temperature, and a stable equilibrium to which minor deviations naturally return. To date, this is still the operating condition of choice in modern fluorine reactors worldwide (with exception of some high temperature electrolyzers in operation in England).

Prior to 1940 nearly all applications for fluorine were academic in nature. The discovery of nuclear fission and particularly the race for development of the atom bomb instigated a need for production of fluorine on an industrial scale. Fluorine was required for synthesis of uranium hexafluoride that is used for diffusional separation of uranium isotopes U^{235} and U^{238}. Discoveries of numerous commercial applications for fluorine and fluorinated products were byproducts of the intensive war time research and development efforts for fluorine production. The *Journal of Industrial and Engineering Chemistry* devoted its entire March 1947 publication to a comprehensive review of American efforts to industrialize fluorine production. Authors of articles in this publication covered a broad range of topics including historical reviews, advanced applications for fluorine chemistry, electrolyzer design, process scale-up, handling and

storage of fluorine, fluorocarbon chemistry, and nuclear energy applications.[15] Following the surrender of Germany in 1945, investigations of the German fluorine industry performed by the U.S. Chemical Warfare Service and British Atomic Energy Programme disclosed several important technological advances for fluorine production and handling. Reports from these agencies are included a review of the fluorine industry published in the 1951 edition of the National Nuclear Energy Series.[18]

The second world-war put fluorine and fluorine chemistry on the map in terms of commercial significance. Global production increased from less than one ton produced exclusively in research laboratories in 1934 to 480 tons in 1952 produced by many chemical companies, foundaries and government institutions throughout the United States, Great Britain, and Soviet Union.[1] Most of the German infrastructure was dismantled and moved to East Germany under control of the Soviet Union.[1]

Since 1950 most advances in fluorine technology have been ancillary in nature. Improvements have been made for materials of construction, product handling and purification technologies.[19-25] The fundamental process technology has remained unchanged. Significant changes in the industry have come in applications for fluorine chemistry as numerous varieties of fluorinated products have been developed.[26]

DuPont HCl Recycle Process

DuPont holds a patent[27] covering processes for electrolysis of anhydrous hydrogen halides to recover halogens from industrial process waste. An experimental program for technology development and demonstration of a process for chlorine recovery was conducted at Experimental Station from 1994 through 1997. This program provided support for and took advantage of some very good mathematical modeling work

performed at University of California Berkeley,[28,29] University of South Carolina,[30-32] and fundamental membrane transport and thermochemical measurements obtained at Los Alamos National Laboratory.[33,34] In 1997 DuPont licensed the technology to DeNora Inc. (Milan, Italy). DeNora has commercialized the technology and developed several HCl recycle systems in operation today.[30]

The electrolyzer is similar in design to polymer-electrolyte-membrane (PEM) fuel cells. It employs a Nafion® membrane as a proton conducting separator and carbon-based gas-diffusion-electrodes (GDE). Catalyst layers are laminated to the membrane surface as a membrane-electrode-assembly (MEA) or coated on the surface of the GDE in ELAT (Electrode Los Alamos Type) electrodes.

Anhydrous hydrogen chloride (AHCl) gas is fed to the anode of the reactor. The gas diffuses to the catalyst layer where it is oxidized to produce chlorine gas. Chlorine gas diffuses away from the catalyst and is swept away along with the unreacted AHCl feed. Protons are conducted across the membrane to the cathode and reduced to hydrogen gas. Dilute hydrochloric acid or water is fed to the cathode of the reactor. The cathode feed hydrates the membrane allowing it to maintain ionic conductivity and the cathode feed sweeps away hydrogen gas that accumulates in the cathode GDE. A schematic diagram is presented in figure 1-1 that represents the electrolytic process in the PEM reactor.

Current collector plates for the reactor consist of a graphite-fluoropolymer composite material with grooves cut in a patterned flow-field that allows for distribution of reactant and removal of product gases. The current collector plates contact the GDE allowing for delivery of electronic current to the catalyst layer. The catalyst layer for

MEA and ELAT cells consists of a mixture of electronic conducting materials (typically carbon black and/or platinum black), ruthenium dioxide catalyst, and proton conducting Nafion© solution.

External to the reactor, vapor-liquid separators (flash and column distillation) are employed for reactant delivery and product separation. Overall, hydrochloric acid exits the plant at a lower concentration than that which entered and hydrogen and chlorine gas are recovered as products. A process-flow-diagram is illustrated in figure 1-2. Hydrochloric acid is fed to a distillation column where a fraction of the HCl is distilled to AHCl vapor. The diluted hydrochloric acid from bottoms of the column is employed as the cathode feed for the reactor. The cathode feed sweeps hydrogen gas from the reactor and also picks up additional hydrogen chloride due to electroosmosis in the PEM reactor. The cathode product stream is sent to a phase separator from which hydrogen gas is removed which may be used as fuel for heating the distillation column and reactor or in other areas of the chemical plant. The remaining hydrochloric acid is recycled back to the cathode feed stream. The overhead AHCl vapor from the distillation is fed to the anode as the reactant. A fraction of the AHCl vapor is electrolyzed yielding chlorine gas that is carried away with the balance of the anode feed. The anode product is sent to an adsorption column. Nearly all of the AHCl gas and a small fraction of the chlorine gas are extracted in a stream of hydrochloric acid that is diverted from and returned to the cathode recycle loop. The overhead vapor from the adsorption column consists of

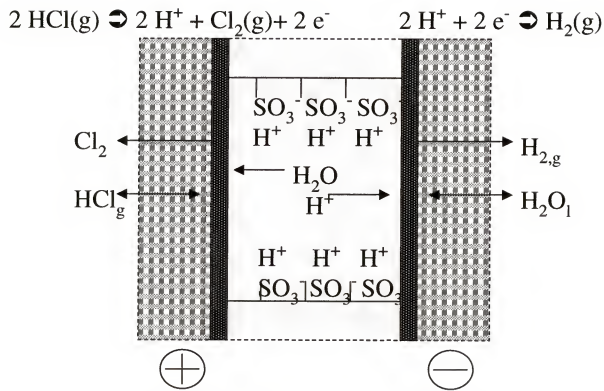

Figure 1-1. HCl PEM Reactor Electrolytic Process

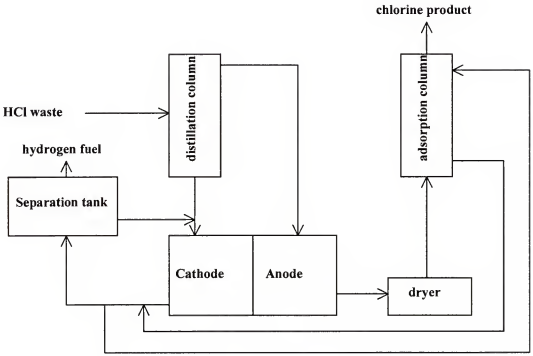

Figure 1-2. HCl Recycle Plant Process Flow Diagram

chlorine gas with trace amounts of AHCl vapor. This is collected as the product that may be sold or recycled in other processes in the chemical plant that use chlorine.

Proton Exchange Membrane Reactors

The work described in this manuscript targeted the development a gas diffusion electrode based PEM (polymer electrolyte membrane) electrochemical reactor for electrolysis of HF to produce fluorine. The traditional electrolysis cell uses a metal diaphragm to separate the anode and cathode in KF·xHF molten salt. Power costs decrease due to reduced IR drop as the diaphragm is made thinner and as the electrodes are moved closer together. The diaphragm is not a true separator, so there is a limit to the proximity of the electrodes. During normal operation, small explosions occur due to mixing and subsequent reaction of a fraction of the products H_2 and F_2. This is accepted in most industrial cells as a source of inefficiency. If the diaphragm is too thin or if the electrodes are too close together, mixing of a larger fraction of the products can lead to a catastrophic explosion. A PEM reactor has a true separator in the polymer membrane itself. The electrodes are in direct contact with the membrane minimizing IR drop in bulk solution. In this type of reactor, the reactants may be gases. This reduces mass transfer limitations on the rate of reaction.

Traditional fluorine production is a semi-batch process. The PEM reactor based process is conceived as a continuous process. The reactant (anhydrous HF) is fed as a gas through a flow-field contacting a gas diffusion electrode. HF diffuses through the electrode to the surface of a catalyst contacting the membrane. An applied voltage electrolyzes HF producing fluorine gas, protons, and possibly other oxidized products. Fluorine (and other products) diffuses back to the reactant stream and flows out of the

reactor. This product stream containing HF, F_2, and other oxidized products is then sent to a series of separation units. Protons are conducted through the membrane and recombine to form hydrogen at a catalyst surface in the opposite chamber. Hydrogen diffuses through a gas diffusion electrode in this chamber to a flow-field. A catholyte stream picks up the hydrogen as it travels through the flow field. The catholyte stream is sent to a scrubber and the hydrogen is vented.

The primary reactions expected to occur in the PEM reactor and their thermodynamic potentials[35-38] are as follows:

Anode: $HF(g) \rightarrow H^+(aq) + \frac{1}{2} F_2(g) + e^-$, $E° = 2.83$ V

(If water present) $HF(g) + \frac{1}{2} H_2O(l) \rightarrow \frac{1}{2} OF_2(g) + 2H^+(aq) + 2e^-$, $E° = 2.82$ V

$H_2O(l) \rightarrow \frac{1}{2} O_2(g) + 2H^+(aq) + 2e^-$, $E° = 1.23$ V

Cathode: $H^+(aq) + e^- \rightarrow \frac{1}{2} H_2(g)$, $E° = 0.0$ V

The formation of oxygen based products (O_2, OF_2) is a result of the presence of water in the cell. With a suitably chosen nonaqueous catholyte, the primary electrolysis products should be fluorine and hydrogen.

Proton Transport in Nafion® Membranes

The Nafion® perfluorinated ionomeric membrane is a DuPont commercial ion-exchange membrane available in film, resin, and solution forms. It is most commonly used in the membrane chlor-alkali process and in PEM fuel cells. The sulfonic acid form, called Nafion® XR, has the following structure:

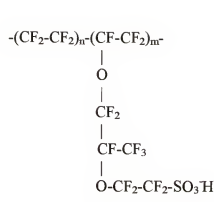

The phenomenon of proton transport through ionomeric membranes has been well documented for aqueous systems.[7,29,30,32] For HF electrolysis, an analogous process to the DuPont HCl process would use anhydrous HF gas as the anolyte and water as the catholyte. A drawback to the use of water as a catholyte is that water would inevitably be introduced into the anolyte leading to the generation of O_2 and OF_2 as the primary products rather than fluorine. This system is still worth investigating because OF_2 can be used as a fluorinating agent. A viable process that generates OF_2 as a primary product from HF would have industrial value. The traditional route to generation of OF_2 is to bubble F_2 into caustic water; thus the cost of OF_2 exceeds that of F_2.

Since the ultimate goal of HF electrolysis is the generation of fluorine, a nonaqueous process must be developed. Nafion® membranes do not conduct ions without the presence of a solvating medium. Fortunately, water is not the only solvent that facilitates proton transport in Nafion® membranes. It has been shown[7] that a variety of organic solvents and acids provide high ionic conductivity when imbibed into Nafion® membranes. The challenge is to devise a solvent system with both high ionic conductivity and stability in the presence of the reactant (HF) and the product (F_2).

The first anhydrous system we tested employed anhydrous HF gas as both anolyte and catholyte streams solvating a dry Nafion® membrane. Anhydrous HF is a very strong

acid. If the solvent (AHF) is a stronger acid than the membrane, it is likely that proton transport would be hindered or nonexistent. The following equilibria drive the transport of protons in acidic solutions:

Typical System: $R\text{-}SO_3H + H_2O \rightarrow H_3O^+ + R\text{-}SO_3^-$

Savinell System[7]: $2\ R\text{-}SO_3H + H_3PO_4 + H_2O \rightarrow H_4PO_4^+ + 2\ R\text{-}SO_3^- + H_3O^+$

HF System: $R\text{-}SO_3H + HF \leftarrow H_2F^+ + R\text{-}SO_3^-$

Unlike the aqueous acid systems, the equilibrium for HF dissociation lies strongly to the left. It is expected that very few if any protons will be available for transport. Experiments were performed to show whether this is or is not the case. These experiments involved direct conductivity measurements of Nafion® membranes saturated with liquid HF and mixtures of HF and several ionic salts. Electrolysis cell performance was also used to evaluate each system.

The second anhydrous system we investigated employed anhydrous HF as the anolyte and a solution of ionic salts in HF as the catholyte. Addition of ionic salts incorporates a mobile electrolyte to the membrane and aids in the dissociation of protons. Alkali fluoride salts were studied; however the use of these salts revisited many of the material compatibility issues that are undesirable in the current industrial process. Material compatibility issues were assessed for these systems prior to and following their use in the PEM reactor.

CHAPTER 2
RESEARCH PROGRAM

Overview

The principal goal of this research program was to develop a viable commercial process for production of fluorine and fluorinated gases in a PEM reactor. DuPont holds a patent related to PEM reactor technologies and production of halogen and halogenated gases.[27] This is an entirely new approach for fluorine production offering an opportunity for study of fundamental transport and reaction engineering problems. Key areas of study included fluorine chemistry, proton transport, electrocatalysis and reaction engineering, corrosion, thermodynamics, separations, and process control.

It was expected that many aspects of the technologies developed for the chlorine process would also apply to fluorine production. This turned out not to be the case. Attempts to engineer the process as a direct analog to the chlorine process by simply substituting HF for HCl were unsuccessful. First and foremost, fluorine is not stable in an aqueous environment. Second, thermodynamics favors oxygen evolution and this reaction can not be sufficiently suppressed on any catalyst at the electrode potential required for fluorine evolution. Third, the kinetics for direct oxidation of anhydrous HF from the gas phase was simply too slow.

Preliminary cell testing experiments demonstrated a nonaqueous environment was required and focus was shifted to discovery of a suitable solvent system for the membrane. A solvent was needed that would swell the membrane to allow proton

transport at a sufficient rate, and that would exhibit stability in the presence of fluorine. The most suitable solvents were determined to be anhydrous HF and HF-metal fluoride molten salts. An experimental program was implemented that focused on the following subjects: characterization of the thermodynamics and vapor-liquid equilibria for HF-metal fluoride molten salt systems, measurement of proton and cation conductivity for Nafion® membrane swollen with HF and HF-metal fluoride molten salts, screening of catalysts for utility in fluorine evolution, and evaluation of the performance of the PEM reactor for a variety of operating conditions.

Thermochemical Characterization and Conductivity Measurements

Inspection of existing literature provided very little thermodynamic data[16,17] and no conductivity data published with respect to Nafion® membranes employing HF-based solvent systems. Facilities were constructed to support an experimental effort to generate useful vapor-liquid equilibrium (VLE) and conductivity data. A four-point-probe conductivity cell was constructed for use in a pressure vessel for simultaneous acquisition of membrane conductivity and vapor-liquid equilibrium data. This system was installed and operated at DuPont Chambers Works with the assistance of on-site engineers and student interns.

Anhydrous HF and several HF-metal fluoride binary molten salt systems were each loaded in the vessel to a level immersing a Nafion® membrane loaded on the conductivity cell. The system was given time to equilibrate at several discrete temperature intervals where membrane conductivity and vapor pressure data were recorded.

Another four-point-probe conductivity cell was used to evaluate the conductivity of several alkali and transition metal cations in Nafion® membrane swollen with a variety of nonaqueous organic solvents. This cell was a free-standing apparatus used in a laboratory dry-box. Trends in the conductivity data were empirically evaluated with respect to the following parameters: temperature, cation size, cation valence, membrane thickness, solvent uptake, solvent dipole moment, and solvent dielectric constant. Several excellent models have been published that describe proton and cation transport in Nafion membrane swollen with water.[39-43] These models were re-evaluated to apply to nonaqueous solvent systems and simulations were compared to the empirical trends extracted from the experimental data.

Catalyst Screening

Catalyst screening experiments were designed to incorporate in situ cell testing and kinetic studies with a microelectrode testing apparatus. Catalyst layers were coated on carbon paper or carbon cloth electrodes in the form of ELAT (Electrode-Los Alamos-Type, Etek Inc.) for the majority of cells used in catalyst screening experiments. The following catalysts were evaluated: platinum black, platinum supported on carbon, nickel, nickel supported on carbon, gold, ruthenium, ruthenium oxide, titanium oxide and vanadium oxide. MEAs (membrane-electrode-assemblies) were fabricated by laminating catalyst layers directly on the membrane surface. MEA experiments were limited to catalysts containing platinum black and platinum supported on carbon.

For in-situ cell testing experiments, three criteria were used to evaluate catalyst utility: current efficiency, effective current density, and catalyst stability. Current efficiency is expressed as the stoichiometric charge equivalent of product recovered as a

percentage of total charge passed through the cell. The following example demonstrates calculation of current efficiency. Galvanostatic operation of the cell at 1.0 A for 60 minutes uses 1.0 A*h charge (3600 Coulombs). Quantitative analysis of the anode product gas during operation yields a product recovery of 1200 moles fluorine. The stoichiometric charge equivalent of one mole of fluorine is two coulombs. The resultant calculation for current efficiency is

$$\varepsilon = (2 \text{ coulombs/mole} * 1200 \text{ mole}) / (3600 \text{ coulombs}) = 67\%.$$

Effective current density is an expression of catalyst utilization. Under mass-transfer-limiting conditions a maximum current density is reached. Effective current density evaluated by measuring the mass-transfer-limited current per gram of catalyst. The following example demonstrates calculation of effective current density. A 1 cm^2 cell contains 5.0 mg/cm^2 catalyst loading. Potentiostatic operation at 6.0 V results in a steady-state current of 500 mA. The calculation for effective current density is

$$i_e = (0.5 \text{ A} / 1.0 \text{ cm}^2) / (0.005 \text{ g} / 1.0 \text{ cm}^2) = 100 \text{ A/g}.$$

Catalyst stability is evaluated in terms of corrosive losses over the lifetime of the cell. Direct measurement of corrosive side reactions can be difficult. The best way to monitor corrosive losses is to weigh the catalyst before assembly and after a cell is disassembled. Care must be taken to properly decontaminate and dry the electrodes and to avoid accidental losses due to mechanical abrasion.

The microelectrode testing apparatus was designed to employ a catalyst coated wire electrode imbedded in a planar surface in contact with a Nafion® membrane. The cell employed a three-electrode configuration with a Cu/CuF_2 reference electrode and

monel counter electrode. The microelectrode cell was constructed in a pressure vessel designed to contain HF or HF-metal fluoride molten salt electrolyte.

AC impedance spectroscopy and cyclic voltammetry are electroanalytical methods that are well suited to employ the microelectrode cell. AC impedance spectroscopy is a useful tool for identifying the nature of charge transfer phenomena. The difference between capacitive, resistive, and inductive electronic processes is readily discernible through such data. Cyclic voltammetry is useful to identify reactions and quantify kinetic parameters. Experiments were planned to fully study electrocatalytic properties for a variety of materials using the microelectrode cell.

Reactor Performance Evaluation

The primary focus of the research program was to assess the performance of the PEM reactor for production of fluorine and fluorinated gases. Initially the objective was to demonstrate fluorine production under guidelines represented in the DuPont patent.[27] Optimization of operating parameters, material compatibility issues, process scale-up, and production of fluorinated gases were each areas of investigation that would arise following demonstration of the fluorine process. The most direct approach for this assessment was repeated operation of the reactor under a variety of operating conditions. The following conditions were varied during the course of experimental work.

Monel, nickel, platinum and a graphite-fluoropolymer composite were each evaluated as materials of construction for the current collector plates of the PEM reactor. Viton®, Neoprene® and Kalrez® were tested as gasket materials. Carbon steel was the only material used for the cell body since it should not be exposed to HF or F_2 and

corrosion would be a good indicator of leaks. PFA Teflon®, PTFE Teflon® and Tefzel® were each tested as materials for tube fittings to the reactor inlet and outlet.

Two types of electrodes were evaluated. ELAT electrodes consisted of carbon cloth or carbon paper coated with catalyst. MEA electrodes consisted of catalyst laminated directly on the surface of the membrane and contacted with a carbon cloth, carbon paper, or metal mesh gas diffusion electrode. Most experiments were performed on cells with 1 cm^2 electrodes. A few experiments were performed on cells with 9 cm^2 electrodes due to hydrodynamic constraints associated with use of KF·xHF molten salt.

Platinum black, platinum supported on carbon, nickel, nickel supported on carbon, gold, ruthenium, ruthenium oxide, titanium oxide and vanadium oxide were each evaluated as catalysts. Catalyst layers for both ELAT and MEA electrodes consisted of a blend of catalyst particles and Nafion® solution binder. The amount of catalyst loaded on the electrode ranged from 0.2 mg/cm^2 to 10.0 mg/cm^2. The mass ratio of catalyst to (dry) Nafion® solution binder was also a variable ranging from 2:1 to 15:1.

Sulfonic acid form Nafion® membrane was the type of separator employed in most cells. A few cells were tested with porous Teflon® film separators. Nafion® membranes of three different thickness were evaluated: 2 mil, 5 mil and 7 mil. The thickness of Teflon® films was varied by stacking layers of 2 mil sheet. The cation conducting species in the Nafion® membrane was also a potential variable. Acid form Nafion® (proton conductor) was employed for most experiments. A few experiments were done with potassium or tetrabutyl ammonium cation exchanged membranes. The solvent used to swell the membrane was an important factor in development of the process. Preliminary tests precluded the use of an aqueous solvent. Anhydrous HF,

$KF{\cdot}xHF$ molten salt, and a few low molecular weight fluorocarbons were each tested as membrane solvents.

Systems for delivery of reactant (HF or HF_2^-) to the anode and removal of products (H_2, F_2, O_2, OF_2, CF_x) from the reactor were designed in four basic modes of operation. The first mode employed liquid water fed to the cathode and anhydrous HF gas fed to the anode. The second mode employed anhydrous HF gas fed to both the anode and cathode coupled with a cooling system for internal condensation of liquid anhydrous HF. The third mode employed $KF{\cdot}xHF$ molten salt flooding the cathode and anhydrous HF gas fed to the anode. The fourth mode employed $HF{\cdot}xHF$ molten salt flooding both the anode and the cathode. The reactor was heated to maintain the molten salt in the liquid phase.

The remaining variables for evaluation of PEM reactor performance each had to do with specific operating conditions for individual experiments. Current, voltage, temperature, and flow-rates were the primary operating variables. A data acquisition and control system was constructed to monitor and control these parameters. Details describing design and operation of the electrolysis system are provided in chapter 3. Experimental results are detailed in chapters 4 and 5.

Gaseous Coreactants

The process previously discussed contemplates the use of a PEM reactor to electrolyze gas phase HF producing fluorine. In addition to electrolyzing HF directly to fluorine, it may also be possible to carry out gas phase electrochemical fluorinations in the same reactor. In this case, the anodic feed stream would contain a gas phase mixture of anhydrous HF with other coreactants. The oxidation of HF in the presence of another

component may fluorinate said component depending on the species involved and the operating conditions. This gives a novel and robust method to fluorinate chemicals without using expensive fluorine gas as the fluorinating agent.

The electronic gases industry requires highly fluorinated gases (e.g., C_2F_6, NF_3, ClF_3, OF_2, etc.) as chamber cleaning agents. Generation of OF_2 has already been discussed. It may also be possible to cofeed hydrocarbons, carbon monoxide and dioxide, ammonia, lower halogens, or other gases to generate fluorinated products useful to this and other industries.

Several experiments were initiated in an attempt to generate NF_3 in our laboratory. This work was not completed to a degree worth presenting in this manuscript, however some of the insights gained from these experiments led to refinement of procedures for product analysis. Product analysis for the above mentioned fluorinated gases may be performed using gas chromatography and mass spectrometry. The laboratory facility was equipped with an HP 6890 series gas chromatograph and a mass spectrometer detector installed outside the hood downstream of the PEM reactor system. Product analysis was conducted on-line during cell operation. DuPont employs many scientists and technicians highly skilled in GC/mass spec analysis, several of whom specialize in fluorocarbon products. Separation of NF_3 and CF_4 is difficult as both molecules have nearly identical boiling points and very similar physical and chemical properties. A cryogenic procedure was used for this separation.

CHAPTER 3
PROCESS DESIGN

Overview

The PEM reactor system and the pressure vessels used in experimental work can each be described in terms of basic chemical engineering unit operations. The processes were designed to employ the following operations: mass transport, separation, chemical reaction, heat transfer, mixing, and process control. The design and operational details of the processes used for experimental work are provided in this chapter. It is useful to first lay out the overall design of the process and then provide greater detail for specific components and subsystems.

Experimental work was performed in laboratory facilities at DuPont Experimental Station and also in a pilot plant at DuPont Chambers Works. An HF electrolysis system was constructed in a hood located in the primary laboratory. The system consisted of a PEM reactor, gas feed systems, cooling and heating water, product treatment scrubbers, process control electronics a gas chromatograph and a mass spectrometer. Conductivity measurements for Nafion® membrane swollen with organic solvents were obtained using a conductivity cell inside a laboratory dry-box. Conductivity and VLE data for HF-KF molten salt were obtained using another conductivity cell and pressure vessel at the pilot plant facility.

Material and energy balances and process diagrams are provided for the overall electrolysis process, for the pressure vessel, and for the following subsystems: anode flow

system, PEM reactor, and product separation systems (scrubbers). Calculations based on the material and energy balances were used to determine the capacity of the systems, safe operating parameters, and energy requirements. Design and operating equations for individual unit operations are the result of these calculations.

Process Hazards Assessment

Anhydrous hydrogen fluoride and fluorine present extreme hazards that necessitate excellent safe work practices and safety training. All personnel working with HF undergo annual training. Any work with HF and its oxidation products is done in a laboratory hood environment with proper personal protective equipment and safety interlocks in place. A team of DuPont research associates and safety officers conducted thorough process safety management prior to start-up.

Any process attempting to make one extremely hazardous chemical into another will have intrinsic safety hazards. This PEM-cell configuration is envisioned as a safer alternative to the present industrial process in which hydrogen and fluorine are generated without a true separator. In the PEM cell, rigorous separation of these gases is achieved and hazard associated with explosive recombination of the gases is decreased. Pressure relief devices were installed to prevent over-pressurization due to plugged process lines or product recombination.

The process hazard assessment process consisted of the following stages: a preliminary brainstorming session to identify potential hazards, a thorough review of each component of the process during the design process, comprehensive documentation in a Process Hazard Report filed with the DuPont Occupational Safety and Health Office, and an inspection of the process prior to start-up. A copy of the PHR manual was stored

outside the laboratory. The PHR was updated every time changes were made to the process or when new standard operating procedures were implemented.

The following list of process hazards and measures taken to eliminate or minimize danger to personnel summarizes issues resolved during the process hazard assessment. Standard operating procedures were listed in the PHR. Material Safety Data Sheets (MSDS) were listed in the PHR and in a separate binder outside the laboratory. First aid procedures were also included in the PHR and in separate emergency training documents posted outside the laboratory.

Hazards and Corrective Actions Identified from Process Hazard Assessment

Chemical exposure (hazardous chemicals are HF, F_2, KF, KOH and HNO_3):

Training for HF and chemical handling, first aid training, Proper Protective Equipment (PPE), fail-safe process design, leak sensors, proper hood ventilation, proper waste disposal

Explosive recombination of H_2 and F_2:

Proper design of gaskets, inspection of separators, safety interlock designed to shut down process if pressure too high, installation of pressure relief valves

Electrical equipment (shock and fire):

Proper grounding of equipment, electrical training, fireproof insulation

N_2 or He gas cylinder malfunction (asphixiation or projectile hazard):

Cylinder handling and storage training, storage in ventilated enclosure, proper regulators and cylinder clamps

Overpressurization of HF cylinder due to accumulation of hydrogen:

Do not store HF cylinders for more than 18 months, monitor pressure gauge when opening a new cylinder, installation of pressure relief valve

Overpressurization of reactor due to plugged process lines:

Purge nitrogen through process prior to start-up, weekly inspection of process lines, safety interlock shuts down process if pressure reaches pre-set limit, installation of pressure relief valves

Melting and decomposition of Nafion® membrane (may release PFB):

Process safety interlock shuts down if cell temperature exceeds 200°C, MEA hot-press temperature limit is 220°C, hot-press located in ventilated enclosure

Catalyst fire (Pt, RuO_2):

Keep dry catalysts away from alcohols, alcohol/water ratio in ink can not exceed 0.5, dry catalyst inks in oxygen-free environment (nitrogen purged oven)

Electrolysis Reactor Design

A PEM reactor was constructed for use in the electrolysis experiments. An expanded view schematic of the reactor is displayed in figure 3-1. The components of the reactor are listed in table 3-2. Engineering drawings were made for each set of current collector plates and for the heat exchanger plates. The drawings are filed with DuPont Engineering as design object numbers D1364043 and D1369368, respectively.

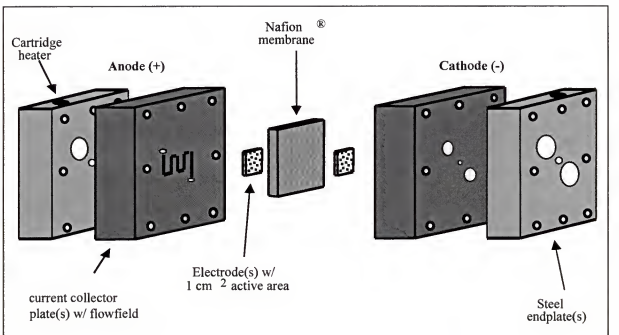

Figure 3-1. Expanded view of the laboratory scale PEM reactor

Table 3-1. PEM Reactor Components

Component	Materials of Construction	Function
Load bearing heat exchanger plates	Stainless steel	Distribute force of bolts uniformly and regulate cell temperature PEM separator
Current collector plates with flow channel	Graphite, Monel, Platinum, Nickel	Electronic conductor with serpentine flowfield for delivery of reactants
Gaskets	Viton®, Kalrez®	Separate electrodes and prevent leaks
Torque bolts	Stainless steel	Compress cell plates
Gas diffusion electrode (GDE)	Carbon paper, Pt mesh, Monel mesh, Ni mesh	Electronic conductor which allows diffusion of reactants to catalyst layer
Catalyst layer	Various catalysts in ELAT or MEA form	Catalyze electrochemical reaction
Membrane Separator	Nafion® membrane, Celgard® membrane, Porous Teflon® membrane	Separate anode and cathode compartments while allowing ionic conduction
Reference electrode	Cu / CuF_2 or Pt / H_2	Provide stable reference potential

Each component was designed to withstand prolonged exposure to anhydrous HF while retaining the mechanical and electrochemical properties required of its purpose. The load bearing plates were not exposed to HF, but they were made of stainless steel in case of accidental exposure. The current collector plates were composed of graphite, nickel, monel, or platinum with a flow channel machined into the broad face for gaseous reactant and product flow. The gas diffusion electrode (GDE) was made from carbon paper, carbon cloth, monel mesh, or platinum mesh. The GDE allowed diffusion of gases to the catalyst layer. The catalyst layer was coated on carbon cloth for ELAT (Electrode-

Los Alamos-Type) electrodes. For an MEA (Membrane-Electrode-Assembly), the catalyst was hot pressed directly on the surface of the membrane.

The process of making and testing MEA is a critical component to achieving high performance PEM reactors. Experiments were conducted to evaluate both ELAT and MEA. ELAT-based electrodes are easier to use because they are commercially available (E-Tek, Inc.). MEA, though not commercially available, are more useful for experimental evaluation because they allow direct manipulation of the variables that control catalyst layer performance. MEA may be fabricated by mixing an "ink" and depositing it on the surface of the membrane by spray coating, screen or ink jet printing, or the decal method. The catalyst layers are dried then hot pressed on the membrane surface. This method creates excellent adhesion between the catalyst layer and the membrane.

The MEA employed in this work were fabricated by the following process: Nafion® solution was mixed with the catalyst particles in a solvent to form an ink. The ink consisted of a 50/50 wt.% isopropanol-water solvent with an approximate ratio of 5:2 platinum to polymer solids from Nafion® solution by weight. Ethylene glycol was added to the ink at approximately 5 wt.% as a plasticizer to improve coating quality. The ink was cast from solution onto a Kapton® film masked to the appropriate area and slowly dried in air. The dried ink consisted of catalyst particles held together with polymer binder from the Nafion® solution. This catalyst layer was then hot pressed onto a Nafion® 115 membrane at 140°C and 5000 psi for three minutes to adhere the layers firmly to the membrane. The result was a high surface area thin layer of catalyst particles

with electronic contact between particles and ionic contact with the proton exchange membrane phase in all locations.

The variables in the hot press procedure, (time, temperature, and pressure), provided some control over the final properties of the catalyst layer. Many different catalysts and additives can be used in MEAs to control the hydrophobicity, porosity, adhesion, electronic conductivity, and other properties. Techniques for MEA optimization[32,33,34] have been established in the PEM-fuel cell industry that was useful for development of the MEA structures employed in this work.

Gas diffusion layers are located adjacent to the catalyst layer on both sides of the cell. These layers serve the dual purpose of allowing reactants (e.g. HF vapor) to diffuse into the electrode regions and serving as an electrical contact. The barrier properties of the gas diffusion layers are important because typically transport of certain species is more favorable than others (e.g., in the PEM fuel cell, transport of gaseous reactants O_2 and H_2 is accomplished while hindering transport of water). As with other cell components, the gas diffusion layers must be both chemically and electrochemically resistant to the reactants and products in the cell.

The other cell layers, (gaskets, current collector plates, and backing plates), are less integral to the electrochemical performance of the cell. Materials of construction reflect concerns over chemical stability, function, and cost. Choice of materials of construction and an optimized design would be important in scaling up the process, but was not a critical factor for preliminary experimental work.

The reactor was assembled in a symmetric sandwich configuration. The membrane was placed between the gaskets. Each gasket had either a 1 cm^2 or a 9 cm^2

hole in its center. The ELAT (Electrode-Los-Alamos-Type) and the gas diffusion electrode were placed in the hole. The active area of the electrochemical cell was 1 cm^2 in all experiments unless noted otherwise. ELAT were purchased from E-TEK Inc. They consisted of catalyst particles coated on one side of a woven carbon cloth. When an MEA (Membrane-Electrode-Assembly) was used, the catalyst layer was part of the membrane and no ELAT was used. The gaskets separated the current collector plates. The outer load-bearing heat-exchanger plates compressed the current collector plates providing a seal against the gasket. The sandwich cell was bolted together using eight bolts at 50 in-lbs. torque.

Fluid Flow and Product Separation Systems

A process diagram for the laboratory process is displayed in figure 3-2. Anhydrous HF used in the process originated from a three-pound cylinder located inside the laboratory hood. The cylinder was partially immersed in a water bath that was used for temperature control. The normal boiling point of HF is 19.5°C. HF is a liquid under pressure inside the cylinder. Cool water circulated through the bath when the process was idle. This minimized vapor pressure reducing the risk of cylinder failure. Warm water circulated through the bath during normal operation. This increased vapor pressure to a level sufficient to operate a Hastings mass flow controller located downstream of the cylinder.

1/4 inch stainless steel tubing and Swagelok fittings were used for essential plumbing on the front end of the process from the cylinder regulator through the mass flow controller. The stainless steel tubing, fittings and mass flow controller were

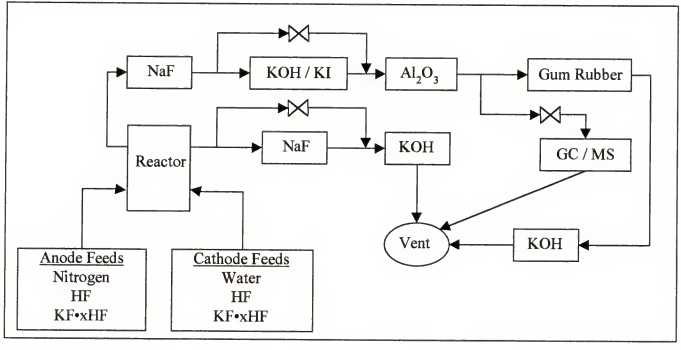

Figure 3-2. General laboratory process flow diagram

wrapped with heat tape to prevent condensation of liquid HF. 1/8 inch Teflon® tubing was used to connect the mass flow controller to the PEM reactor.

The anode side of the process was configured to allow gas phase flow of HF and nitrogen through the anode, or for flooding molten salt electrolyte through the anode in a circulating loop. The cathode side of the process was configured the same way, but also allowed for liquid-phase flow of deionized water through the cathode.

A metered valve system was designed to allow nitrogen to flow through the process lines and also to allow mixed flow of nitrogen and HF. The nitrogen source was a standard fifty-pound cylinder located in a laboratory cylinder closet outside the hood. Plumbing for nitrogen was connected to a fitting through the wall of the hood and tied in to the process at the 3-way valve immediately downstream of the HF regulator, and also at a needle valve allowing mixed flow downstream of the mass flow controller.

Experimental plans called for HF flow rates ranging from 10 to 200 cc/min. Volumetric flow rates for HF may be related to molar flow rates by the ideal gas law (PV = nRT). The corresponding range for molar flow rate is 4.0E-04 to 8.0E-03 mole/min. This range of operation is conservatively low with respect to production standards but sufficient for experimental work. The entire anode flow system would require much more stringent design if the process warrants scale-up.

Downstream from the anode, the following product separation scrubbers and analytical devices were employed in series. A scrubber packed with sodium fluoride pellets was used to remove HF from the product stream. A bypass line allowed for diversion of the product to a bubbler filled with KI solution for analysis of fluorine and oxygen difluoride. An automated 6-port sampling valve was used to extract samples to

inject in a gas chromatograph equipped with a mass spectrometer for analysis of fluorinated gases and other byproducts. A pipe filled with alumina pellets was used to remove fluorine. A gum-rubber trap was used to absorb oxygen difluoride. A tank filled with 15 wt.% KOH solution was installed at the end of the process as a fail-safe in the event any HF or fluorinated gases escaped the scrubber series.

HF scrubbers were made by filling monel cylinders with NaF pellets. These scrubbers were placed in the product lines to remove HF by the following reaction.

$$HF_{(g)} + NaF_{(s)} \rightarrow NaHF_{2(s)}.$$

For purposes of effective regeneration, it is not desirable for this reaction to proceed any further than 0.2 moles HF per mole of NaF. $NaHF_2$ was regenerated to NaF by heating the cylinder to approximately 200°C reversing the reaction. HF gas was released into a nitrogen-purge stream.

A fluorine scrubber was made by filling a stainless steel pipe with alumina pellets. This scrubber was placed in the anode product line to remove fluorine by the following reaction:

$$Al_2O_{3(s)} + 3\ F_{2(g)} \rightarrow 2\ AlF_{3(s)} + 3/2\ O_{2(g)}\ .$$

This scrubber cannot be regenerated. An OF_2 scrubber was made by filling a stainless steel cylinder with gum rubber particles. This scrubber was used to absorb OF_2.

Neutralization scrubbers were made by dissolving KOH pellets with DI water to a concentration of 15 wt.% in a Nalgene® tank. These scrubbers were used to neutralize any HF remaining at the end of the process line. The end of the process gas line was attached to a dip-leg that allowed the effluent (nitrogen under normal operating conditions) to bubble through the KOH solution. The overhead vapor from the KOH

tank was released to the roof through a tube vented at the top of the hood. The neutralization reaction is:

$$KOH_{(aq)} + HF_{(g)} \rightarrow KF_{(aq)} + H_2O_{(l)}.$$

The amount of F_2 or OF_2 in the anode product stream was periodically measured by sending the anode exit gas through a KI scrubber located between the NaF scrubber and the alumina scrubber. The KI scrubber was made by dissolving the desired amount of KI in a K_2HPO_4-buffered aqueous solution contained in a Nalgene® tank. After the process was shut down, samples withdrawn from this scrubber were titrated with $Na_2S_2O_3$ using a starch indicator (iodometric titration). The reaction that occurs in the KI scrubber is liberation of iodine due to reduction of F_2 and/or OF_2.

$$2\ KI_{(aq)} + F_{2(g)} \rightarrow 2\ KF_{(aq)} + I_{2(g)}$$

$$4\ KI_{(aq)} + OF_{2(g)} + H_2O_{(l)} \rightarrow 2\ KF_{(aq)} + 2\ KOH_{(aq)} + 2\ I_{2(g)}$$

These reactions proceed to completion in slightly acidic media without any interference from O_2. The K_2HPO_4 buffer was used to insure the solution did not become basic due to formation of KOH. It is also important to insure that all the HF in the product stream is scrubbed in the NaF scrubber. If the solution takes on too much HF it becomes hydrofluoric acid, a potential safety hazard. The same situation could result if all the KI is exhausted by reaction with fluorine. Continued addition of fluorine beyond the KI capacity of the scrubber results in liberation of OF_2 leaving hydrofluoric acid.

$$2\ F_{2(g)} + H_2O_{(l)} \rightarrow OF_{2(g)} + 2\ HF_{(aq)}$$

Downstream from the cathode, the product steam (N_2, HF, H_2, DI water) was passed through a condenser to separate gas and liquid phases. The overhead gas phase was fed to a sodium fluoride scrubber to remove HF and then bubbled through a tank

containing 15 wt.% KOH. The liquid phase bottoms were drained directly to the same KOH tank for neutralization of hydrofluoric acid.

Process Operation

Systems for reactant delivery and product handling were constructed for each of four modes of operation of the PEM reactor.

Mode I: Aqueous HF Electrolysis

DI water is metered through a rotometer and fed to the cathode flow-field. Liquid (dilute HF_{aq}) and gas (cathodic product H_2) exiting the cathode flow-field are sent to a KOH scrubber. Anhydrous HF gas is metered through a Tylan General mass-flow-controller and fed to the anode flow-field. Gases (HF and anodic electrolysis products such as O_2 and OF_2) exiting the anode flow-field are sent to the following series of scrubbers: NaF, Alumina, Gum Rubber, and KOH. Figures 3-3 and 3-4 show process diagrams for the mode I flow system and for the PEM reactor.

Mode II: Anhydrous HF Electrolysis

Anhydrous HF gas is metered through a mass-flow-controller and fed to the cathode flow-field. Gases (HF and cathodic product H_2) exiting the cathode flow-field are sent to a NaF scrubber followed by a KOH scrubber. Anhydrous HF gas is metered through a mass-flow-controller and fed to the anode flow-field. Gases (HF and anodic product F_2) exiting the anode flow-field are sent to the following series of scrubbers: NaF, Alumina, Gum Rubber, and KOH. Figures 3-5 and 3-6 show process diagrams for the mode II flow system and for the PEM reactor.

Mode III: Liquid Catholyte HF Electrolysis

A liquid electrolyte consisting of KF dissolved in anhydrous HF is generated by loading a prescribed mass of KHF_2 into a monel mixing cylinder and allowing the salt to equilibrate with 1 atm. anhydrous HF vapor at a prescribed temperature. Anhydrous HF vapor is fed to the mixing cylinder to maintain 1 atm. pressure as HF condenses and dissolves the salt. The resulting liquid generated is a solution of KF in HF with composition dictated by thermodynamic equilibrium at the prescribed temperature with 1 atm. vapor pressure. The liquid electrolyte is drained into the cathode flow-field where it remains stagnant during the course of the experiment.

A vent is opened from the cathode vapor space to a tube through which anhydrous HF gas flows at 1 atm. This gas and the cathodic product (H_2) exiting the vent are sent to a NaF scrubber followed by a KOH scrubber. Anhydrous HF gas is metered through a mass-flow-controller and fed to the anode flow-field. Gases (HF and anodic product F_2) exiting the anode flow-field are sent to the following series of scrubbers: NaF, Alumina, Gum Rubber, and KOH. Figures 3-7 and 3-8 show process diagrams for the mode III flow system and for the PEM reactor.

Mode IV: Batch Electrolysis

A liquid electrolyte consisting of KF dissolved in anhydrous HF is generated by loading a prescribed mass of KHF_2 into a monel mixing cylinder and allowing the salt to equilibrate with 1 atm. anhydrous HF vapor at a prescribed temperature. Anhydrous HF vapor is fed to the mixing cylinder to maintain 1 atm. pressure as HF condenses and dissolves the salt. The resulting liquid generated is a solution of KF in HF with composition dictated by thermodynamic equilibrium at the prescribed temperature with

1 atm. vapor pressure. The liquid electrolyte is drained into both the anode and cathode flow-fields where it remains stagnant during the course of the experiment.

A vent is opened from the cathode vapor space to a tube through which nitrogen is purged. The nitrogen purge gas and the cathodic product (H_2) exiting the vent are sent to a NaF scrubber and then to a KOH scrubber. A vent is opened from the anode vapor space to a tube through which nitrogen is purged. The nitrogen purge gas and the anodic product (F_2) exiting the vent are sent to a NaF scrubber followed by an alumina scrubber and then to a KOH scrubber. Figures 3-9 and 3-10 show process diagrams for the mode IV flow system and for the PEM reactor.

Chemical Reactions

A summary of the primary reactions expected to take place in the PEM cell and the thermodynamic potentials of these reactions follows:

Anode: $HF_{(g)} \rightarrow H^+_{(aq)} + \frac{1}{2} F_{2(g)} + e^-$, $E^0 = 2.83$ V

$HF_{(g)} + \frac{1}{2} H_2O_{(l)} \rightarrow \frac{1}{2} OF_{2(g)} + 2 H^+_{(aq)} + 2 e^-$, $E^0 = 2.82$ V

$H_2O_{(l)} \rightarrow \frac{1}{2} O_{2(g)} + 2 H^+_{(aq)} + 2 e^-$, $E^0 = 1.23$ V

Cathode: $H^+_{(aq)} + e^- \rightarrow \frac{1}{2} H_{2(g)}$, $E^0 = 0.0$ V

The formation of oxygen-based products such as O_2 and OF_2 depends on the presence of water in the cell. The expected electrolysis products for the first mode of operation are O_2, OF_2, and H_2. The second and third modes of operation do not have water present. The expected electrolysis products are F_2 and H_2.

1 atm. vapor pressure. The liquid electrolyte is drained into both the anode and cathode flow-fields where it remains stagnant during the course of the experiment.

A vent is opened from the cathode vapor space to a tube through which nitrogen is purged. The nitrogen purge gas and the cathodic product (H_2) exiting the vent are sent to a NaF scrubber and then to a KOH scrubber. A vent is opened from the anode vapor space to a tube through which nitrogen is purged. The nitrogen purge gas and the anodic product (F_2) exiting the vent are sent to a NaF scrubber followed by an alumina scrubber and then to a KOH scrubber. Figures 3-9 and 3-10 show process diagrams for the mode IV flow system and for the PEM reactor.

Chemical Reactions

A summary of the primary reactions expected to take place in the PEM cell and the thermodynamic potentials of these reactions follows:

Anode: $HF_{(g)} \rightarrow H^+_{(aq)} + \frac{1}{2} F_{2(g)} + e^-$, $E^0 = 2.83$ V

$HF_{(g)} + \frac{1}{2} H_2O_{(l)} \rightarrow \frac{1}{2} OF_{2(g)} + 2 H^+_{(aq)} + 2 e^-$, $E^0 = 2.82$ V

$H_2O_{(l)} \rightarrow \frac{1}{2} O_{2(g)} + 2 H^+_{(aq)} + 2 e^-$, $E^0 = 1.23$ V

Cathode: $H^+_{(aq)} + e^- \rightarrow \frac{1}{2} H_{2(g)}$, $E^0 = 0.0$ V

The formation of oxygen-based products such as O_2 and OF_2 depends on the presence of water in the cell. The expected electrolysis products for the first mode of operation are O_2, OF_2, and H_2. The second and third modes of operation do not have water present. The expected electrolysis products are F_2 and H_2.

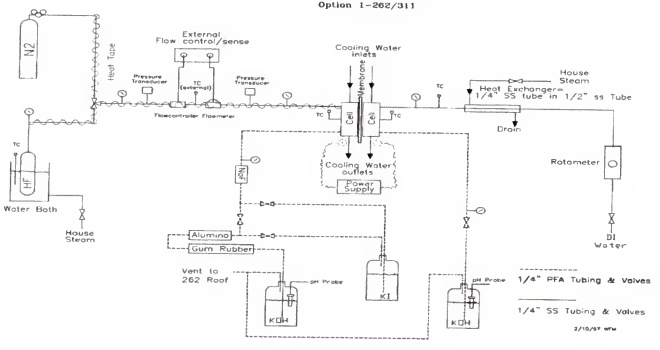

Figure 3-3. Process Flow Diagram for Mode I Operation

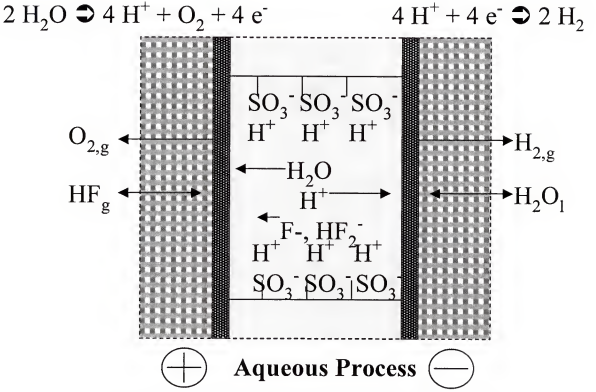

Figure 3-4. Mode I PEM Reactor Internal Process Diagram

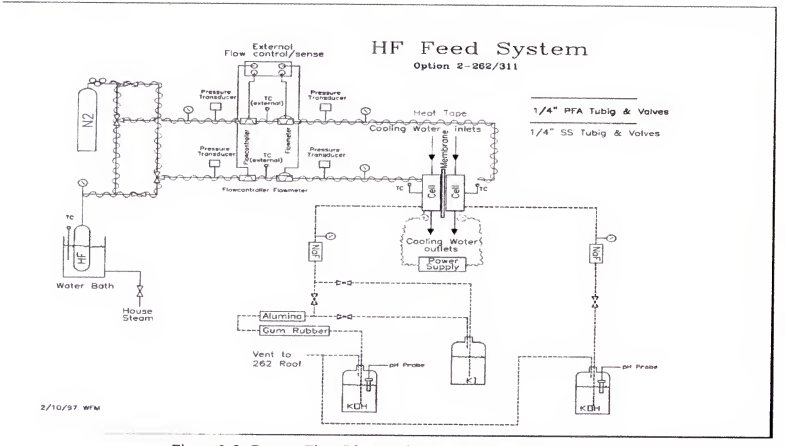

Figure 3-5. Process Flow Diagram for Mode II Operation

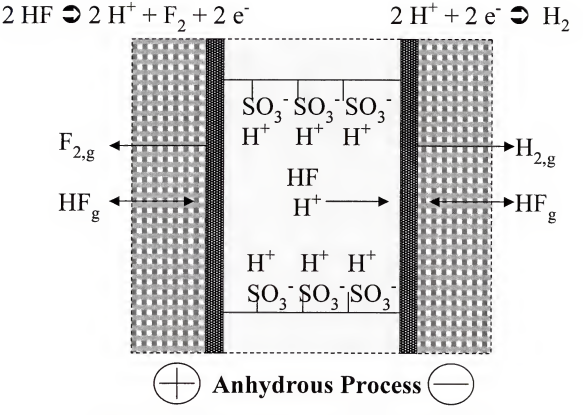

Figure 3-6. Mode II PEM Reactor Internal Process Diagram

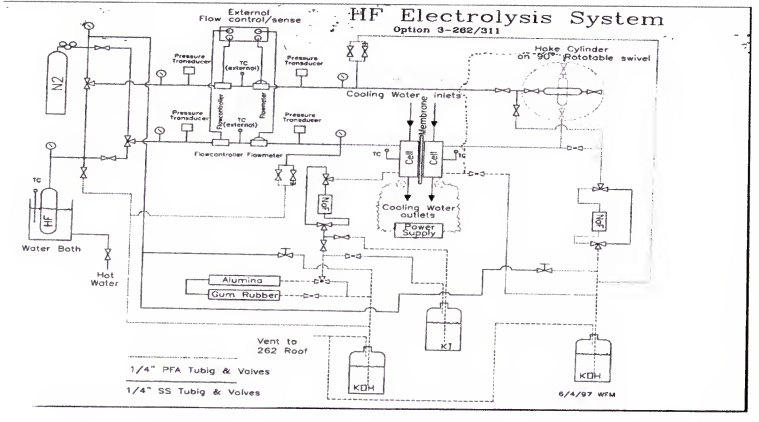

Figure 3-7. Process Flow Diagram for Mode III Operation

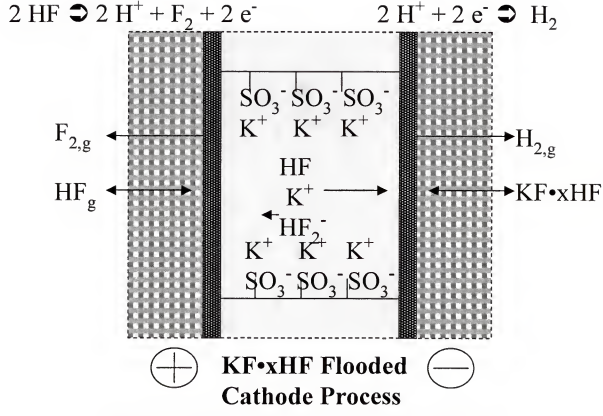

Figure 3-8. Mode III PEM Reactor Internal Process Diagram

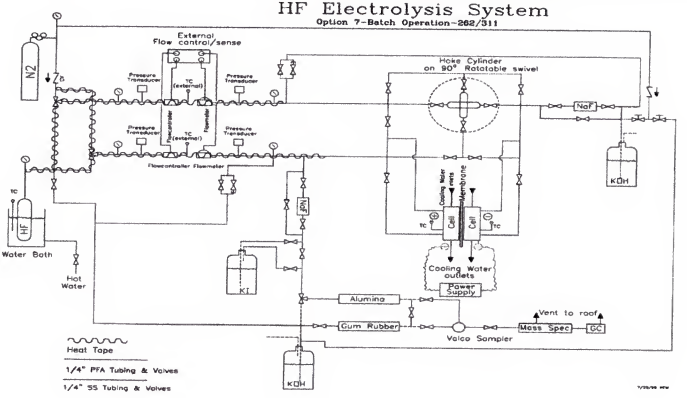

Figure 3-9. Process Flow Diagram for Mode IV Operation

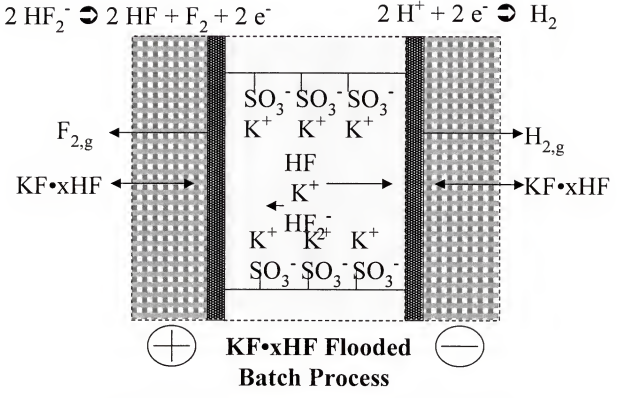

Figure 3-10. Mode IV PEM Reactor Internal Process Diagram

The listed anodic reactions occur only if the current collector and electrode materials are chemically and electrochemically inert under normal operating conditions. Side reactions are concerns for the following materials of construction:

Carbon: $x\ HF_{(g)} + C_{(s)} \rightarrow CF_{x(s)} + x\ H^+_{(aq)} + x\ e^-$

$2\ HF_{(g)} + C_{(s)} + H_2O_{(l)} \rightarrow COF_{2(g)} + 4\ H^+_{(aq)} + 4\ e^-$

Nickel: $x\ HF_{(g)} + Ni_{(s)} \rightarrow NiF_{x(s)} + x\ H^+_{(aq)} + x\ e^-$

Platinum: $x\ HF_{(g)} + Pt_{(s)} \rightarrow PtF_{x(s)} + x\ H^+_{(aq)} + x\ e^-$

Monel: $x\ HF_{(g)} + Cu_{(s)} \rightarrow CuF_{x(s)} + x\ H^+_{(aq)} + x\ e^-$

Stoichiometric Current

An important expression for an electrochemical process is the conversion in terms of the current density and reactant molar flow rate. The stoichiometric current (I_{st}) is defined as the maximum current that can be passed when the reactants react to completion.

$$I_{st} = N_{HF}F[\chi_{F2} + 2\ \chi_{OF2}]$$

N_{HF} represents the molar flow rate of HF. F is Faraday's constant (96487 Coulombs per mole-equivalent). With respect to HF electrolysis, the stoichiometric current depends on the relative product conversions (χ) for F_2 and OF_2. Fluorine requires one electron per mole of HF. Oxygen difluoride requires two electrons per mole of HF.

$$2\ HF \rightarrow F_2 + 2\ H^+ + 2\ e^-$$

$$2\ HF + H_2O \rightarrow OF_2 + 4\ H^+ + 4\ e^-$$

The stoichiometric current may be used to express the conversion of reactant (HF) in terms of the molar feed rate and product conversions at a given current density. This expression is used in both material and energy balances for the reactor.

$$\chi_{HF} = i \cdot A / I_{st} = i \cdot A / N_{HF} F[\chi_{F2} + 2\,\chi_{OF2}]$$

Data Acquisition and Process Control

A data acquisition system was run through Testpoint software on a Dell Electronics PC that logged the following data: flow-rates, process temperatures, reactor pressure, cell voltage, and current. Electroanalytical experiments were performed using a Solartron model 1287 potentiostat, a Solartron model 1260 frequency response analyzer (FRA), and a Xantrax model HPD power supply. A Hewlett Packard model 6890 gas chromatograph and a Hewlett Packard model 5973 mass spectrometer were used to identify fluorinated gases. Table 3-3 lists the different types of experiments performed, the equipment used, and the form of data acquired.

Safety interlocks were installed that responded to critical process upsets. In the event of a hydrogen fluoride leak, HF sensors located in strategic locations in the hood were hardwired to automatically sound an alarm, switch flow from HF to nitrogen, and to shut down the power supply. If a pressure sensor or thermocouple exceeded critically set limits, the software was programmed to shut down power and all process flows. Pressure relief valves were positioned to vent to the back of the hood in the event of a catastrophic explosion. If cell voltage exceeded 20 V, the power supply was shut down.

Table 3-2. Experimental Methods and Devices

Experimental Method	Equipment	Form of Acquired Data
Potentiostatic Operation	Potentiostat or Power Supply, PEM Reactor, Temperature Controller, Flow Controllers	I (E, T, F): steady-state current as a function of potential, temperature or flowrate
Galvanostatic Operation	Potentiostat, PEM Reactor, Temperature Controller, Flow Controllers	E (I, T, F): steady-state potential as a function of current, temperature or flowrate
Cyclic Voltammetry	Potentiostat, PEM Reactor, Reference Electrode	I (E, t): current as a function of potential and sweep-rate
Cyclic Amperometry	Galvanostat, PEM Reactor, Reference Electrode	E (I, t): potential as a function of current and sweep-rate
AC Impedance Spectroscopy	Potentiostat, Frequency Response Analyzer, PEM Reactor, Ref. Electrode	$\Omega(E,\omega)$: impedance as a function of bias potential and current frequency
Open Circuit Potential Decay	Potentiostat, PEM Reactor, Reference Electrode	E(t): potential as a function of time at open circuit
Iodometric Titration	Titration Solutions, Burret	ε: efficiency as a function of operating conditions
EMF Titration	Titration Solutions, Fluoride Ion Selective Electrode	ε: efficiency as a function of operating conditions
Gas Chromotography / Mass Spectrometry	Gas Chromotograph, Mass Spectrometer, Autosampler	c_i: concentration of species (fluorinated gas) in sample
Conductivity Measurement	Conductivity Cell, Frequency Response Analyzer	κ: cationic conductivity of Nafion® membrane as a function of cation size, valence, temperature, and solvent uptake
Vapor Liquid Equilibrium	Pressure Vessel, Temperature Controller, Pressure Gauge	$P^{vap}(T, x_{HF})$: vapor pressure as a function of temperature and composition of molten salt

Material and Energy Balances

Predictive calculations of mass and energy balances were used to estimate the worst-case scenario process conditions. The pertinent calculations involved the heating

or cooling requirements of the reactor, scrubber tanks, and HF cylinder. Process temperature extremes from 5°C (chilled water) to 250°C (maximum output cartridge heater) were used to estimate heat duties. HF throughput within the limits of the mass-flow-controller from 2 cc/min to 200 cc/min was used to gauge scrubber capacities. The following sections detail energy and mass balances for each component in the process.

Analytical Scrubber

This unit was a 1.0 L Nalgene bottle with inlet and outlet gas tubing fixed to the lid. The bottle was charged with 750 ml of 0.2 M KI solution with phosphate buffer. This provides a net capacity of 0.15 moles KI. KI reacts with fluorine and oxygen difluoride according to the following reactions. The heats of reaction provided were used to predict temperature rise due to exothermic reaction.

$$2\ KI\ (aq) + F_2(g) \rightarrow 2\ KF(aq) + I_2(g)\ \ (\Delta H^\circ = -448.8\ kJ/mol)$$

$$4\ KI(aq) + OF_2(g) \rightarrow 2\ KF(aq) + 2\ I_2(g) + 2\ KOH(aq)\ \ (\Delta H^\circ = -473.5\ kJ/mol)$$

Assuming complete conversion of HF to F_2 at the maximum HF flow-rate (200 cc/min ≈ 0.008 mole/min) as the worst case scenario, 0.004 mole/min F_2 is the maximum flow rate the scrubber should encounter. This would consume KI at a rate of 0.008 mole/min. At maximum capacity this provides an operating window for collecting samples of 20 minutes before the KI supply is exhausted. The rate of heat generation during this process is approximately 30 W according to the following calculation:

$$(0.004\ mole/min * 450\ kJ/mole) / 60\ sec/min\ =\ 0.03\ kJ/s\ =\ 30\ W$$

With a heat capacity of 4.2 J/g*K, under adiabatic conditions, the temperature of 750 g of solution will increase at a rate of approximately 0.6°C/min according to the following calculation:

$$30 \text{ J/s} * 60 \text{ sec/min} / (4.2 \text{ J/g*K} * 750 \text{ g}) = 0.6 \text{ K/min}$$

This temperature rise would be a concern only if the analytical scrubber is employed at maximum capacity for over three hours. It was shown previously that the reactant KI would be exhausted within 20 minutes, therefore sampling should be limited by the capacity of the reactant rather than concern for overheating the scrubber.

Sodium Fluoride Scrubbers

HF is removed from the process gas downstream from the reactor by passing the product gas through a double-ended stainless steel Hoke cylinder packed with approximately 1 kg sodium fluoride pellets. The following reaction is carried out to completion between NaF and HF to 100% conversion as long as sufficient unreacted NaF solid surfaces remain in the packing.

$$HF(g) + NaF(s) \rightarrow HNaF_2(s) \quad (\Delta H^\circ = -68.7 \text{ kJ/mol})$$

At the maximum flow rate of 0.008 mol/min HF, this reaction will generate approximately 9 W of heat in the cylinder according to the following calculation:

$$(0.008 \text{ mol/min} * 68.7 \text{ kJ/mol}) / 60 \text{ s/min} = 9.1 \text{ J/s}$$

Assuming a heat capacity for the packing of approximately 1 J/g*K, the temperature rise in the scrubber during operation at maximum flow rate would be approximately 0.5°C/min according to the following calculation:

$$(9.0 \text{ J/s} * 60 \text{ s/min}) / (1 \text{ J/g*K} * 1000 \text{ g}) = 0.5 \text{ K/min}$$

This rate of heating might be a concern under adiabatic conditions, however the cylinder walls provide an excellent heat sink for distributing heat to both the atmosphere and to the support structure on which the cylinder is mounted. Nonetheless some localized

melting of the NaF pellets was experienced during high capacity operation at the cylinder inlet.

According to manufacturer's specifications, under normal packing conditions NaF pellets absorb approximately 0.1 grams HF per gram NaF pellets (approximately 1/5 NaF mass is available for reaction near the pellet surface). For a 1 kg NaF scrubber, the HF capacity therefore is 100 g or 5 moles. At a maximum molar flow rate of 0.008 mole/min, the time to saturation would be 624 minutes (10.5 hours). This capacity insures that maximum flow rate operation may run continuously during the period of one standard 8-hour workday.

Once the NaF scrubber is saturated with HF, it is necessary to regenerate the NaF pellets. This is accomplished by wrapping the cylinder with heat tape and heating the cylinder at temperature in excess of 250°C while purging the cylinder with an inert nitrogen carrier gas to remove HF. HF is then neutralized in a KOH tank downstream from the NaF scrubber. Though the process of absorbing and volatilizing HF from NaF pellets is reversible, over time the pellets lose mechanical integrity and disintegrate into a powder. It was necessary to replace the NaF scrubbers approximately every 6 months.

Potassium Hydroxide Scrubber

The KOH scrubber was placed at the end of the process as a fail-safe to neutralize any HF or fluorinated gases that might escape the primary separation scrubbers and traps. It was also used during regeneration of NaF scrubbers and therefore its capacity must be sufficient to neutralize HF from a completely saturated NaF scrubber. The HF neutralization reaction in KOH solution is:

$$HF(g) + KOH(aq) \rightarrow KF(aq) + H_2O(l) \quad (\Delta H° = -98.7 \text{ kJ/mol})$$

For a maximum regeneration capacity of 5.0 moles HF and assuming complete HF removal from the scrubber distributed evenly over the course of 2 hours (experience has shown it actually takes much longer than this, closer to 20 hours), the heat generation rate in the KOH scrubber would be 68 W according to the following calculation:

$$(2.5 \text{ moles/h} * 98.7 \text{ kJ/mol}) / 3600 \text{ s/h} = 0.068 \text{ kJ/s} = 68 \text{ W}.$$

For a 2.7 gallon tank (10 L) containing 3.0 M KOH (15 wt.%) solution, the molar capacity for neutralization is 30 moles KOH. This is more than sufficient for neutralization of HF from a completely saturated NaF scrubber. The heat rise at 68 W is negligible in this size tank.

Electrochemical Cell

The material and energy balances in the reactor depend upon the relative conversion of HF to F_2 and OF_2, and to a lesser extent depend on side reactions such as water electrolysis and corrosion of electrodes. Assuming HF is oxidized only to F_2 and OF_2, the heat of reaction (q) can be expressed in terms of conversion to these species.

$$HF(g) \rightarrow 1/2\ F_2(g) + 1/2\ H_2(g) \quad (\Delta H° = 268.8 \text{ kJ/mole})$$

$$HF(g) + 1/2\ H_2O(l) \rightarrow 1/2\ OF_2(g) + H_2(g) \quad (\Delta H° = 424.1 \text{ kJ/mole})$$

$$q\ (J/s) = n_{HF}(mol/s)\ [\chi_{F2}\Delta H°_{F2} + \chi_{OF2}\Delta H°_{OF2}]$$

The cell reaction is endothermic in both cases. As a result, the cell must be heated to maintain a steady temperature at the electrodes. The consequences of a drop in cell temperature are condensation of HF and an increased cell voltage due to increased overpotential associated with decreased electrode kinetics at lower temperature.

Two methods are available for control of temperature in the cell. With water as the catholyte, the temperature of the cell may be controlled by preheating the catholyte

stream. An energy balance was used to determine the heat duty required to maintain steady temperature at the electrode. Estimates were based on a minimum catholyte flow rate of 10 cc/min, complete conversion of HF to F_2, and maximum HF feed rate of 200 cc/min. Detailed calculations modeling temperature distributions as a function of process flow rates and heat inputs are provided in the appendix. According to these calculations, the catholyte must be pre-heated to approximately 35°C to maintain the anode temperature at approximately 25°C. When potassium bifluoride molten salt is used as the catholyte, the cell body must be heated in excess of 80°C using cartridge heaters in order to prevent solidification of the molten salt.

Pressure Vessel and Conductivity Cell Design

A four-point-probe conductivity cell was constructed for use in a pressure vessel for simultaneous acquisition of membrane conductivity and vapor-liquid equilibrium data. Anhydrous HF and several HF-metal fluoride binary molten salt systems were each loaded in the vessel to a level immersing a Nafion® membrane loaded on the conductivity cell. The system was given time to equilibrate at several discrete temperature intervals where membrane conductivity and vapor pressure data were recorded.

Figure 3-11 displays a schematic of the pressure vessel and conductivity cell. The vessel was machined from Hastelloy steel. The conductivity cell was constructed from Teflon® parts with platinum wires insulated by polypropylene shrink-wrap. A process diagram for pilot plant facilities used to load and operate the pressure vessel is shown in figure 3-12. A process hazard report containing process details and operating procedures is on file with DuPont Chambers Works OSH office. Details from experiments using this facility are provided in Chapter 6 of this work.

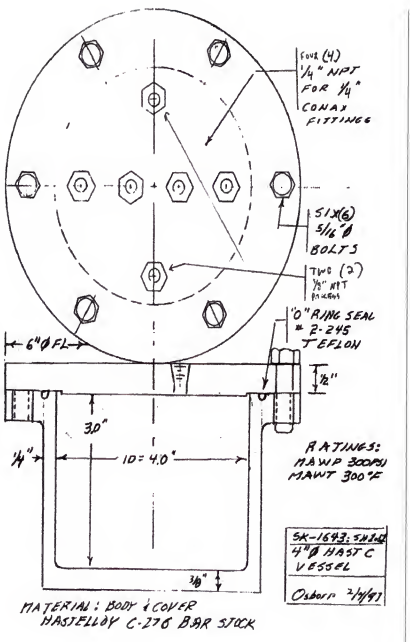

Figure 3-11. Schematic of Pressure Vessel with Conductivity Cell

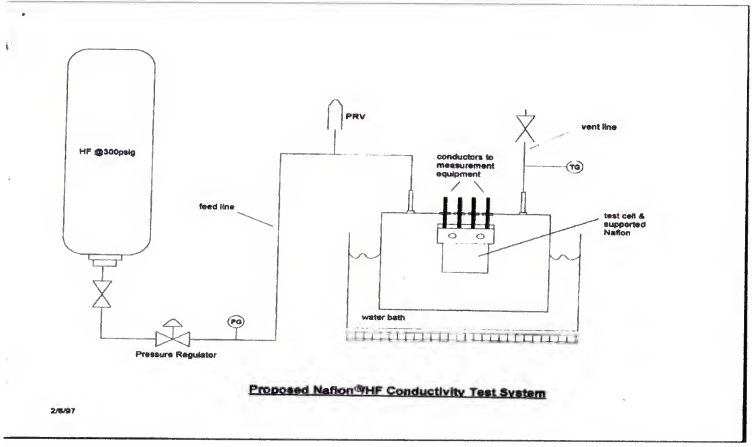

Figure 3-12. Process Flow Diagram for Pressure Vessel System

CHAPTER 4
DIRECT OXIDATION OF ANHYDROUS HF GAS

Introduction and Background

Fluorine is produced commercially by bulk electrolysis of KF·xHF molten salt ($1<x<4$).[1,2,44] Fluorine is used in several processes including uranium refining, direct fluorination reactions, and electronic gas syntheses. The lifetime of a fluorine cell is limited by corrosion of the carbon anode and other components such as the electrode-current collector connections.[2]

We are pursuing an alternative route for fluorine production by direct oxidation of anhydrous HF in a proton exchange membrane (PEM) reactor. This process is similar in concept to the anhydrous HCl process which utilizes a PEM reactor to electrolyze anhydrous HCl forming chlorine and hydrogen gas.[6,28,30] Advantages of the PEM reactor over conventional electrolyzers include higher current densities or production rates per unit cell cost, lower operating voltages due to reduction of the interelectrode gap distance, and better product gas separations leading to improved safety.

The thermodynamic potential for fluorine evolution is approximately 1.8 V more positive than the potential for chlorine evolution. Materials of construction used for an HF PEM reactor must be stable to higher voltages than materials used for an HCl PEM reactor. In aqueous media such as the water-swollen Nafion® membrane used in the HCl process, there is an inherent oxidative stability limit due to the oxygen evolution reaction. This limit may preclude an aqueous process for fluorine production as oxidation of water

to form oxygen occurs well below the thermodynamic fluorine evolution potential (1.23 V H_2O/O_2 vs. NHE, 2.85 V HF/F_2 vs. NHE).[38] Due to these constraints, HF electrolysis presents new challenges as compared with HCl electrolysis.

When water is completely removed from the Nafion® membrane, the ionic conductivity of the membrane drops so low as to be essentially unusable in room temperature electrochemical reactors. Fortunately, Nafion® membranes conduct cations when swollen with a variety of polar solvents.[7,45] The membrane solvent must not oxidize at high voltage or must generate fluorine as an oxidation product. Two logical choices are anhydrous HF and KF·xHF molten salt since both have the potential to produce fluorine as an oxidation product.

Electroorganic fluorination reactions in liquid anhydrous HF have been reported for cells employing a Nafion® membrane separated reactor.[46] To the best of our knowledge, our experiments represent the first efforts to produce fluorine in a PEM reactor.[52] Results are compared from experiments performed with a PEM reactor employing water, anhydrous HF, and KF·xHF molten salt as the membrane solvent introduced at the cathode and anhydrous HF gas fed to the anode.

Experimental

The PEM reactor utilized flow-through gas-diffusion-electrodes (GDE) separated by a Nafion® 115 membrane. A schematic of the reactor is shown in (chapter 3) figure 3-1. The effective area of the reactor was 1 cm^2. Load bearing heat-exchanger plates distributed compressive load on the cell and controlled cell temperature using isolated electric heating cartridges or cooling water. Tefzel®-graphite composite, monel and platinum current collector plates were machined with serpentine flow-fields for delivery

of reactants and removal of products. The GDE were either carbon cloth ELAT (E-TEK, Inc.), monel mesh (Cleveland Wire Cloth & Mfg. Co.) or platinum mesh. Catalyst layers were either coated on the GDE in ELAT form or laminated directly on the membrane surface in the form of a membrane-electrode-assembly (MEA). Each of the following catalysts was tested in ELAT form: platinum black, platinum supported on carbon, nickel supported on carbon, carbon black, and ruthenium dioxide. Platinum black was the only catalyst tested in MEA form.

Fabrication procedures used to construct MEAs were based on procedures developed at Los Alamos National Laboratory for catalyst-coated-membranes used in PEM fuel cells.[33] Several inks consisting of fuel cell grade platinum black catalyst (E-TEK, Inc.), Nafion® solution, and FC-40 (3M Co.) solvent were developed. The mass ratio of platinum catalyst to Nafion® solution binder was 12:1. The catalyst inks were milled to particle sizes on the order of 1 micron, solution cast on Kapton® films masked to the appropriate area, and slowly dried in a nitrogen-purged atmosphere at room temperature. The catalyst layers were hot pressed onto Nafion® 115 K^+ form membranes at 180°C and 800 psi for five minutes. For experiments with water or anhydrous HF as the membrane solvent, the MEA was acid exchanged in 1 M HNO_3 prior to use. Experiments with KF·xHF molten salt as the membrane solvent used a K^+ form MEA.

Attempts were made to employ a Cu/CuF_2 reference electrode by placing a copper wire between the gasket and the membrane in close proximity to the anode. This electrode appeared stable following sufficient equilibration time with an HF swollen membrane but did not give a reproducible potential with respect to a hydrogen evolving cathode. The drift in potential may depend on extent of corrosion or deposition at the

cathode and to a lesser degree concentration overpotential and impurities in the membrane. For consistency, all applied voltage and cell potential measurements presented are full cell voltage. Some half-cell impedance spectra are presented which employed this reference electrode.

Three modes of reactor operation were employed with different combinations of feed streams:

1) Deionized water cathode feed and anhydrous HF gas anode feed
2) Anhydrous HF gas anode and cathode feeds
3) KF·xHF molten salt cathode feed and anhydrous HF gas anode feed

Deionized water and anhydrous HF feed streams flowed continuously through the current collector flow-fields at flow rates from 10 to 200 cc/min. Anhydrous HF gas was delivered by heating a technical grade anhydrous HF gas cylinder (Air Products Co.) to generate pressure driven flow regulated by a series of mass-flow-controllers (Tylan Co.).

KF·xHF molten salt was prepared *in situ* by equilibrating KHF_2 salt with 1 atm. anhydrous HF gas in a mixing cylinder at room temperature. The resulting liquid was drained into the cathode flow-field by gravity feed within a Teflon® PFA reservoir. A fairly dilute composition by industrial standards was used in order to operate at ambient temperature and pressure. In a separate experiment the concentration of KF equilibrated with HF at room temperature which results in 1 atm. vapor pressure was determined to be approximately 2.5 mole/kg (KF·xHF; x=20). The KF concentration of the molten salt increased with time as HF vapor was entrained in an overhead nitrogen purge. Bubbling anhydrous HF gas through the reservoir periodically restored the original concentration.

A scrubber sequence was installed for separation and neutralization of the product streams. A process flow diagram is shown in (chapter 3) figure 3-2. Scrubbers packed with NaF·xHF pellets (Engelhard Co., x=1 as received) absorbed HF. These scrubbers were activated and periodically regenerated by heating to 200°C and purging with nitrogen for 24 hours. To quantify F_2 and OF_2 content, the anode product stream bubbled through a 0.2 M KI solution with 0.1 M KH_2PO_4 buffer. A scrubber packed with alumina pellets was used to remove fluorine by conversion to oxygen when the KI solution was bypassed. In the course of experiments described in chapter 5 of this manuscript, product samples were periodically injected into a gas chromatograph with mass selective detector (Hewlett Packard 6890/5973 series) for analysis of CF_4 and other fluorinated gases. Any OF_2 formed as a side product by electrolytic fluorination of adventitious water was absorbed in a gum rubber trap.

Experiments were conducted at temperatures ranging from 5°C to 80°C. A data acquisition system logged the following data: flow rates, process temperatures, reactor pressure, cell voltage, and current. Cell resistance measurements were obtained using a Hewlett Packard model 4338B milliohmmeter. Electroanalytical experiments were performed using a Solartron model 1287 potentiostat, a Solartron model 1260 frequency response analyzer, and a Xantrax model HPD power supply.

Results and Discussion

Aqueous Operation--Deionized Water Catholyte

Direct oxidation of anhydrous HCl gas in a PEM reactor has been demonstrated as a viable commercial process for recovery of chlorine from HCl waste.[30] In this reactor

oxygen evolution kinetics are suppressed as chlorine is evolved preferentially on RuO_2 catalyst. No efforts are reported in the literature investigating fluorine evolution on RuO_2 electrodes. Commercial fluorine cells use various forms of carbon anodes. Pure metals and metal alloys have been studied extensively, and the only metals that develop reasonably conductive surface films and exhibit some degree of passivation during fluorine evolution are platinum, nickel and some nickel alloys (monel).[47,48]

Addition of water amplifies corrosion issues. No electrode material has been reported as stable for electrolysis in hydrofluoric acid. Depending on water concentration, three gas phase products are formed during bulk electrolysis of hydrofluoric acid: oxygen, oxygen difluoride (OF_2), and ozone. Fluorine is formed as an intermediate product at low water concentration but it immediately reacts with water in the bulk solution yielding O_2 and OF_2.[49]

Despite evidence suggesting fluorine can not be generated and electrode corrosion would be problematic, experiments were conducted for HF electrolysis as a direct analog to the anhydrous HCl PEM electrolyzer with water as the membrane solvent. Platinum, carbon, ruthenium dioxide and nickel were each tested as potential catalysts on ELAT gas diffusion anodes. Platinum, Tefzel®-graphite composite and monel were tested as current collector materials.

Oxygen was the primary gas-phase anodic product for all cells run with deionized water fed to the cathode and anhydrous HF gas fed to the anode. Anode product streams bubbled through a KI scrubber liberated no iodine indicating negligible production of F_2, OF_2 or O_3. Steady-state current-voltage curves for two cells are displayed in figure 4-1. Both cells had an acid form Nafion® 115 membrane separator and platinum black

catalyst-coated ELAT electrodes with 2 mg/cm^2 catalyst loading. The first cell employed Tefzel®-graphite composite current collector plates. The second cell employed a platinum anode plate and monel cathode plate.

The mass-transfer-limited current approached 2.3 kA/m^2 in the cell with Tefzel®-graphite composite current collectors. The cell with a platinum anode current collector reached a mass-transfer-limited current of 25 kA/m^2. The increase in effective current is likely due to an increase in active area. Water from the Nafion® membrane condensed in the anode flow-field of both cells as hydrofluoric acid and provided an ionic pathway to the current collector. Slugs of liquid were observed periodically emerging from the anode outlet. The applied voltage ($E < 3$ V) did not exceed the overvoltage required for oxygen evolution on the Tefzel®-graphite composite current collector therefore no additional electrode area was active beyond the ELAT for this cell. The applied voltage was sufficient for oxygen evolution on platinum. Exposure of the platinum current collector to hydrofluoric acid resulted in additional active electrode area beyond that available in the ELAT.

Substantial corrosion occurred in both cells. The ELATs flaked apart on disassembly and the catalyst layer adhered to the membrane. The Tefzel®-graphite composite anode current collector exhibited pitting damage and mechanical collapse of the flow-field. The platinum anode current collector retained its mechanical integrity but was mildly tarnished with an orange surface precipitate.

Two control experiments were conducted to determine whether HF contributed in any way to the overall current in the reactor. In a cell of identical construction with a platinum anode current collector, deionized water was fed to the cathode and nitrogen

was purged through the anode, then deionized water was fed to both cathode and anode. Figure 4-2 compares steady-state current voltage data obtained from cells with anhydrous HF gas, nitrogen gas, and deionized water anode feed streams. Tafel slopes were nearly identical in each case at approximately 1180 mV/decade. This Tafel slope is not typical for oxygen evolution on a pristine platinum metal surface. The expected Tafel slope for oxygen evolution on platinum in aqueous media is 58 mV/decade.[50]

A number of factors may contribute to additional overvoltage in PEM reactors using gas diffusion electrodes that can not be distinguished by steady-state polarization data alone. However by comparing Tafel slopes we conclude that the reaction kinetics for oxygen evolution was similar for each type of anode feed. The only difference was the magnitude of mass-transfer-limited current. The mass-transfer-limited current was 2.0 kA/m^2 with nitrogen anode feed, 3.5 kA/m^2 with deionized water flowing through the anode and 25 kA/m^2 with anhydrous HF gas anode feed. With no change in Tafel slope and no detection of F_2 or OF_2, condensation of hydrofluoric acid activating additional electrode area best explains the increased current for the cell with anhydrous HF gas anode feed and a platinum anode current collector.

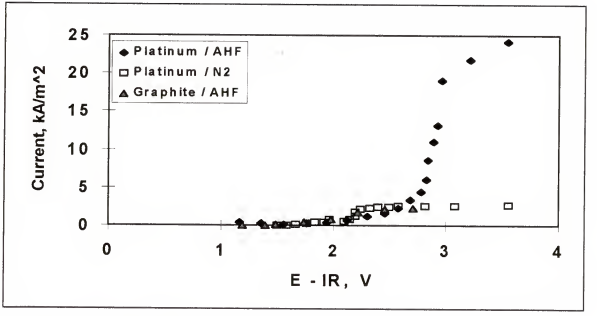

Figure 4-1. Steady-state polarization data from two cells with different anode current collector materials. Deionized water purged the cathode and nitrogen or anhydrous HF purged the anode.

Anhydrous Operation--Anhydrous HF Gas Catholyte

Previous experiments demonstrated that substantial current passed through the Nafion® membrane with water as the membrane solvent and anhydrous HF gas purging the anode. All of the current was a result of water electrolysis and corrosion. The next step was to remove water from the system and replace it with anhydrous HF. Several cells were constructed for evaluation with anhydrous HF gas purging both the anode and cathode. Five different catalyst materials were tested in cells with carbon cloth ELAT gas diffusion electrodes: platinum black, carbon black, platinum supported on carbon, nickel supported on carbon, and ruthenium dioxide. Cells with platinum black MEA were also tested.

The Nafion® membrane was dried in a nitrogen-purged vacuum oven prior to assembly or *in situ* by purging nitrogen through the anode and cathode flow-fields overnight. In both cases the cell resistance decreased from greater than 1 megaohm to less than 1 ohm shortly following initiation of anhydrous HF feed to both sides of the cell. After extended pre-electrolysis at 2.5 V for removal of the last traces of water, the bulk impedance increased slightly to 1.7 ± 0.5 ohmcm^2 (an average of 8 cells with 0.24 ohmcm^2 standard deviation). Steady-state open-circuit bulk impedance measurements for several cells are tabulated in table 4-1. During the course of electrochemical experiments that included both static and dynamic operation at potentials exceeding 3 V, the impedance response of each cell exhibited subtle changes consistent with formation of fluoride species at the catalyst surface. The bulk impedance increased in each cell and a charge-transfer loop appeared better resolved at moderate frequencies ($\omega > 1$ Hz). Data obtained from a typical cell presented in figure 4-3 compare the initial open-circuit

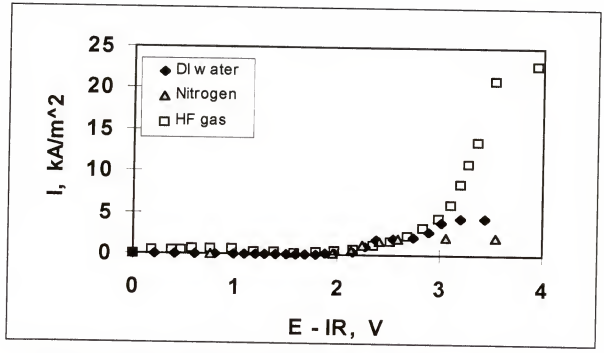

Figure 4-2. Steady-state polarization data for different anode feed streams from a cell with platinum black ELAT and platinum anode current collector

impedance response and the open-circuit impedance response approximately 30 minutes after termination of potentiostatic operation at 5.0 V.

The Arrhenius plot displayed in figure 4-4 shows the temperature dependence of bulk impedance for an anhydrous HF humidified PEM cell with a platinum black MEA before and after the last traces of water were removed by bulk electrolysis. Prior to electrolysis, the bulk impedance remained reasonably low ($R < 5$ ohm·cm^2) at temperatures as high as 50°C indicating good proton conductivity. Following electrolysis, the upper temperature limit for low bulk resistance (arbitrarily chosen as 5 ohm·cm^2) decreased to approximately 35°C. The boiling point of anhydrous HF is 19°C, however substantial boiling point elevation likely occurs due to the presence of fixed sulfonate groups within the pores of the membrane. Prior to electrolysis, residual water also provided additional boiling point elevation and proton conductivity.

Table 4-1. Bulk impedance of PEM reactors following pre-electrolysis

Catalyst, Electrode	**Z(bulk): ohm·cm^2** **(-) $AHF_{(g)}$ / $AHF_{(g)}$ (+)**	**Z(bulk): ohm·cm^2** **(-)$KF{\cdot}xHF_{(l)}$ / $AHF_{(g)}$ (+)**
Pt black, ELAT	1.4	-
Pt black, ELAT	1.6	1.3
Pt/C, ELAT	2.3	1.1
Ni/C, ELAT	2.0	1.2
Pt black, MEA	1.8	0.9
Pt black, MEA	1.6	1.2
Pt black, MEA	1.7	1.4
RuO_2, ELAT	1.5	-

Current was not sustained in any of the cells tested during potentiostatic operation up to 60 V. Transient current was observed due to electrolysis of residual water retained in the membrane and corrosion of some of the catalyst materials. A typical cyclic voltammogram for these cells is demonstrated in figure 4-5. All cells tested exhibited a broad irreversible oxidation peak between 1.5 and 2.5 V which may be attributed to bulk electrolysis of residual water coupled in some cases with corrosion of carbon catalyst support. This peak decreased in magnitude on repeated cycling and ultimately disappeared following extended potentiostatic operation. Other peaks observed in various cells were not as reproducible with peak potentials depending on catalyst type and extent of cycling. Quasireversible oxidation peaks were observed at potentials less than 1.0 V, most noticeably in cells with platinum catalyst.

Cells with ruthenium dioxide catalyst exhibited sustained corrosion for several minutes above 1.0 V. At room temperature, cells employing carbon cloth ELAT GDE sustained corrosion current above 2.3 V for longer duration ranging from several minutes to nearly an hour. This may be attributable to activation of additional electrode area within the carbon cloth GDE due to condensation of HF and possibly more substantial catalyst oxidation. Figure 4-6 displays quasi-steady-state current-voltage curves obtained from cells at room temperature with platinum black, nickel, and ruthenium dioxide catalyst coated ELAT, and from a cell with platinum black ELAT at 50°C. Current was not sustained for substantial duration at any potential. Each data point in figure 4-6 represents current recorded after a few minutes at a fixed voltage when the decay slowed to less than 0.1 mA/s. At 50°C no condensation was observed in the reactor outlets. The absence of corrosion current in the cell operated at 50°C is consistent with the premise

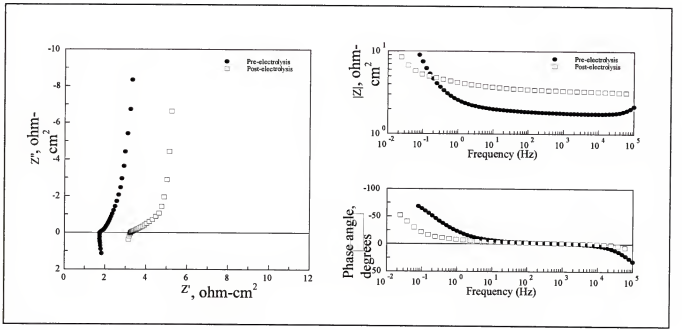

Figure 4-3. Open-circuit impedance spectra obtained during operation of PEM reactor with anhydrous HF gas purged anode and cathode: 1 cm² Pt black MEA cell with carbon paper GDE.

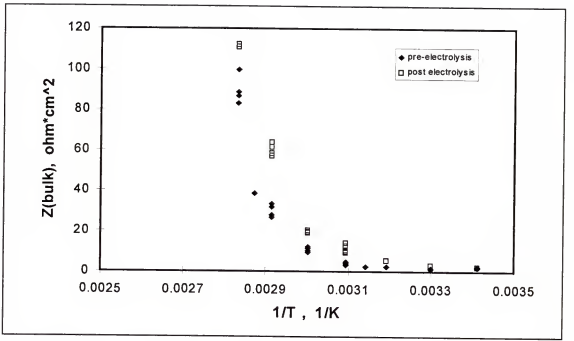

Figure 4-4. Arrhenius plot for bulk impedance of PEM reactor with anhydrous HF gas purged anode and cathode: 1 cm^2 Pt black MEA cell with Monel mesh GDE.

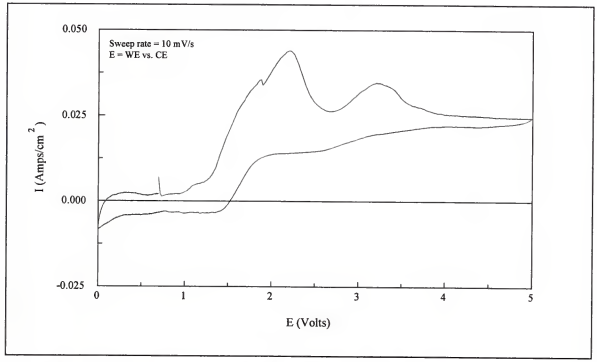

Figure 4-5. Cyclic voltammogram obtained from a cell with 40 cc/min. anhydrous HF gas purging both the anode and cathode at 20°C. Electrodes were 1 cm^2 ELAT with platinum black catalyst loaded at 2.0 mg/cm^2

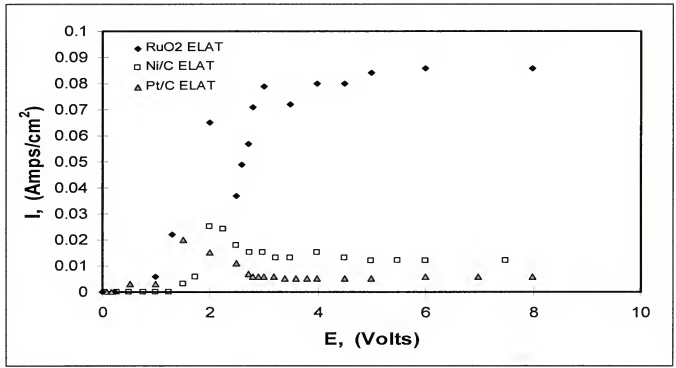

Figure 4-6. Psuedo-steady-state polarization data for three cells with different ELAT catalyst run with anhydrous HF gas purging the anode and cathode

that condensation in the ELAT at room temperature allows activation of additional electrode area promoting corrosion of the carbon cloth GDE.

Based on these results we conclude that anhydrous HF gas was not directly oxidized at the anode to yield fluorine on any of the catalysts evaluated with an anhydrous HF swollen membrane. The bulk resistance of each cell was low indicating that proton conductivity was not limiting the process. Two hypotheses may explain this result. Either transport of an essential reacting species to the catalyst surface is severely restricted by the membrane and catalyst binder, or the fluorine evolution reaction will not proceed at a substantial rate on any of the catalysts tested.

Anhydrous Operation--KF·xHF Molten Salt Catholyte

Current was not sustained with anhydrous HF swelling the Nafion® membrane. Flooding the cathode with KF·xHF molten salt was expected to fully saturate the membrane with solvent and provide additional conductivity in the form of a supporting electrolyte. The same types of cells used for evaluation with anhydrous HF purging both the anode and cathode were tested with KF·xHF molten salt flooding the cathode. Under stagnant non-operating conditions, the anode of each cell was purged with nitrogen. Steady-state flow of anhydrous HF was established through the anode prior to most electrochemical experiments. A few experiments employed a nitrogen anode feed stream.

Platinum, nickel, and carbon have all been demonstrated as fluorine evolving electrodes for bulk electrolysis of MF·xHF molten salts in reactors with no true separator between the anode and cathode. The reacting species is HF_2^- for fluorine evolution in such reactors.[44,51] The Nafion® membrane separator employed in the PEM reactor is an

anion exclusion membrane. Production of fluorine by bulk electrolysis of KF·xHF molten salt was expected to be negligible with the molten salt introduced at the cathode due to mass transport restrictions of the reacting species HF_2^-. In this case, current should be sustained only by direct oxidation of HF from the gas phase or by oxidation of catalyst or cell components.

The resistance of each cell with anhydrous HF gas purging the anode flow-field and KF·xHF molten salt flooding the cathode was again less than 1 ohm but not substantially lower than that observed in cells with anhydrous HF gas purging both anode and cathode flow-fields. The bulk impedance increased slightly to approximately 1.2±0.3 ohm·cm^2 (an average of six cells with 0.17 ohm·cm^2 standard deviation) after extended pre-electrolysis at 2.5 V for removal of residual water. Switching the anode gas feed from HF to N_2 increased the cell resistance approximately two orders of magnitude. This indicates a partial depletion of solvent at the anode-membrane interface resulting in decreased conductivity.

Steady-state open-circuit bulk impedance measurements for several cells are tabulated in table 4-1. Following potentiostatic operation, the impedance response was again altered yielding higher bulk resistance and resolution of a charge transfer loop at moderate frequencies. In time the impedance response returned to its original state. Such recovery was not observed with anhydrous HF gas purging the cathode. This observation is consistent with formation of a fluoride film at the anode that dissolves in KF·xHF molten salt. Figure 4-7 compares a typical anode half-cell open-circuit impedance response for a cell with a platinum black MEA. Spectra were obtained prior to and following loading of KF·xHF molten salt at the cathode before potentiostatic operation,

shortly following cut-off of applied voltage, and approximately 45 minutes following the return to steady-state open-circuit conditions.

Figure 4-8 displays linear current sweep data for three cells. One cell employed platinum black catalyst coated ELAT electrodes with KF·xHF molten salt fed to the cathode. The other two cells were constructed with a platinum black catalyst MEA with either KF·xHF molten salt or anhydrous HF gas fed to the cathode. Each cell had a mass-transfer-limited current less than 0.5 kA/m^2. The cells that contained KF·xHF molten salt exhibited transient activity at potentials greater than 3 V that may indicate fluorine evolution or catalyst fluorination.

Current was not sustained in any of the cells tested for more than a few minutes. The maximum current densities observed during start-up were less than 1.0 kA/m^2. Anode product streams bubbled through an aqueous KH_2PO_4 buffered KI scrubber liberated no iodine. The coulometric fluorine equivalent for the amount of current passed, however, did not reach the lower detection limit for iodometric titration of the KI scrubber. Open-circuit potential decay following operation at 6 V is exhibited in figure 4-9 for a cell with platinum black ELAT operating with KF·xHF molten salt fed to the cathode. Changes in slope are observed initiating at 2.9 V and 2.4 V that indicate two separate oxidation processes occurred with equilibrium potential greater than 2.0 V. A second substantial potential decay is evident initiating at approximately 2.0 V. Potential subsequently decayed slowly ultimately approaching an equilibrium potential at less than 1.0 V beyond the time scale of figure 4-9.

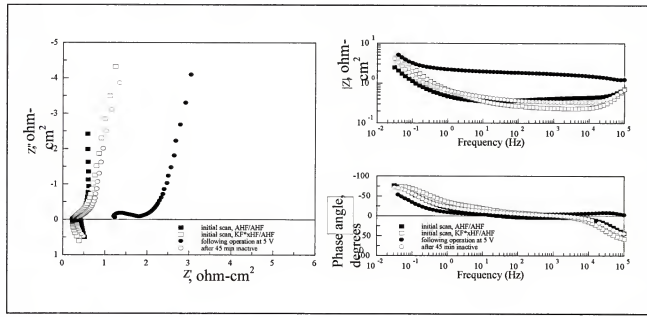

Figure 4-7. Open-circuit anode half cell impedance spectra obtained over various stages of operation: 1 cm² platinum black MEA, carbon paper GDE

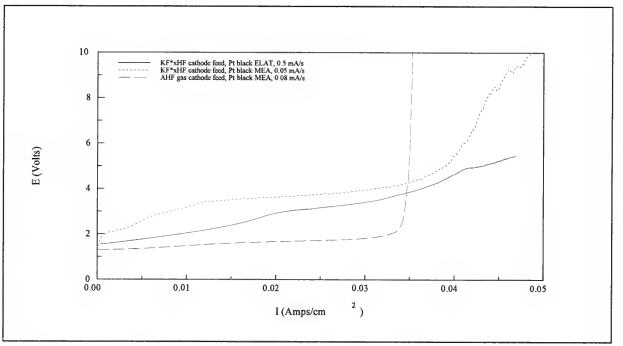

Figure 4-8. Linear current sweeps obtained from cells with different cathode feeds and electrode type. 50 cc/min. anhydrous HF gas anode feed for each cell.

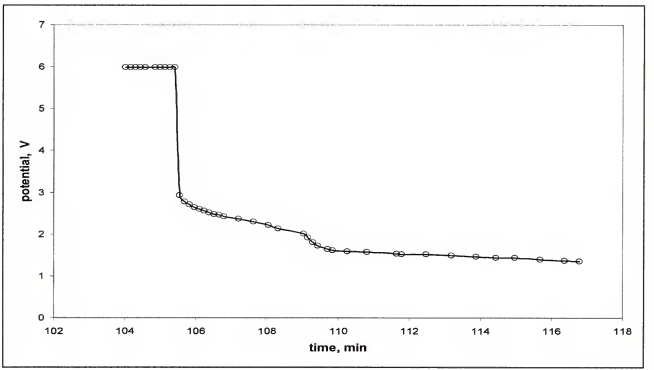

Figure 4-9. Open-circuit potential following operation at 6 V with KF•xHF molten salt cathode feed and anhydrous HF gas anode feed. 1 cm^2 Pt black ELAT electrodes

Interpretation of Impedance Spectra

A breakdown of the various cell impedance components is helpful to better understand charge transfer limitations in the PEM reactor. Equivalent circuit models of impedance spectra are commonly used to develop electrical analog circuits with elements that represent physical parameters for electrochemical cells. Interpretation of such models is complicated in PEM reactors due to non-uniformity of properties in the catalyst layer and membrane.[34] However, for the purpose of distinguishing charge-transfer processes and quantifying some general bulk properties, equivalent circuit analysis can provide some insight.

Three equivalent circuit models composed of various combinations of passive circuit elements listed below were fit to full-cell and anode half-cell open-circuit impedance spectra. A fourth model was used to fit spectra obtained during operation at biased potential. Circuit diagrams are shown in figure 4-10 for each model. Figures 4-11 and 4-12 respectively present open-circuit and biased-potential impedance spectra derived from model simulations for a typical cell. Model parameters are presented in table 4-2. The cell employed a platinum black MEA with a Cu/CuF_2 reference electrode adjacent to the anode. KF·xHF molten salt flooded the cathode and anhydrous HF gas was fed to the anode.

Model 1: Resistor in series with a capacitor

Without pinpointing the source of capacitance in the cell, it may be attributed to an overall geometric cell capacitance. The capacitance is modeled in series with the bulk resistance of the cell. The impedance spectrum generated from such a model represents the expected response for an electrolysis cell under open-circuit conditions when the

main reactions are inactive and side reactions are nonexistent. Full-cell and anode half-cell impedance spectra were fit to this model.

Model 2: Resistor in series with a parallel R-C combination

The parallel R-C combination represents an interface between the electrolyte and a single electrode. The R-C combination is modeled in series with the bulk resistance of the cell. One might expect this model to describe adequately an electrolysis cell under open-circuit conditions with at least one side reaction occurring at a finite rate. This model applies to cells in which the interfacial impedance of one electrode greatly exceeds that of the other or for half-cell measurements employing a reference electrode. Full-cell and anode half-cell impedance spectra were fit to this model.

Model 3: Resistor in series with two parallel R-C combinations

Each parallel R-C combination represents the interface between electrolyte and an electrode. The interfaces for both electrodes are modeled in series with the bulk resistance of the cell. This model applies to cells in which the interfacial impedance of each electrode is of the same order of magnitude. Full-cell impedance spectra were fit to this model. Prior to application of applied voltage, symmetric cells should fit this category. Following electrolysis, impedance at the anode exceeds that of the cathode due to formation of surface films. These surface films may also be represented by an additional R-C element in series with other elements. The order of elements in series is inconsequential to the model therefore this model may also represent impedance at a single electrode with two charge transfer interfaces: electrode-film, and film-electrolyte. Half-cell impedance spectra were fit to this model. Distinction between interface types

can be made based on the order of magnitude of capacitance. Capacitance of surface films should be several orders of magnitude less than that of the electrode.

Model 4: Resistor in series with multiple R-C combinations in a parallel network

This model represents multiple charge transfer phenomena occurring at the anode. Sources of charge transfer at biased potential may be due to oxidation of catalyst, corrosion of the GDE and bulk electrolysis of HF, KF·xHF and residual water. Each charge transfer process may be represented by an R-C combination. Independent charge transfer processes each contribute to cell impedance as parallel pathways. Bulk resistance and the anode-electrolyte interface contribute to cell impedance in series with the parallel network. This model was developed by adding R-C elements to the parallel network until further additions yielded negligible contributions from new circuit elements and offered no substantial improvement to the quality of fit. For full-cell impedance spectra at biased potential, an additional R-C element in series representing the cathode is not employed on the assumption that the hydrogen evolution reaction offers no substantial contribution to cell impedance. The model was fit to impedance spectra obtained at biased potential. Current decayed to less than 0.01 kA/m^2 prior to obtaining each spectrum. The biased potential model parameters presented in table 4-2 were all fit to anode half-cell impedance spectra.

The 2.9 V arrest potential observed during open-circuit potential decay, the mass-transfer-limited low frequency impedance response at bias voltage greater than 3 V, and the activity observed above 3 V are all consistent with the following hypothesis. A supply of HF_2^- is initially available to the anode with liquid KF·xHF saturating the membrane. When the fluorine evolution potential is exceeded, HF_2^- is consumed and can

not be replaced at an appreciable rate due to severe mass-transfer limitations. The Nafion® membrane is a cation exchange membrane that effectively restricts transport of anions by electrostatic repulsion. A logical way to test this hypothesis was to make HF_2^- continuously available to the anode without interference from the Nafion® membrane by substituting a porous PTFE film in place of the Nafion® membrane or by flooding the anode with KF·xHF molten salt. Results from such experiments are presented in chapter 5 of this manuscript describing bulk electrolysis of KF·xHF molten salt in a PEM reactor.

Conclusions

A direct analog to the PEM HCl electrolyzer was ineffective for electrolysis of anhydrous HF. Neither anhydrous HF gas nor liquid anhydrous HF could be oxidized directly to yield fluorine under the conditions investigated. Good proton and potassium ion conductivity was observed in HF-swollen Nafion® 115 membranes indicating that cation conductivity was not limiting the process. Based on an analysis of potential decay and impedance data, it is believed that transport of HF_2^- through the perfluorinated ionomer solution catalyst binder and membrane separator was restricted by electrostatic repulsion and was not sufficient to sustain fluorine evolution at the catalyst.

Table 4-2. Equivalent circuit elements fit to PEM reactor impedance spectra

(R: $\Omega \cdot cm^2$, C: mF)

Model	State	R_{bulk}	R1	C1	R2	C2	R3	C3
1	Open circuit Pre-electrolysis	0.886	-	88.2	-	-	-	-
2	Open circuit Pre-electrolysis	0.884	54.0	87.3	-	-	-	-
3	Open circuit Pre-electrolysis	0.852	115.1	103.2	0.677	90.2	-	-
4	3 V bias voltage $i < 0.01$ kA/m^2	4.96	18.3	0.0919	16.8	6.24E-4	10.7	9.54E-4
4	4 V bias voltage $i < 0.01$ kA/m^2	8.36	25.1	2.59	36.0	6.93E-5	46.5	2.98E-4
4	5 V bias voltage $i < 0.01$ kA/m^2	6.58	184	1.04	178	5.59E-5	115	1.26E-6
1	Open circuit Post-electrolysis	1.84	-	838	-	-	-	-
2	Open circuit Post-electrolysis	1.80	7.54	753	-	-	-	-
3	Open circuit Post-electrolysis	1.39	9.61	796	0.596	0.138	-	-

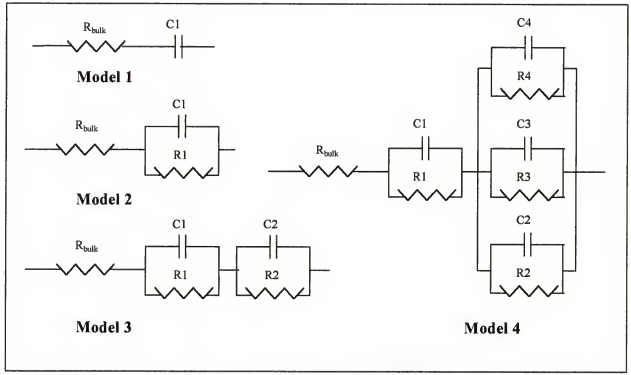

Figure 4-10. Equivalent circuit models used to fit PEM reactor impedance spectra

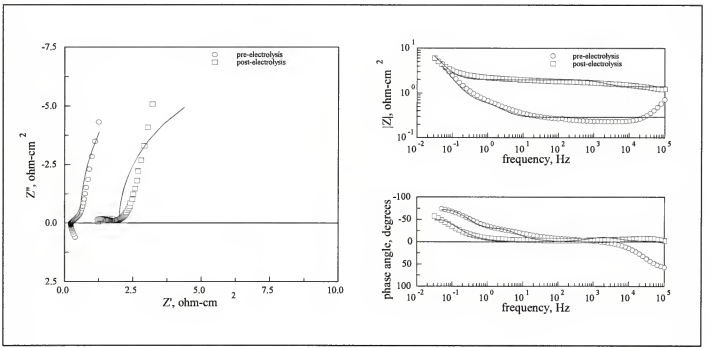

Figure 4-11. Equivalent circuit model 3 fit to anode half-cell open-circuit impedance spectra obtained from a cell with a platinum black MEA. Solid lines indicate simulated model fit to experimental data

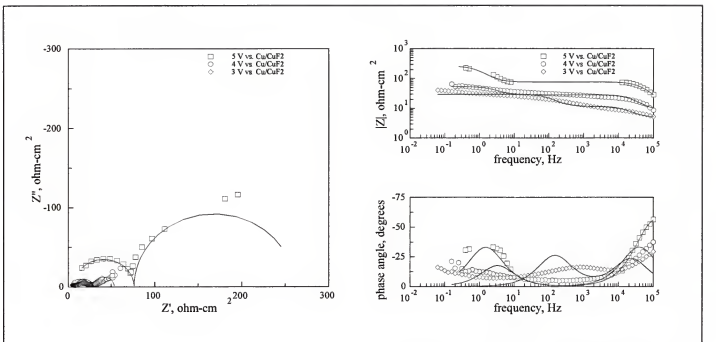

Figure 4-12. Equivalent circuit model 4 fit to anode half-cell open-circuit impedance spectra obtained at biased potentials from a cell with a platinum black MEA. Solid lines indicate simulated model fit to experimental data

CHAPTER 5
BULK ELECTROLYSIS OF KF·XHF MOLTEN SALT

Introduction and Background

This process is similar in concept to the anhydrous HCl recycle process which utilizes a PEM reactor to electrolyze anhydrous HCl directly from the gas phase forming chlorine and hydrogen gas.[6,28,30] Previous efforts to generate fluorine gas in a proton-exchange-membrane (PEM) reactor by direct oxidation of anhydrous HF gas are described in chapter 4. We concluded that HF can not be oxidized directly from the gas phase and that Nafion® 115 membranes exhibit good cation conductivity when swollen with anhydrous HF.[52] The reactant necessary for fluorine evolution is HF_2^-. An HF_2^- solvating medium for which stability has been established in the presence of fluorine is HF in the form of KF·xHF molten salt. Commercial reactors generate fluorine by bulk electrolysis of KF·xHF molten salt ($1<x<4$).[1-5] In the PEM reactor, transport of HF_2^- is hindered by electrostatic repulsion in Nafion® 115 membranes. HF_2^- must be provided directly to the anode to generate fluorine in a PEM reactor.[52]

Two mechanisms were evaluated for delivery of HF_2^- to the anode. It is desirable to employ a gas-purged anode in order to prevent activation of the interior of the gas-diffusion-electrode (GDE) and the current collector plate. A porous Teflon® membrane separator was employed in a reactor with KF·xHF molten salt flooding the cathode and either anhydrous HF gas or nitrogen purging the anode. HF_2^- was delivered to the anode surface in contact with the KF·xHF molten salt-saturated membrane. It is also desirable

to employ an ionomeric membrane separator. These two desires can not be met simultaneously. When a cation exchange membrane separator is employed, HF_2^- can only be delivered to the anode by flooding the anode with KF·xHF molten salt. A Nafion® 115 membrane separator was employed in a reactor with KF·xHF molten salt flooding both the anode and cathode.

Advantages envisioned by employing flow-through GDE in a fuel cell type PEM reactor can not be realized when the anode feed is switched from anhydrous HF gas to KF·xHF molten salt. Gas phase electrode kinetics no longer applies and the current collector is exposed to electrolyte. Some benefit with respect to process safety may be realized through the use of an ionomeric membrane separator. The process is not radically different than existing commercial reactors that produce fluorine by bulk electrolysis of KF·xHF molten salt. Fluorine production in an electrochemical membrane reactor by bulk electrolysis of KF·xHF molten salt is described in this chapter.

Experimental

The reactor, electrolysis unit, and procedure for preparation of KF·xHF molten salt are described in chapters 3 and 4. Three types of cell configuration were evaluated. One cell configuration consisted of platinum catalyst-coated ELAT separated by three layers of porous Teflon® membrane each having 2 mil thickness. KF·xHF molten salt flooded the cathode and either anhydrous HF gas or nitrogen flowed through the anode. Another cell configuration employed a platinum catalyst-coated membrane-electrode-assembly (MEA) with monel mesh GDE. KF·xHF molten salt flooded both the cathode and the anode. The reactor was scaled up employing 9 cm^2 electrodes to allow molten salt to drain freely in and out of the reactor. The third cell configuration employed

platinum catalyst-coated ELAT with a Nafion® 115 K^+ membrane separator. The reactor was again scaled up to 9 cm^2 and KF·xHF molten salt flooded both the cathode and the anode.

MEAs were fabricated with fuel cell grade platinum black catalyst laminated on a Nafion® 115 K^+ membrane according to procedures described in chapter 4. Two types of catalyst binder were used in different MEA cells. Nafion® solution catalyst binder was used to promote cation conductivity in the catalyst layer. Teflon® AF solution catalyst binder was used to determine whether catalyst utility would improve if transport restrictions imposed by the Nafion® solution catalyst binder on the reactant anion HF_2^- were eliminated.

Modifications were made to the procedure for quantitative analysis of product gas following the porous membrane reactor experiments. A 5.0 M KOH solution analytical scrubber was installed in series preceding a 0.1 M KH_2PO_4 buffered 0.2 M KI solution analytical scrubber. Fluoride ion concentration in the KOH scrubber was determined by EMF measurement. Iodine concentration in the KI scrubber was determined by titration with 0.1 M $Na_2S_2O_3$ in the presence of starch indicator.

Standards simulating KOH scrubber concentrations were generated ranging from 10 to 1000 ppm fluoride by mixing appropriate amounts of KOH solution with NaF standard (Orion Research, Inc.). The KOH scrubber samples and standards were each diluted 9:1 with 4 M potassium acetate pH 5 buffer and an equal volume of TISAB II buffer (Orion Research, Inc.). A fluoride ion selective combination electrode (Orion Research, Inc.) was used to measure EMF of the scrubber samples and standards. The

fluoride concentration of samples was calculated by linear interpolation between standard measurements on a logarithmic scale.

Calibrations of the KI scrubber with mixtures of fluorine and nitrogen revealed that iodine was not liberated in quantities stochiometric to fluorine. Error exceeded 10% unaccounted fluorine and depended on flow rate and nitrogen dilution. An excess of 99% recovery of fluorine was achieved for all calibrations with KOH and KI scrubbers in sequence. Depending on flow-rate and dilution in nitrogen, some fluorine escaped the KOH scrubber in the form of OF_2 that liberated iodine in the KI scrubber. The lowest ratio of fluorine quantified from the KOH scrubber vs. fluorine quantified from the KI scrubber was 20:1 from a 50 vol.% mixture of fluorine in nitrogen at 200 cc/min.

Results and Discussion

Operation with a Porous Teflon® Membrane Separator

Experiments for cells with a porous Teflon® membrane separator were designed to characterize the fluorine evolution reaction on a fuel cell grade platinum black catalyst-coated ELAT. Fluorine evolution on bright platinum metal has been demonstrated as an autocatalytic reaction.[51] Dissolution of platinum during anodic operation precludes its use in commercial fluorine cells.[1,47,51] The same was anticipated for platinum black catalyst, with the rate of dissolution retarded by the Nafion® solution binder employed in the ELAT catalyst layer. We found instead that the ionomeric nature of the catalyst binder prevented the fluorine evolution reaction from occurring on the catalyst at all. Therefore the rate of catalyst dissolution was minimal, but catalyst utilization was poor to nonexistent.

Cells were constructed in the same manner described in chapter 4. Fuel cell grade platinum black catalyst coated ELAT (E-tek, Inc.) were employed for both the anode and cathode. The separator was comprised of three 2 mil thick sheets of porous Teflon® film (DuPont). KF·xHF molten salt was drained into the cathode reservoir. The anode was continuously purged with either nitrogen or anhydrous HF gas. Electroanalytical experiments performed on one specific cell are detailed herein.

Figure 5-1 displays cyclic voltammograms obtained from one cell. The first scan shows a broad peak with poor resolution between 1.0 V and 3.8 V. This peak was generated by the combined transient currents attributed to catalyst oxidation from 1.0 V to 1.5 V, oxygen evolution above 1.5 V, and catalyst fluorination between 2.5 V and 3.0 V. Sustained fluorine evolution is observed at potentials greater than 4.0 V. A reversible couple around 1.5 V is better resolved on subsequent scans giving further evidence for catalyst oxidation and reduction. The contribution of oxygen evolution is greatly diminished in these scans indicating nearly complete removal of water from the molten salt. Again the onset of fluorine evolution appears to occur near 4.0 V. These potentials may be roughly interpreted as potential vs. NHE since the reference electrode was shorted to the hydrogen-evolving cathode.

The cell was operated potentiostatically at 2.5 V, 5.0 V, and 7.5 V for 5 minutes at each potential. Figure 5-2 shows the current measured at each potential. At 2.5 V the current quickly decayed to a baseline of 20 mA/cm^2 oxygen evolution. At 5.0 V oxygen evolution and/or OF_2 formation briefly contributed to a current of 180 mA/cm^2, but the

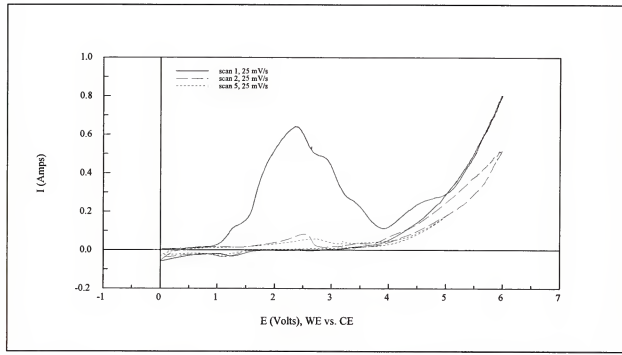

Figure 5-1. Cyclic voltammograms obtained from a cell employing porous PTFE membrane separator and 1 cm^2 platinum black ELAT electrodes

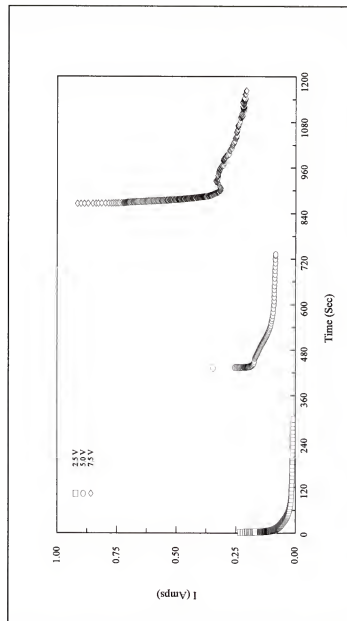

Figure 5-2. Potentiostatic operation of a cell with porous PTFE membrane separator and 1 cm^2 ELAT electrodes

current quickly decayed to a baseline of 100 mA/cm^2 fluorine evolution. Similar behavior is seen at 7.5 V with an initial current of 350 mA/cm^2 decaying to a baseline of 250 mA/cm^2 fluorine evolution.

The current was somewhat unstable at 7.5 V possibly due to poor anode surface wetting, bubble formation, and periodic corrosion of the current collector plate. KF·xHF molten salt likely seeped beyond the ELAT membrane interface allowing activation of the current collector plate in the perimeter space between the gasket and the ELAT. Further evidence of this effect was apparent when the cell was disassembled. A distinct etching pattern was observed on the anode current collector plate in the area between the gasket and the ELAT.

The cell was operated galvanostatically at 200 mA/cm^2 for the purpose of quantifying the fluorine content of the product stream. Nitrogen purged the anode at 50 cc/min. After steady-state product evolution was established, the product stream was passed through a KI scrubber for 30 minutes to liberate iodine for iodometric titration. Table 5-1 lists current efficiency calculations for several experiments. This cell is listed as cell#1 in table 5-1. Figure 5-3 shows the cell potential during the course of this experiment. The potential was initially somewhat erratic ranging from 6.5 V to 7.5 V, but stabilized after 15 minutes.

The color of the KI scrubber was dark red or purple at the end of this experiment. Iodometric titration with $Na_2S_2O_3$ established an iodine concentration of 5.4±0.9E-04 M. The size of the scrubber was 667 ml. and the amount of iodine liberated was 3.6±0.6E-04 moles. The current passed while the product stream was sent through the KI scrubber

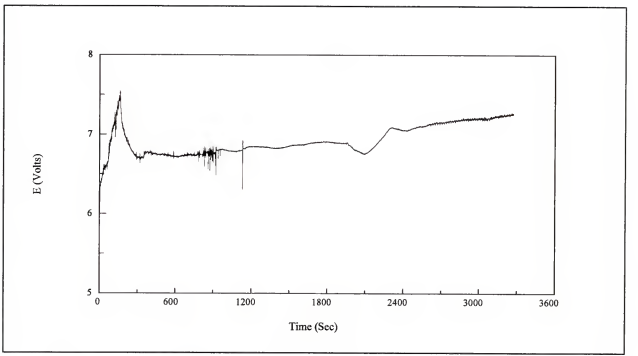

Figure 5-3. Galvanostatic operation at 200 mA of a cell employing a porousPTFE membrane separator and 1 cm^2 ELAT electrodes

was 0.1 amp-hours (360 coulombs) which is equivalent to a maximum fluorine output of $1.9x10^{-3}$ moles. The current efficiency was 18±4% based on iodine liberated as a percentage of maximum fluorine output. Subsequent calibrations showed that this iodometric titration method underestimates fluorine content in the product stream by more than 10%, however this does not account for the observed 82% inefficiency. Inefficiency may be attributed to side reactions and direct recombination of hydrogen and fluorine due to gas crossover.

The following interpretation of reactions and reaction locations in the porous membrane reactor is consistent with the observed results. When nitrogen purged the anode, the GDE was cleared of molten salt and the reaction (bulk electrolysis of KF·xHF) was confined to the ELAT surface in contact with the wetted porous membrane. A mass-transfer-limited current density was reached that gradually decreased with time following application of voltage, ultimately approaching a somewhat unstable steady-state current. The cause of this decrease in current is unclear. Two contributing factors may be depletion of solvent in the pores of the membrane and loss of active electrode area as molten salt freezes out coating some of the electrode surface that is not in direct contact with the wetted membrane. During potentiostatic operation at 5.0 V current was initially observed at 180 mA/cm^2 and dropped as low as 100 mA/cm^2 within 5 minutes. When anhydrous HF gas purged the anode, molten salt penetrated further into the GDE and drained into the perimeter space between the ELAT and gasket. Corrosion patterns verify this. Additional electrode area was active in the GDE and current collector plate that led to superficial current densities in excess of the (2 A) output limit of the potentiostat.

This effect is illustrated in figure 5-4. A cell was operated potentiostatically at 5.0 V for 30 minutes. Nitrogen purged the anode prior to application of voltage and during the first 5 minutes of operation. After 5 minutes elapsed, the anode feed was switched from nitrogen to anhydrous HF gas. Within one minute current began to rise. When current exceeded 350 mA/cm^2, the anode feed was switched back to nitrogen. Approximately 2 minutes elapsed as current continued to rise. Current decreased to less than 250 mA/cm^2 over the next 5 minutes and ultimately reached a steady state of 200 mA/cm^2 for the remainder of the experiment. The residence time of the anode feed line is estimated to be 40 seconds at 50 cc/min flow-rate. This adequately accounts for the majority of process lag time. Left unchecked, when anhydrous HF gas purged the anode, current would continue to rise during potentiostatic operation at potentials 5 V and greater. This indicates free corrosion of the anode with no mass transfer limiting current.

Additional iodometric titrations were performed with anhydrous HF gas purging the anode. Cells were operated galvanostically to avoid the continuous increase of current. The cell was operated galvanostatically again at 200 mA/cm^2. After steady-state product evolution was established, the product stream was passed through a KI scrubber for 30 minutes to liberate iodine for iodometric titration. Iodine was not detected indicating fluorine was not generated within the detection limits of the KI scrubber. The scrubber remained colorless throughout the experiment. This result was initially puzzling, but on disassembly it was apparent substantial corrosion occurred on the anode current collector plate around the perimeter of the ELAT. The decreased cell potential, lack of fluorine production, and etch pattern observed on the current collector plate each indicate free corrosion was the predominant reaction during this experiment.

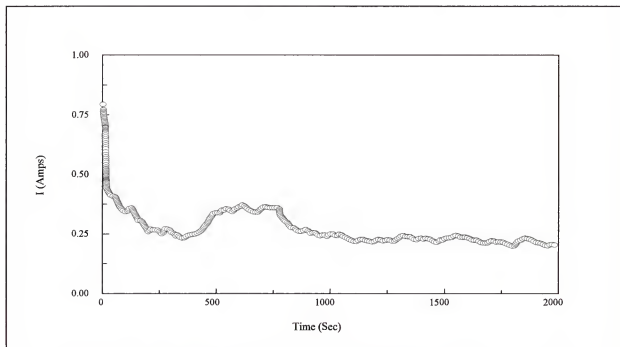

Figure 5-4. Potentiostatic operation at 5.0 V for a cell with a porous PTFE membrane separator and 1 cm^2 platinum black ELAT electrodes. Anode feed switched from nitrogen to anhydrous HF during time interval 300 to 600 seconds.

Operation with a Nafion® Membrane Separator

To evaluate cell performance for bulk electrolysis of KF·xHF molten salt, the PEM reactor was operated with both the anode and the cathode of the reactor flooded with KF·xHF molten salt. This configuration was chosen to determine whether a Nafion® membrane separator could be used in a commercial fluorine cell and to evaluate catalytic activity for fluorine production on ELAT and MEA electrodes. Cells were constructed in the same manner described in chapter 4. The combined methods of fluoride ion EMF in KOH solution and iodometric titration of KI solution were employed for quantitative analysis of fluorine in the product stream.

Hydrodynamic problems were encountered in cells with 1 cm^2 area. Product gas built up inside the reactor that forced liquid out both the outlet and inlet of the cell. The reactor was scaled up to employ 9 cm^2 electrodes. At this size the gasket no longer restricted flow at the inlet and outlet. A continuous recycle of liquid was established as product gas exited at the reactor outlet and liquid in the reservoir spilled over and flowed into the inlet. Results from two 9 cm^2 cells are presented for comparison. The first cell employed platinum black catalyst-coated ELAT electrodes separated by a Nafion® 115 potassium-form membrane. The second cell consisted of an MEA with platinum black catalyst laminated on Nafion® 115 potassium-form membrane and Monel mesh gas-diffusion-electrodes.

Current-voltage data are presented in Figure 5-5 for ELAT and MEA cells with molten salt flooded anodes. The current density and primary anode product gas depended on the type of anode used. A platinum-catalyst-coated ELAT cell with Monel current

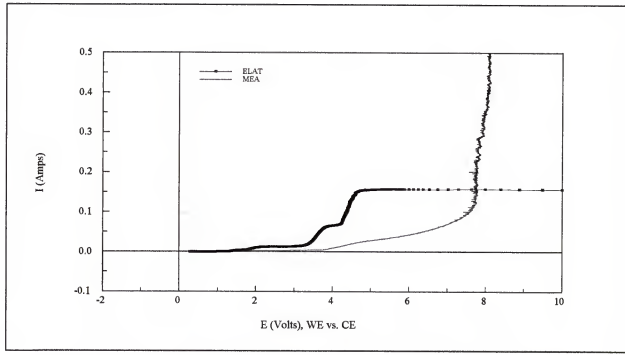

Figure 5-5. Pseudo-steady-state current obtained from cells operating with KF•xHF molten salt flooding both the cathode and anode. One cell employed 9 cm^2 platinum black ELAT electrodes. The other cell employed a 9 cm^2 platinum black MEA.

collector plates yielded a mass-transfer-limited current of 180 mA (20 mA/cm^2). The primary anode product gas was identified as CF_4 by mass spectrometry. Presumably the source of CF_4 was decomposition of the carbon cloth ELAT. Fluorine was not detected in the analytical scrubbers. If any fluorine was generated in this cell it likely attacked the carbon cloth ELAT yielding CF_4. An etch pattern observed on the perimeter of the anode current collector suggested electrochemical reactions were confined to the gap between the ELAT and the gasket. This may be explained by anodic polarization preventing wetting of the interior of the ELAT with electrolyte.

The same types of ELAT electrodes were employed in the cells with a porous Teflon® membrane separator. Fluorine did not completely react with the ELAT in these experiments. Two factors may explain this contradiction. The residence time of product in the reactor was much shorter for cells with a gas-purged anode then for cells with a molten-salt-flooded anode. Cells with a molten-salt-flooded anode also had much greater active surface area subject to corrosion.

A platinum-catalyst-coated MEA cell with monel mesh GDE and monel current collector plates had no apparent mass-transfer-limited current, likely due to corrosion of nickel from monel. Figure 5-6 displays cell potential during the course of galvanostatic operation with current ranging from 180 mA (20 mA/cm^2) to 540 mA (60 mA/cm^2). These potentiograms exhibit two interesting features. Following start up, polarisation occurs in the cell causing potential to quickly rise to a maximum value exceeding 8.0 V. Potential subsequently decays to a steady-state value between 6.0 V and 7.0 V that is relatively insensitive to current density.

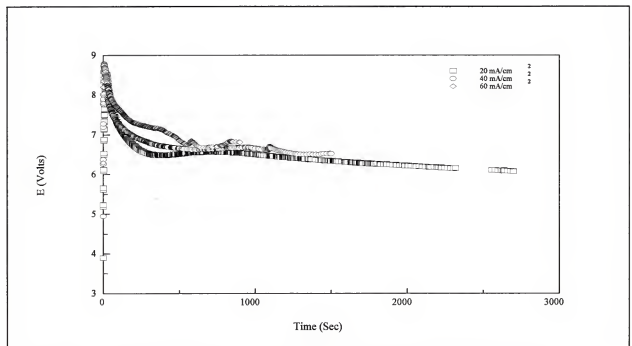

Figure 5-6. Galvanostatic operation of a cell employing a 9 cm^2 platinum black MEA with KF•xHF molten salt flooding the anode and cathode.

After extended periods of operation, the color of molten salt in the reservoir changed from transparent and colorless to transparent with violet color. K_2NiF_6 was identified by x-ray diffraction from a solid corrosion byproduct that had finite solubility in the melt. The primary anode product gas was fluorine. Table 5-1 presents current efficiency calculations derived from measurements of fluoride recovery in the analytical scrubbers. This cell is listed as cell #2. A maximum current efficiency of 61% was obtained at 50°C and 20 mA/cm^2. Repeated experiments at identical current densities did not result in consistent efficiencies. Efficiency depended on cell history to a greater extent than temperature or current density.

Without the presence of a carbon cloth ELAT, electrochemical reactions occurred uniformly throughout the entire anode compartment of MEA cells as evidenced by a uniform etch pattern on the current collector plate. Based on visible corrosion of the current collector plate and relatively little damage to the MEA, we believe that the fluorine evolution reaction occurred preferentially on the current collector rather than on the platinum catalyst layer of the MEA. This result is counterintuitive since it has been demonstrated that the overpotential for fluorine evolution on platinum is lower than that on monel.[47,51] However, if one considers the constitution of the catalyst binder then mass transfer can explain this result.

These results demonstrate that fluorine can be produced in a PEM reactor. The anhydrous KF·xHF molten-salt-swollen Nafion® membrane separator does not appear to limit current and the advantages of a continuous flow-through-electrode membrane-separated cell design are within reach. However, the corrosion sustained in this cell indicates that efficient use of the catalyst was not achieved. Attempts were made to

improve fluoride ion transport to the catalyst surface by replacing the Nafion® solution catalyst binder with Teflon® AF solution.

Operation with Teflon® AF Solution Catalyst Binder

Transport of fluoride ion to the catalyst surface in ELAT and MEA cells was hindered by electrostatic exclusion from the Nafion® solution catalyst binder. An MEA employing Teflon® AF solution catalyst binder was assembled to evaluate whether a non-ionomeric catalyst binder would allow fluoride ions to reach the catalyst. The function of Nafion® solution catalyst binder in PEM reactors is to promote cation conductivity within the catalyst layer and to physically secure the catalyst to the surface of an ELAT or MEA. Use of a non-ionomeric catalyst binder requires that the catalyst layer be saturated with a cation-conducting electrolyte. We anticipated that operation with the anode flooded with KF·xHF molten salt would provide the necessary electrolyte saturation.

Results from this cell employing an MEA with Teflon® AF solution binder were nearly identical to results obtained in cells with Nafion® solution-based MEAs. Again, no activity for fluorine evolution was observed on the platinum catalyst and fluorine evolved preferentially on the monel mesh GDE and current collector plate. Cell efficiency was evaluated during cell operation at effective current density ranging from 25 mA/cm^2 to 75 mA/cm^2 at room temperature and at 40°C. Efficiency calculations tabulated in table 5-1 obtained from this cell are listed as cell #3. During room temperature galvanostatic operation at 225 mA (25 mA/cm^2), current efficiency of this cell was approximately 32% fluorine detected by fluoride ion EMF in KOH solution as a percentage of coulometric equivalent current. Quasi-steady-state current voltage curves are compared in figure 5-7 for cells of identical construction with platinum black MEA

employing Teflon® AF solution and Nafion® solution catalyst binder. No significant differences in current-voltage behavior were observed.

Two explanations adequately account for lack of catalyst activity in the cell with Teflon® AF solution catalyst binder. The catalyst binder, though non-ionomeric, still provided a barrier for transport of fluoride ion to the catalyst. Having no protective coating, the monel mesh GDE and current collector remained the preferential site for fluorine evolution. The non-ionomeric catalyst binder may also not have allowed sufficient cation conductivity in the catalyst layer. KF·xHF molten salt may not have adequately wetted the interior of the catalyst layer to provide the necessary electrolyte.

Table 5-1. Coulometric efficiency for fluorine production in selected cells.
(Cell #1 employed a porous Teflon® membrane separator and ELAT electrodes. Cell #2 employed an MEA with Nafion® solution catalyst binder. Cell #3 employed an MEA with Teflon® solution catalyst binder.)

Cell – size	T, °C	I, mA/cm^2	Time, sec	Charge, C	Equiv F_2	sample F_2	ε
1 – 1 cm^2	20	200	1800	360	1.87E-03	3.60E-04	18%
2 – 9 cm^2	20	50	1200	540	2.80E-03	1.32E-03	47%
2 – 9 cm^2	40	20	3600	648	3.36E-03	1.82E-03	54%
2 – 9 cm^2	45	20	4500	810	4.20E-03	2.39E-03	57%
2 – 9 cm^2	50	20	2700	486	2.52E-03	1.54E-03	61%
2 – 9 cm^2	55	20	3600	648	3.36E-03	1.64E-03	49%
2 – 9 cm^2	50	25	2400	540	2.80E-03	1.58E-03	56%
2 – 9 cm^2	50	50	1200	540	2.80E-03	1.06E-03	38%
2 – 9 cm^2	50	75	900	608	3.15E-03	1.32E-03	42%
2 – 9 cm^2	50	25	2400	540	2.80E-03	1.20E-03	43%
3 – 9 cm^2	20	25	3600	810	4.20E-03	1.36E-03	32%
3 – 9 cm^2	20	50	1800	810	4.20E-03	1.67E-03	40%
3 – 9 cm^2	20	75	1800	1215	6.30E-03	1.69E-03	27%
3 – 9 cm^2	40	50	2700	1215	6.30E-03	1.64E-03	26%

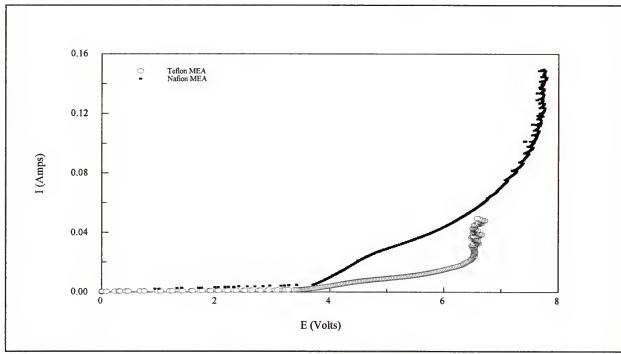

Figure 5-7. Pseudo-steady-state current obtained from cells operating with KF•xHF molten salt flooding both the cathode and anode. Each cell employed a 9 cm^2 platinum black MEA. One cell contained Teflon solution MEA binder and the other cell contained Nafion solution MEA binder.

Operation with a Bare Platinum Mesh Anode

As previously stated it was counter-intuitive that fluorine evolved preferentially on the monel GDE and current collector plate and not on the platinum catalyst. Consideration of transport restrictions in the catalyst binder adequately explains this result. In an attempt to completely eliminate transport restrictions and generate a baseline for comparison of fluorine evolution on platinum, a cell was constructed with no catalyst layer using bare platinum metal mesh electrodes separated by a Nafion® 115 membrane. The anode and cathode of the reactor were flooded with KF·xHF molten salt.

The cyclic voltammograms presented in figures 5-8 and 5-9 show two distinct processes occuring at potentials below the fluorine evolution potential. Initially at 0.4 V an irreversible oxidation occurs which is likely formation of PtF_2 on the surface of the platinum mesh. This peak decreases in magnitude on successive scans but activity is observed in each scan initiating at 0.4 V. In the range 0.4 V to 2.8 V current appears to be limited by an ohmic resistance. The magnitude of this resistance extracted from the slope of the current-voltage curves is approximately 20,000 ohm. This resistance may be attributed to impedance of a fluoride film causing nearly complete passivation of the anode. At 2.8 V a second oxidation peak is observed which is coupled with a reduction peak at approximately 0.4 V. Scans to potentials at or below 2.8 V did not exhibit the reduction peak. This redox couple is likely attributed to further oxidation of platinum to PtF_3 and reduction back to PtF_2. The potential of the reduction peak is not likely coincidental with the potential attributed to onset of passivation. The wide potential gap between the redox couples may be caused by passivation of the anode between 0.4 V and 2.8 V.

Figure 5-10 compares quasi-steady-state current-voltage data obtained from this cell with the data obtained from ELAT and MEA cells. Total measured current is presented for qualitative comparison. The true electrode areas of these cells substantially differ. Though the active area of the catalyst layer appears to be negligible, the active area of the ELAT carbon cloth GDE is uncertain. The area of the monel and platinum mesh GDE are respectively estimated to be 2.4 cm^2 and 0.15 cm^2. Additional electrode area was available in each cell at the exposed current collector plate. The ELAT and MEA cells each had 9 cm^2 gasket holes. The bare platinum mesh cell had a 1 cm^2 gasket hole.

At potentials greater than the fluorine evolution potential two irreversible oxidation processes are observed. The first process appears to initiate above 3.0 V and reaches a mass transfer limited current. This is likely fluorine evolution on the platinum mesh. The second process is likely free corrosion of the monel current collector plate initiating at approximately 10 V. This potential is higher than the potential observed in other cells, however it should be noted that new current collector plates were used in this cell which may not have been adequately "broken in". Hydrodynamic considerations may also account for increased overvoltage and apparent instability. The 1 cm^2 gasket area did not allow for free circulation of molten salt. Fluorine did not bubble freely from the reactor but rather in slugs as pressure exceeded the liquid head of the molten salt reservior.

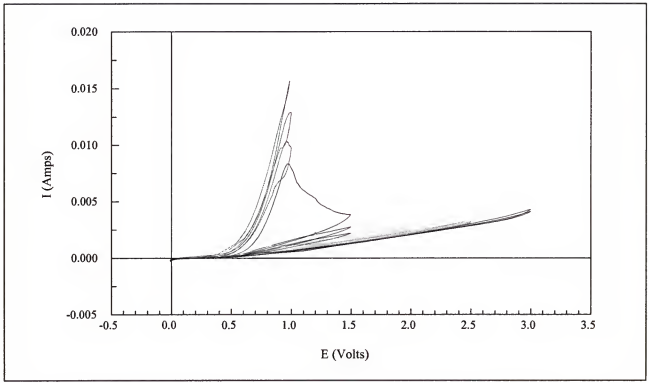

Figure 5-8. Cyclic voltammograms obtained from a cell employing porous Nafion membrane separator and 1 cm^2 bare platinum mesh electrodes

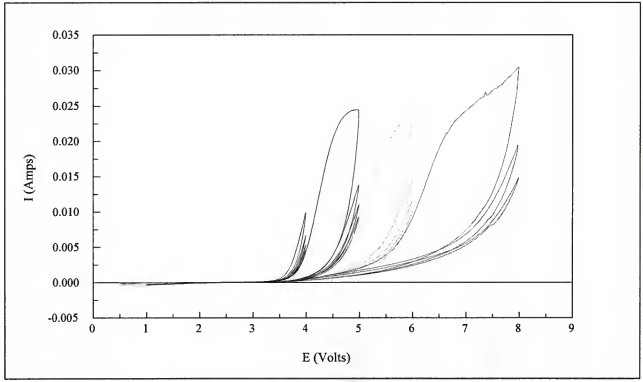

Figure 5-9. Cyclic voltammograms obtained from a cell employing porous Nafion membrane separator and 1 cm^2 bare platinum mesh electrodes

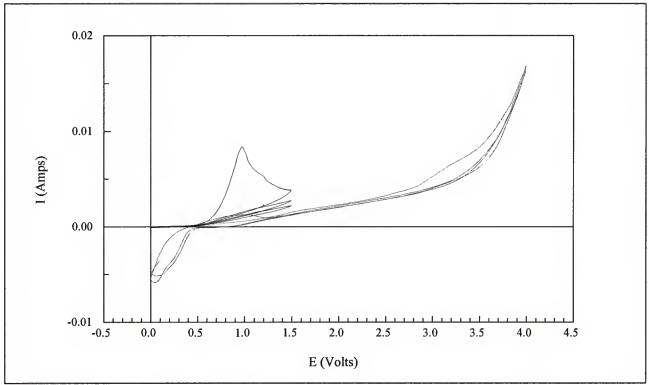

Figure 5-10. Cyclic voltammograms obtained from a cell employing porous Nafion membrane separator and 1 cm^2 bare platinum mesh electrodes

Conclusions

Fluorine production was demonstrated in a Nafion® 115 membrane-separated-electrochemical reactor. With KF·xHF molten salt fed to the anode in a Nafion®-membrane-separated reactor, fluorine was the primary product with the anodic reaction occurring on the monel current collector. Bifluoride ion (HF_2^-) abundant in KF·xHF molten salt was a necessary reactant for sustained fluorine evolution. Good proton and potassium ion conductivity was observed in HF-swollen Nafion® 115 membranes indicating that cation conductivity was not limiting the process. Transport of HF_2^- through the perfluorinated ionomer solution catalyst binder and membrane separator was restricted by electrostatic repulsion and was not sufficient to sustain fluorine evolution at the catalyst.

Optimization of the KF·xHF molten-salt-flooded PEM reactor to maximize current efficiency and reduce electrode corrosion might result in a process very similar to the existing industrial technology with differences only in the type of separator and the methods of reactant delivery and product removal. A perfluorinated ionomer membrane separator may be used to facilitate bipolar and modular cell designs not currently employed in modern fluorine reactors.

CHAPTER 6
THERMOCHEMICAL ASSESSMENT OF THE HF-KF MOLTEN SALT SYSTEM

Introduction

The investigations detailed in Chapter 5 for production of fluorine in a PEM reactor made use of a liquid phase solution of KHF_2 dissolved in HF as the reactant. Under the conditions of operation (P_{HF} = 1.0, 10°C < T < 100°C) the liquid phase was technically not a molten salt but instead a binary solution of HF and KHF_2. This distinction will become apparent through the development of a phase diagram for this binary system. The equilibrium concentration of KHF_2 under conditions of operation ranged between mole fractions of 0.01 to 0.1. For KHF_2 mole fraction less than 0.14, the liquidus is defined by equilibrium between solid HF and liquid solution. The solvent species is liquid HF. Concentrations with KHF_2 mole fraction greater than 0.14 meet the definition of molten salt as the solvent species is a molten stoichiometric compound KF·xHF. The liquidus in this case is defined by equilibrium between solid KF·xHF and liquid solution.

The following description summarizes the operating conditions for the process detailed in Chapter 5. KHF_2 and HF were equilibrated at ambient temperature and 1 atm. pressure. The resulting liquid solution of KHF_2 in HF was drained into the anode and cathode flow reservoirs of the PEM reactor with concentration maintained by bubbling HF at 1 atm. through the liquid. The reactor was then heated or chilled to the desired

operating temperature. The two operating parameters that define the equilibrium of the liquid solution in the flow reservoirs are reactor temperature and partial pressure of HF in the vapor bubbled through the liquid.

To better define the conditions of operation of the reactor it was useful to evaluate existing thermochemical data for the KF-HF system. Very little data has been published for the system KF-HF likely due to the difficulty involved in safe handling of HF. The data that does exist primarily involves studies of the compound KHF_2 and the molten salts KF·xHF in the concentration range $1<x<4$. This is the concentration range of interest for commercial fluorine production. The composition range employed in the PEM reactor was much more dilute (0.01 – 0.1 mole fraction KF in HF). New experimental data was generated to assist in evaluation of the phase diagram and thermochemical properties over the entire composition range. A free energy model was developed that is used to predict composition of the reactant solution as a function of process control parameters (temperature and HF partial pressure).

Thourey, Perachon and Germain reported measurements of the enthalpy of dissolution at 298 K for various concentrations of KF in anhydrous HF obtained by calorimetry.[53] Bottomley, Farrow, and Lincoln reported measurements of equilibrium pressure of HF over solid KHF_2.[54] Davis and Westrum reported measurements of the enthalpy of fusion and decomposition for KHF_2 obtained by a direct calorimetric approach.[55] White and Pistorus studied the high pressure phase diagram of KHF_2 employing differential thermal analysis and volume displacement.[56] Cady published liquidus and vapor pressure measurements for the system KF-HF over a broad

concentration range.[16] His work included a thorough development of the phase diagram and is referenced by most authors studying this system as the original source data.

Experimental Methods

Data available from literature sources exists in the form of liquidus measurements, vapor pressure measurements and calorimetric determination of heat capacity.[16,53-56] While adequate for the purposes of this study, it was determined that additional vapor pressure measurements would be useful for composition and temperature ranges in which literature data is scarce.

Vapor pressure measurements were obtained as a function of temperature and composition for the binary system HF-KF. Liquid solutions of KF in HF were formed at compositions ranging from 0.01 m to 5 m. Each solution was prepared by dissolving a prescribed amount of KF in 365 grams of HF. Table 6-1 provides the mass of salt required for each discrete molar composition. Vapor pressure was measured for each solution at temperatures ranging from 4 °C to 100 °C.

Table 6-1. Loading Requirements for KF in 365 grams HF

Concentration	5.0 m	1.0 m	0.5 m	0.1 m	0.05 m	0.01 m
HF:MF ratio	10:1	50:1	100:1	500:1	1000:1	5000:1
mass KF, g	106.0	21.2	10.6	2.1	1.1	0.2

Figure 3-12 displays a process diagram for the experimental system. The liquid solution for each composition tested was formed in a 0.707 L hastelloy pressure vessel by the following procedure:

- The appropriate mass of KF for each composition with respect to a common base of 365 g HF was loaded into the vessel
- The vessel was purged with nitrogen and then evacuated

- 365 grams HF was loaded in a stainless steel transfer cylinder
- The transfer cylinder was gently heated and the valve for the HF feed line connecting to the pressure vessel was opened allowing transfer of the cylinder contents (365 g HF) to the pressure vessel
- The transfer line was closed and pressure vessel was cooled to 4 °C.

The vessel was immersed in a water bath with temperature maintained by an immersion heater. Following sufficient equilibration time, the vessel temperature was increased at approximately 2.0 °C/min. Temperature was measured with a Kalrez® elastomer coated Type J (ungrounded) thermocouple located in the vapor space of the pressure vessel. The pressure of the vessel was measured with pressure transducer. Both temperature and pressure were recorded on a Hewlet Packard data logger. Measurements were obtained to limits of either 100 °C or 30 psig.

When the temperature or pressure limit was reached, the power for the immersion heater was turned off and the vessel was allowed to cool. Temperature and pressure were recorded during the cooling process. A slight hysteresis was apparent for each data set with a higher vapor pressure measured during heating. For the purpose of the modeling work to follow, data obtained during heating was disregarded. The mean cooling rate of approximately 0.5 °C/min provided conditions closer to equilibrium conditions than the heating process as evidenced by the slight hysteresis in P(T) data.

Following completion of the cooling process and data acquisition, the vessel was pressurized to 10 psig. with nitrogen. The drain valve at the bottom of the vessel was opened allowing bulk liquid to drain to a neutralization tank containing 15 wt.% KOH solution. The drain valve was then closed and the vessel was purged with nitrogen for 8

hours to remove residual HF vapor and allow residual liquid to solidify. The vessel was then decontaminated and cleaned to prepare for the next experiment.

Results

Figure 6-1 displays vapor pressure curves as a function of temperature for each discrete composition of KF-HF solution. The solid line represents vapor pressure of pure anhydrous HF. Vapor pressure for compositions less than 0.5 m was indistinguishable from that of pure anhydrous HF.

Discussion

The phase diagram for the system KF-HF is well known.[16] A single liquid phase forms over the entire composition range. The system contains five stoichiometric compounds: KF·HF, KF·2HF, 2KF·5HF, KF·3HF and KF·4HF. Liquidus points and vapor pressure are reported in the literature for a range of composition and temperature.[16] Additional vapor pressure measurements were obtained from experimental work reported herein.

The optimization technique presented by Bale and Pelton[57] may be employed in development of a free energy model for the binary system HF – KHF_2. Burt Diemer (DuPont Engineering) utilized such a model for the binary system HF-KHF_2 as part of basic data compilation for development and commercialization of molten salt fluorination technology.[58] He fit a free energy model using Cady's data[16] and pure component properties[59,60]. The same model was employed in this work to predict the composition of the HF – KHF_2 solution as a function of the control parameters for the PEM reactor (temperature and HF partial pressure). The new measurements presented in this work were also used to fit the model and compared to the fit obtained from Cady's data.

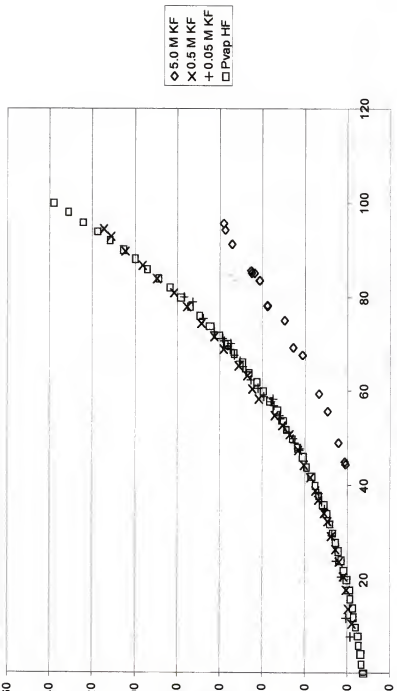

Figure 6-1 Vapor Pressure Measurements for Dilute Solutions of KF in Anhydrous HF

Additional optimization techniques are available in the form of algorithmic software packages. One software package available is the F*A*C*T system provided by Polytechnique Université de Montréal. Another software package is Thermocalc provided by the Royal Institute of Technology, Stockholm, Sweden.

Binary Solution Theory

Development of the free energy model should begin with a review of binary solution theory. The following model describes solution behavior for a binary system of compounds A and B in phase j with respect to the free energy of solution (G_j). Phase j may be either a liquid or a solid. A general development of this model may be found in any number of textbooks covering the subject of thermodynamics.

The free energy of a binary solution may be described in terms of the contributions of the pure components ($G°_{i,j}$ i = species, j = phase) and the free energy of mixing (ΔG^{mix}) relative to the pure components.

$$G_j = x_A G°_{A,j} + x_B G°_{B,j} + \Delta G^{mix}$$

$$\Delta G^{mix} = RT(x_A \ln(x_A) + x_B \ln(x_B)) + G^{ex}$$

The terms x_A and x_B are the mole fractions of each species. The terms $G°_A$ and $G°_B$ represent the free energy of the pure component species A and B. The free energy of HF and KHF_2 will be defined in a later description of pure component properties. The crux of the model lies in the excess free energy (G^{ex}) which is expressed as a polynomial function with respect to composition that is fit to measured data. The following polynomial function is a variation of that employed by Bale and Pelton.[57]

$$G^{ex} = {}_{j=1}\Sigma^{M} K_{mn}(x_A)^m(x_B)^n \text{ , sum j over M coefficients } K_{mn}$$

The excess term (G^{ex}) accounts for deviations from ideal behavior. These deviations are either enthalpic (heat of mixing, ΔH^{mix}) or entropic (excess entropy, S^{ex}) and relate to excess free energy as follows:

$$G^{ex} = \Delta H^{mix} - TS^{ex}$$

The coefficients K_{mn} are expressed as linear functions of temperature containing two fitted parameters. The first parameter (C^{H}_{mn}) contains the enthalpic contribution and the second parameter (C^{H}_{mn}) contains the entropic contribution.

$$K_{mn} = C^{H}_{mn} - TC^{S}_{mn}$$

The partial molar free energy ($\underline{G}_{i,j}$) and partial molar excess free energy ($\underline{G}^{ex}_{i,j}$) for compound i (i = A or B) in a solution (phase j) may be derived resulting in the following equations.

$$G_j = x_A G^{\circ}_{A,j} + x_B G^{\circ}_{B,j} + RT(x_A \ln(x_A) + x_B \ln(x_B)) + G^{ex}$$

$$\underline{G}_{i,j} = (\partial(G_j)/\partial(N_i))_{T,N\neq Ni} = G_j - \Sigma_{k\neq i} x_k (\partial(G_j)/\partial(x_k))_{T,x[k,i]}$$

$$\underline{G}_{i,j} = G^{\circ}_{i,j} + RT\ln(x_i) + \underline{G}^{ex}_{i,j}$$

$$\underline{G}^{ex}_{i,j} = (\partial(G^{ex}_j)/\partial(N_i))_{T,N\neq Ni} = G^{ex}_j - \Sigma_{k\neq i} x_k (\partial(G^{ex}_j)/\partial(x_k))_{T,x[k,i]}$$

Application of partial molar derivatives to the polynomial function for excess free energy produces the following expressions.

$$G^{ex} = \Sigma_{j=1}^{M} K_{mn} (x_A)^m (x_B)^n$$

$$\underline{G}^{ex}_{A,l} = \Sigma_{j=1}^{M} K_{mn} (m x_A^{m-1} + (1-m-n) x_A^{m}) x_B^{n}$$

$$\underline{G}^{ex}_{B,l} = \Sigma_{j=1}^{M} K_{mn} (n x_B^{n-1} + (1-m-n) x_B^{n}) x_A^{m}$$

The activity of compound i in a solution (phase j) is defined according by the following expression:

$$RT\ln(a_i) = \underline{G}_{i,j} - G^{\circ}_{i,j} = RT\ln(x_i) + \underline{G}^{ex}_{i,j}$$

The excess term is zero in an ideal solution. The ideal activity of compound i in the solution is equivalent to the mole fraction of compound i in the solution. Deviation from ideal behavior is accounted for by the partial molar excess free energy. As a result the partial molar excess free energy may be correlated to an activity coefficient ($\gamma i = a_i/x_i$) using the following relationship:

$$\underline{G}^{ex}_{i,j} = RT\ln(a_i/x_i) = RT\ln(\gamma_i)$$

The requirement for equilibrium between phases (j and k) is that the partial molar free energy for each species is the same in both phases.

$$\underline{G}_{i,j} = \underline{G}_{i,k} \text{ for all species "i".}$$

Vapor-Liquid Equilibrium

The expression for free energy in the gas phase requires an additional term to accounts for pressure dependence.

$$G_g = x_A G^\circ_{A,g} + x_B G^\circ_{B,g} + \Delta G^{mix} + G^p$$

$G^p = RT\ln(P/P^\circ)$, where P = pressure in the gas phase, and P° = 1 atm.

The partial pressure of species i in the gas phase is the mole fraction of species i multiplied by the total pressure ($p_i = x_i P$). The preceding terms may be combined to yield:

$$\Delta G^{mix} + G^p = RT(x_A\ln(p_A) + x_B\ln(p_B)) + G_g^{ex}$$

This leads to the following expressions for partial molar free energy for species i in the gas phase and free energy of vaporization:

$$\underline{G}_{i,g} = G^\circ_{i,g} + RT\ln(p_i) + \underline{G}^{ex}_{i,g}$$

$$\Delta G^\circ_{i,vap} = G^\circ_{i,g} - G^\circ_{i,l} = RT\ln(x_{i,l}/p_i) + \underline{G}^{ex}_{i,l} - \underline{G}^{ex}_{i,g}$$

Cady's data for partial pressure of hydrogen fluoride over HF-KHF_2 solution was obtained from measurements at relatively low pressures.[16] The data may be treated as an ideal gas with excess free energy of zero. This simplifies the expression for free energy of vaporization to the following expression:

$$\Delta G^{\circ}_{i,vap} = RT\ln(x_{i,l}/p_i) + \underline{G}^{ex}_{i,l}$$

For a pure liquid, the liquid excess term is zero with a mole fraction of 1.0. The pressure of compound i in equilibrium with pure liquid phase i is defined as the vapor pressure of compound i (P_i^{vap}). Free energy of vaporization for compound i may then be correlated to its vapor pressure.

$$\Delta G^{\circ}_{i,vap} = -RT\ln(P_i^{vap})$$

The preceeding expressions may be combined to create a general model for binary vapor-liquid equilibrium represented by the following two equations.

$$p_i = a_{i,l}P_i^{vap}$$

$$\underline{G}^{ex}_{i,l} = \Delta G^{\circ}_{i,vap} + RT\ln(p_i/x_{i,l})$$

Published vapor pressure data for HF-KHF_2 solution[16] combined with an expression for vapor pressure of pure HF as a function of temperature may be used as data points to fit the excess free energy model for the solution. This model may be then extended to project pressure of HF in the gas phase at higher pressures using an equation of state ($P = P(T,\underline{V})$) for pure HF in the gas phase.

$$P^{IG} = p_i = x_{i,l}(\exp(((\underline{G}^{ex}_{i,l})/RT) + \ln(P_i^{vap})))$$

$$\underline{V} = RT/P^{IG}$$

$P = P(T,\underline{V})$, input T, $\underline{V}$ in E.O.S. model

Glenn Sweany (DuPont Polymer Products) developed the following Peng-Robinson equation of state model for hydrogen fluoride.[61] This model was used for determination of vapor pressure of pure HF and as the equation of state for P(T,$\underline{V}$).

$$P = (RT/(\underline{V} - b)) - a/(\underline{V}^2 + 2\underline{V}b - b^2)$$

a = Peng-Robinson constant, atm(cc/gmol)^2

b = Peng-Robinson constant, cc/gmol

$\underline{V}$ = molar volume, cc/gmol

P = pressure, atm

T = temperature, K

R = gas constant = 82.059 atm·cc/(gmol·K)

The vapor phase was assumed to be a mixture of HF monomer and HF hexamer. The Peng-Robinson constants were determined through application of mixing rules for HF monomer and HF hexamer where y_1 is the mole fraction of hexamer in the vapor phase.

$$a = y_1^2(a_1+a_6-2(a_1a_6)^{1/2}) + 2y_1((a_1a_6)^{1/2}-a_6)+a_6$$

$$b = b_1(6-5y_1)$$

The parameters a1, a6, b1 and y1 were fit to experimental data subject to the constraints of equilibrium for each species (monomer and hexamer) and the equation of state.

Solid-Liquid Equilibrium

Free energy of fusion is derived from the requirement for equilibrium between liquid and solid phases.

$$\Delta G^\circ_{i,fus} = G^\circ_{i,l} - G^\circ_{i,s} = RT\ln(x_{i,s}/x_{i,l}) + \underline{G}^{ex}_{i,s} - \underline{G}^{ex}_{i,l}$$

If the liquid is in equilibrium with pure solid, the solid excess term is zero and the solid mole fraction is 1.0. The partial molar excess free energy for species i in the liquid phase then defined by the following expression:

$$\underline{G}^{ex}_{i,l} = -\Delta G^{\circ}_{i,fus} - RTln(x_{i,l})$$

This equation is useful for evaluating deviations from ideal behavior based on measurements of melting temperature (liquidus measurements).

The previous equation for partial molar excess free energy applies only to the portion of the liquidus curve where the solid phase in equilibrium with the liquid is a pure solid. For stoichiometric compounds (e.g. KF*xHF, $1 < x < 4$) in a binary A - B system, the partial molar free energy may be deduced from the following model.[57]

$$\underline{G}^{ex}_{AyB(1-y)} = \sum_{j=1}^{M} K_{mn}((1-m-n)x_A^m x_B^n + (ymx_B + (1-y)nx_A)x_A^{m-1}x_B^{n-1} - y^m(1-y)^n)$$

The stoichiometric solid may be treated as a pure component by transforming the concentration variable space.

$$X_{st,i} = m_i x_i + b_i \quad \text{where i = species A or B}$$

$$\text{e.g. } X_{A*2B,A} = -3x_A + 1\ ,\ X_{A*2B,B} = -(3/2)x_B + 3/2$$

Treating the stoichiometric compound as a pure species in the newly defined composition variable space, free energy of fusion for the stoichiometric solid may be computed for each measured liquidus datum using the free energy model.

$$\Delta G^{\circ}_{st,fus} = -RTln(X_{st}) - \underline{G}^{ex}_{st,l}$$

$$\text{note: } \underline{G}^{ex}_{st,l} = n\underline{G}^{ex}_{AyB(1-y)}\ ,\ \text{e.g. } KF*2HF = 3(((KH)_{1/2}F)_{2/3}*HF_{1/3}),\ n = 3$$

The resulting data set for free energy of fusion for the stoichiometric solids may be fit as a linear function of temperature.

$$\Delta G^{\circ}_{st,fus} = \Delta H^{\circ}_{st,fus} - TS^{\circ}_{st}$$

This expression for free energy of fusion may then be reinserted in the liquidus equation to complete the liquidus curve in the region where the stoichiometric solid compound is in equilibrium with the liquid.

$$\Delta G^{\circ}_{st,fus}(T) = - RT\ln(X_{st}(x_i)) - \underline{G}^{ex}_{st,i}(T,x_i)$$

The free energy of the stoichiometric compound relative to the pure components (G^{rl}) may be expressed as the difference between the free energy of mixing (ΔG^{mix}) evaluated at the stoichiometric composition and the free energy of fusion ($\Delta G^{\circ}_{st,fus}$) for the stoichiometric compound.

$$G^{rl} = \Delta G^{mix} - \Delta G^{\circ}_{st,fus}$$

$$\Delta G^{mix}_{(A_yB(1-y))} = RT(x_{A,st}\ln(x_{A,st}) + x_{B,st}\ln(x_{B,st})) + G^{ex}_{st}$$

$$\Delta G^{mix} = n\Delta G^{mix}_{(A_yB(1-y))}, \text{ e.g. } KF*2HF = 3(((KH)_{1/2}F)_{2/3}*HF_{1/3}), n = 3$$

Pure Component Properties

In addition to experimental measurements of partial molar free energy, properties of the end member species HF and KHF_2 were used to fit the solution model. These properties are heat of formation, absolute entropy, and heat capacity for solid and liquid phases. The sources of data for HF and KHF_2 are discussed in the following text. The source of data for stoichiometric compounds is derived from the phase diagram analysis.

To make use of vapor pressure data for the HF, thermodynamic properties in the gas phase were considered in addition to those described for liquid and solid phases. Gas phase properties of anhydrous HF available in JANAF tables[60] are the following:

Heat capacitiy fit by least squares over the temperature range 100 K - 2500 K:

$$Cp,g \text{ (cal/mol/K)} = 6.749 + 4.23E\text{-}02*T + 2.1E+03*T^{-2} + 1.19E\text{-}07*T^{2}$$

Heat of formation of anhydrous HF at 298 K: $\Delta H°_{f,298,g} = -65.14$ kcal/mol

Entropy of anhydrous HF at 298 K: $S°_{298,g} = 41.53$ cal/mol/K

The following liquid phase and solid phase properties of HF were obtained from the DuPont Engineering Unified Physical Property System: Liquid heat capacity was averaged to a constant value of 10.86 cal/mol/K over the range 198 K to 273 K. The normal boiling point for HF is 292.6 K. HF vapor pressure at 273 K is 0.475 atm. HF vapor pressure at 298 K is 1.207 atm. These values may be used to estimate heat of vaporization and entropy of vaporization at the boiling point (292.6 K).

$$\Delta H_{vap,292.6} = 6.04 \text{ kcal/mol}, \quad \Delta S_{vap,292.6} = 20.63 \text{ cal/mol/K}$$

Liquid heat of formation at 298 K and liquid entropy at 298 K were calculated as follows:

$$\Delta H°_{f,298,l} = \Delta H°_{f,298,g} - \Delta H_{vap,292.6} + \int_{298.15}^{292.6} (C_{p,g} - C_{p,l})dT = -71.15 \text{ kcal/mol}$$

$$S°_{298,l} = S°_{298,g} - \Delta S_{vap,292.6} + \int_{298.15}^{292.6} ((C_{p,g} - C_{p,l})/T)dT = 20.98 \text{ cal/mol/K}$$

A solid phase heat capacity of 7.66 cal/mol/K was obtained at 173 K. The melting point of HF is listed at 189.8 K with a heat of fusion of 1.095 kcal/mol and an entropy of fusion of 5.77 cal/mol/K. Solid heat of formation at 298 K and solid entropy at 298 K were calculated as follows:

$$\Delta H°_{f,298,s} = \Delta H°_{f,298,l} - \Delta H_{fus,189.8} + \int_{298.15}^{189.8} (C_{p,l} - C_{p,s})dT = -72.59 \text{ kcal/mol}$$

$$S°_{298,s} = S°_{298,l} - \Delta S_{fus,189.8} + \int_{298.15}^{189.8} ((C_{p,l} - C_{p,s})/T)dT = 13.77 \text{ cal/mol/K}$$

When combined, the liquid and solid properties lead to the following expression for free energy of fusion:

$$\Delta G°_{fus} \text{ (cal/mol)} = 488.71 + 14.18*T - 3.194*T*\ln(T)$$

Setting this expression to zero yields a melting temperature of 189.8 which is in very good agreement with that obtained from the DuPont Engineering Database.

Data for liquid and solid KHF_2 are available in JANAF tables.[60] A glass transition occurs in the liquid phase at 314 K. Two solid phases have been identified. The low temperature solid phase (α) has tetragonal structure. The transition to the α phase occurs at 469.9 K. The high temperature solid phase (β) has cubic structure with random occupancy of the body diagonals by HF_2^- anions. The melting point of the β phase occurs at 512.0 K.

At 298 K, the glassy liquid has a heat of formation of -219.07 kcal/mol and an entropy of 31.71 cal/mol/K. The heat capacity for this glassy liquid is the same as that for the α solid phase. This heat capacity was fit by least squares over the temperature range 100 - 469.9 K resulting in the following expression:

$$C_{p,\alpha}\ (\text{cal/mol/K}) = 13.24 + (17.33\text{E-}03)T - (3.310\text{E+}04)T^{-2} + (3.859\text{E-}06)T^2$$

The normal liquid phase above 314 K has a constant heat capacity of 25.00 cal/mol/K. The heat of formation for this liquid at 314 K is -218.77 kcal/mol with respect to the elements in their stable phases at 298 K. This translates to a heat of formation for the liquid phase at 298 K of -219.17 kcal/mol due to the following correction:

$$\Delta H^\circ_{f298,l} = \Delta H^\circ_{f314,l} + \int_{314}^{298.15} C_{p,l}dT$$

The entropy of the normal liquid phase at 314 K is 32.69 cal/mol/K. This translates to an entropy at 298 K of 31.40 cal/mol/K due to the following correction:

$$S^\circ_{f298,l} = S^\circ_{f314,l} + \int_{314}^{298.15} (C_{p,l}/T)dT$$

The heat of formation and entropy at 298 K for solid phase α are respectively: -222.57 kcal/mol and 24.92 cal/mol/K. The heat capacity of solid phase β is constant at 23.96 cal/mol/K. The heat of formation for solid phase β at 469.9 K is -216.41 kcal/mol

with respect to the elements in their stable phases at 298 K. This translates to a heat of formation for solid phase β at 298 K of -220.53 kcal/mol due to the following correction:

$$\Delta H°_{f,298,\beta} = \Delta H°_{f,314,\beta} + \int_{314}^{298.15} C_{p,\beta} dT$$

The entropy of the solid phase β at 469.9 K is 39.77 cal/mol/K. This translates to an entropy at 298 K of 28.87 cal/mol/K due to the following correction:

$$S°_{f,298,\beta} = S°_{f,314,\beta} + \int_{314}^{298.15} (C_{p,\beta}/T) dT$$

Combining these values leads to the following expressions for free energy of fusion from each solid phase to the normal liquid:

$$\Delta G°_{fus,\beta}\ (\text{cal/mol}) = 1049.92 + (4.439)T - (1.040)T\ln(T)$$

$$\Delta G°_{fus,\alpha}\ (\text{cal/mol}) = 813.402 + (66.731)T - (16550)T^{-1} + (8.666\text{E-}03)T^2$$
$$+ (6.432\text{E-}07)T^3 - 11.756T\ln(T)$$

Setting the free energy of fusion for the β phase solid to zero yields a melting point of 512.3 K. This is in good agreement with the value of 512.0 provided in the JANAF table.[60] The same calculation applied to the α phase solid yields a melting point of 484.5 K. This melting point is never observed because the transition to β phase solid occurs below this temperature. The free energy change for the α-β transition can be calculated from the difference in free energies of fusion at the transition temperature according to the following expression:

$$\Delta G°_{tr,\alpha-\beta} = \Delta G°_{fus,\alpha} - \Delta G°_{fus,\beta}$$

$$\Delta G°_{tr,\alpha-\beta} = -236.52 + (62.292)T - (16550)T^{-1} + (8.666\text{E-}03)T^2$$
$$+ (6.432\text{E-}07)T^3 - (10.716)T\ln(T)$$

Setting the free energy of the solid transition to zero yields a transition temperature of 469.7. This is in good agreement with the value of 269.9 listed in the JANAF table.[60]

Binary Solution Model for HF - KHF_2

The previous discussion of binary solution fundamentals outlined an approach for obtaining partial molar excess free energy ($\underline{G}^{ex}_{HF}$) for HF from partial pressure and liquidus data. A plot of $\underline{G}^{ex}_{HF}$ vs x_{HF} is presented in figure 6-2 based on published vapor pressure measurements for the binary system HF-KF.[16] A point of inflection is apparent near the composition corresponding to KF·2HF.

For treatment of the binary system KF-HF with F^- as the common anion, the KF·HF composition may be represented by $(HF)_{1/2}\cdot(KF)_{1/2}$ or by $(KH)_{1/2}F$. Retaining this stoichiometry requires that the free energy associated with the species $(KH)_{1/2}F$ is one-half that of KF·HF. A new composition variable is useful to distinguish between "free" HF and HF tied up with the species $(KH)_{1/2}F$.

Let: $z_{HF} = 2*x_{HF} - 1$

$z_{(KH)0.5F} = 1 - z_{HF} = 2 - 2*x_{HF}$

Where: x_{HF} = mole fraction HF in HF-KF phase space with values ranging from 0.5 to 1.0 on the HF-rich side of the phase diagram

z_{HF} = mole fraction HF in HF-$(KH)_{1/2}F$ phase space with values ranging from 0.0 to 1.0

$z_{(KH)0.5F}$ = mole fraction $(KH)_{1/2}F$ in HF-$(KH)_{1/2}F$ phase space with values ranging from 0.0 to 1.0

The partial molar excess free energies of HF and $(KH)_{1/2}F$ were recalculated along portions of the liquidus in equilibrium with the corresponding pure solids using the new composition variables. These calculations followed the same model outlined in the

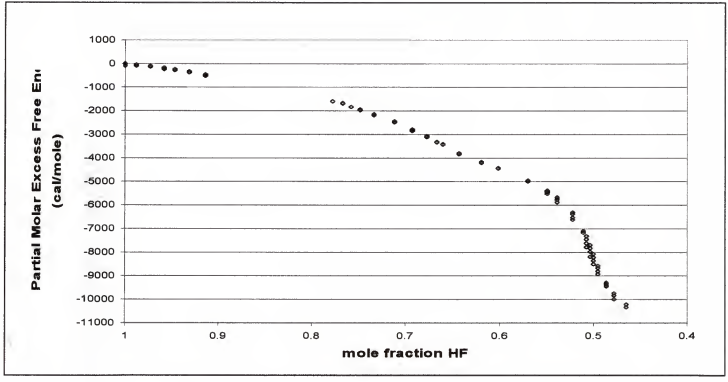

Figure 6-2 Partial molar excess free energy of HF in the liquid phase based on published vapor pressure measurements

discussion of binary solution theory. The partial molar excess free energy of vapor phase HF over the liquid was also recalculated using the new composition variables.

Additional data is also available[59,60] in the form of heat of solution at infinite dilution at 298 K for KF(s) (-21782 cal/mol) and KHF_2(s) (-9540 cal/mol). These values may be used to establish the heat of mixing for $(KH)_{1/2}F$(l) at infinite dilution in HF(l) according to either of the following equations:

$$\Delta H^{mix,\infty}_{(KH)1/2F} = (\Delta H^{\infty}_{sol,KF(s)} - \Delta H^{\circ}_{fus,KF} + \Delta H^{\circ}_{dis,KHF2(l)})/2$$

$$\Delta H^{mix,\infty}_{(KH)1/2F} = (\Delta H^{\infty}_{sol,KHF2(s)} - \Delta H^{\circ}_{fus,KHF2})/2$$

The first equation represents a mixing sequence in which KF(s) melts, then combines with HF(l) to form KHF_2(l), and KHF_2(l) mixes with HF(l). The second equation represents a mixing sequence in which KHF_2(s) melts and then mixes with HF(l). These equations require information for the heat of fusion of KF and KHF_2, and the heat of dissociation for the reaction:

$$KHF_2(l) \leftrightarrow KF(l) + HF(l)$$

According to literature sources[59,60] the values are:

$$\Delta H^{\circ}_{fus,KF,298} = 3379 \text{ cal/mol}$$

$$\Delta H^{\circ}_{fus,KHF2,298} = 3402 \text{ cal/mol}$$

$$\Delta H^{\circ}_{dis,KHF2(l),298} = 15494 \text{ cal/mol}$$

The calculation for heat of mixing using the first equation is -4819 cal/mol. The calculation using the second equation is -6471 cal/mol. These values are not identical, but are of the same order indicating the data obtained from separate sources each have merit.

For this binary model with end members A-B, HF is the "A" end member and $(KH)_{1/2}F$ is the "B" end member. At infinite dilution of B in A, the solution model is evaluated at $x_B = 0$ and $x_A = 1$. Only the 0^{th} term exists in the limit for the partial excess free energy of B, thus:

$$\underline{G}^{ex,\infty}{}_B = C^H{}_0 - TC^S{}_0$$

The infinite dilution heat of mixing of B is equal to the 1^{st} enthalpic term $C^H{}_0$. This coefficient also provides a value for excess free energy of B at infinite dilution and a temperature of 0 K. $\Delta H^{mix,\infty}{}_{(KH)1/2F} = -4819$ cal/mol was selected as there was no specific basis for determining the other value of -6471 cal/mol to be more or less correct. This value was also input as a single highly weighted datum along with the other partial molar excess free energy data for fitting the model.

Excess free energy for the system may be expressed as the following polynomial expansion of the HF mole fraction in HF-$(KH)_{1/2}F$ phase space:

$$G^{ex} = \Sigma\, \phi_{m_i n_i} z_{HF}{}^{m_i}(1-z_{HF})^{n_i}$$

Taking the partial derivatives with respect to mole fraction yields the following expressions for partial molar excess free energy of the end member species HF and $(KH)_{1/2}F$:

$$G^{ex}{}_{HF} = \Sigma\, \phi_{m_i n_i}[m_i z_{HF}{}^{m_i-1} + (1 - m_i - n_i) z_{HF}{}^{m_i}](1-z_{HF})^{n_i}$$

$$G^{ex}{}_{(KH)_{1/2}F} = \Sigma\, \phi_{m_i n_i}[n_i(1-z_{HF})^{n_i-1} + (1 - m_i - n_i) z_{HF}{}^{n_i}] z_{HF}{}^{m_i}$$

The free energy model coefficients $\phi_{m_i n_i}$ were expressed as a linear function of temperature and substituted into the expressions for total free energy and partial molar free energy as follows:

$$\phi_{m_i n_i} = C^H_{m_i n_i} - T \cdot C^S_{m_i n_i}$$

$$G^{ex} = \Sigma \left(C^H_{m_i n_i} - T \cdot C^S_{m_i n_i}\right) z_{HF}^{m_i} (1 - z_{HF})^{n_i}$$

$$G^{ex}_{HF} = \Sigma \left(C^H_{m_i n_i} - T \cdot C^S_{m_i n_i}\right) [m_i z_{HF}^{m_i - 1} + (1 - m_i - n_i) z_{HF}^{m_i}] (1 - z_{HF})^{n_i}$$

$$G^{ex}_{(KH)_{1/2}F} = \Sigma \left(C^H_{m_i n_i} - T \cdot C^S_{m_i n_i}\right) [n_i (1 - z_{HF})^{n_i - 1} + (1 - m_i - n_i) z_{HF}^{n_i}] z_{HF}^{m_i}$$

For development of a regression matrix, these equations may be expressed as a linear expansion (m=1) in terms of a dependent variable, two independent variables, and two fitted coefficients as follows:

$$f(x1,x2) = \Sigma_{i=0,N} \left(C^H_{mn_i}(x_{1i}) + C^S_{mn_i}(x_{2i})\right)$$

Where: f(x1,x2) = Dependent Variable

x1 = Independent Enthalpic Variable

x2 = Independent Entropic Variable

C^H_{mn} and C^S_{mn} = Fitted Coefficients (m=1, n=0,1,2…N, N = model order)

Dependent Variable	Independent Enthalpic Variable	Independent Entropic Variable
$\underline{G}^{ex}_{HF}$	$(1-(n+1)z_{HF})(1-z_{HF})^{n+1}$	$-T(1-(n+1)z_{HF})(1-z_{HF})^{n+1}$
$G^{ex}_{(KH)_{1/2}F}$	$(n+1)z_{HF}^2(1-z_{HF})^n$	$-T((n+1)z_{HF}^2(1-z_{HF})^n)$
G^{ex}	$z_{HF}(1-z_{HF})^{n+1}$	$-T(z_{HF}(1-z_{HF})^{n+1})$

The sum of squared error (SSE) is defined by the following expression:

$$SSE = \Sigma_{i=1,D} (y_i - f(x1,x2))$$

Where: D = total number of data entered into model fit

y_i = measured datum

f(x1,x2) = dependent variable for type of datum entered ($\underline{G}^{ex}_{HF}$, $G^{ex}_{(KH)_{1/2}F}$, or G^{ex})

Setting the partial derivative of the sum of squared error with respect to each model coefficient to zero yields the following matrix that may be used to determine the values for each coefficient.

$$(\partial(SSE)/\partial(C_i))_{Cj\neq Ci} = \Sigma_{k=1,D}[-2(y_k\text{-}f(x_1,x_2)_k)(x_i + \Sigma_{(j=0,1,2\ldots,i\text{-}1,\ldots i+1,\ldots N)}(C_j x_j))] = 0$$

The resulting N equations may be used to solve for N coefficients in the matrix using any number of software packages that include matrix solution algorithms (F*A*C*T and Thermocalc employ such algorithms). Alternatively the equations may be entered into a spreadsheet and solved by iterative trial and error methods. This method was employed in this work to include the new vapor pressure measurements obtained at DuPont.

Models of increasing order were each fit to the data until such point that increasing the order of the model did not substantially reduce the residual squared error. Burt Diemer found a third order model sufficiently represented Cady's data yielding the following equation for excess free energy:[58]

$$G^{ex} = z_A z_B[(-4816 - 2.409T) + z_B(-7134 + 16.21T) + 2628 z_B^2]$$

where A = HF and B = $(KH)_{1/2}F$

A third order model was also fit for this work using Cady's data, and including the experimental data measured at DuPont, yielding the following expression for excess free energy:

$$G^{ex} = z_A z_B[(-4820 - 6.32T) + z_B(-6720 + 16.1T) + z_B^2(1950 - 1.78T)]$$

All pure component free energies were entered in the model as expressions relative to the free energy of the pure end member liquids. The pure end member liquids have zero free energy within the fitting algorithm. The derived liquid phase model was used to calculate the free energy of fusion ($\Delta G°_{fus}$) of the stoichiometric solids for each

published liquidus datum. The resulting data set was then fit to a linear expression with respect to temperature.

$$\Delta G^{\circ}_{st,fus} = -\underline{G}^{ex}_{st,l} - RT\ln(X_{st})$$

$$\Delta G^{\circ}_{st,fus} = \Delta H^{\circ}_{st,fus} - TS^{\circ}_{st}$$

The free energy of the stoichiometric solids relative to the pure components was determined using the fitted results for free energy of fusion.

$$G^{rl} = \Delta G^{mix} - \Delta G^{\circ}_{st,fus}$$

$$\Delta G^{mix}_{(AyB(1-y))} = RT(x_{A,st}\ln(x_{A,st}) + x_{B,st}\ln(x_{B,st})) + G^{ex}_{st}$$

$$\Delta G^{mix} = n\Delta G^{mix}_{(AyB(1-y))}, \text{ e.g. } KF*2HF = 3(((KH)_{1/2}F)_{2/3}*HF_{1/3}), n = 3$$

Table 6-2 lists the resulting expressions for total free energy (G^{rl}) and free energy of fusion ($\Delta G^{\circ}_{st,fus}$) for the stoichiometric solids relative to the pure component liquids.

Table 6-2. Total free energy and free energy of fusion of stoichiometric solids relative to pure component liquids

Compound	G^{rl}_{s} (cal/mol)	ΔG°_{fus} (cal/mol)
KF·2HF(s)	-8456 + 10.09T	2853 - 8.285T
2KF·5HF(s)	-24150 + 33.07T	10380 - 30.82T
KF·3HF(s)	-12880 + 15.35T	5155 - 15.17T
KF·4HF(s)	-12770 + 9.846T	4068 - 11.64T

These expressions may be converted to the mixed reference state as follows for each compound KF·nHF:

$$G^{\circ}_{s,KF*nHF} = G^{rl}_{s,KF*nHF} + G^{\circ}_{l,KHF2} + (n-1)G^{\circ}_{l,HF}$$

A simplifying assumption may be used to determine heat capacity for the stoichiometric complexes. The assumption is that the heat capacity of the complexes (in

solid or liquid phase) is equal to the stoichiometric sum of the pure component species liquid heat capacities.

$$C_{p,(s\text{ or }l),KF\cdot nHF} = C_{p,l,KHF2} + (n-1)C_{p,l,HF}$$

This assumption is implicit in the fact that the computed free energy expressions for fusion and for compounds relative to the pure liquids have only two terms. If heat capacity of the compounds differs from the stoichiometric sum of end member heat capacities by even a constant value, a Tln(T) term would be necessary in the free energy expressions. The two term models employed adequately account for enthalpy differences in the constant terms and for entropy differences with the coefficients of temperature.

The heat capacity assumption establishes that the change in heat capacity for fusion and for formation reactions is zero. This allows direct calculation of properties at 298 K for both solid and liquid phase compounds.

$$G^\circ_{s,KF\cdot nHF,298} = \Delta H^\circ_{f,s,KF\cdot nHF,298} - TS^\circ_{s,KF\cdot nHF,298}$$

$$\Delta H^\circ_{f,s,KF\cdot nHF,298} = \Delta H^{rl}_{s,KF\cdot nHF} + \Delta H^\circ_{f,l,KHF2,298} + (n-1)\Delta H^\circ_{f,l,HF,298}$$

$$S^\circ_{s,KF\cdot nHF,298} = \Delta S^{rl}_{s,KF\cdot nHF} + S^\circ_{l,KHF2,298} + (n-1)S^\circ_{l,HF,298}$$

$$G^\circ_{l,KF\cdot nHF,298} = \Delta H^\circ_{f,l,KF\cdot nHF,298} - TS^\circ_{l,KF\cdot nHF,298}$$

$$\Delta H^\circ_{f,l,KF\cdot nHF,298} = \Delta H^\circ_{f,s,KF\cdot nHF,298} + \Delta H^\circ_{fus,KF\cdot nHF}$$

$$S^\circ_{l,KF\cdot nHF,298} = S^\circ_{s,KF\cdot nHF} + \Delta S^\circ_{fus,KF\cdot nHF}$$

Table 6-3 displays standard heat of formation, standard entropy, and heat capacity for each compound determined according to the preceding set of relationships.

Table 6-3. Standard heat of formation, standard entropy, and heat capacity for intermediate compounds KF·nHF

Compound	Phase	$\Delta H^\circ_{f,298}$ (kcal/mol)	S°_{298} (cal/mol/K)	C_p (cal/mol/K)
KF·2HF	liquid	-295.92	50.576	35.855
KF·2HF	solid	-298.78	42.291	35.855
2KF·5HF	liquid	-665.57	123.49	82.565
2KF·5HF	solid	-675.95	92.673	82.565
KF·3HF	liquid	-369.20	73.176	46.710
KF·3HF	solid	-374.36	58.010	46.710
KF·4HF	liquid	-441.33	96.140	57.565
KF·4HF	solid	-445.39	84.497	57.565

Values for some heats of formation may be compared to values published in literature. Two values of heat of formation published[59,60] for KF·2HF are -296.7 kcal/mol and -296.6 kcal/mol. The same sources provide values of -373.0 kcal/mol and -372.9 kcal/mol for KF·3HF. One of the sources[60] lists a heat of formation for KF·4HF as -449.2 kcal/mol. Each of these values compares favorably to the values derived in this work.

Figure 6-3 displays the phase diagram predicted by the free energy model along with liquidus points taken from literature.[16] The phase diagram is presented in the concentration variable space transformed to the psuedo-binary system HF-$(KH)_{1/2}F$. The model results show excellent agreement with the published data. Figure 6-4 displays the phase diagram after refitting to include the new vapor pressure measurements obtained at DuPont. On comparison of the two model fits, the only substantial difference occurs in the first entropic coefficient. This did not greatly affect the quality of the fit to the liquidus data.

Equilibrium vapor pressure (p_{HF}) may also be derived from the free energy model as detailed in the previous discussion of binary solution fundamentals.

$$\underline{G}^{ex}_{HF,l} = \Delta G°_{HF,vap} + RT\ln(p_{HF}/x_{HF})$$

$$\underline{G}^{ex}_{HF,l} = \partial(G^{ex})/\partial x_{HF}$$

$$\Delta G°_{HF,vap} = -RT*\ln(P_{HF}^{vap})$$

$P_{HF}^{vap} = P(T)$, vapor pressure of pure HF at temperature T

$$P^{IG} = p_i = x_{i,l}(\exp(((\underline{G}^{ex}_{i,l})/RT) + \ln(P_i^{vap})))$$

$$\underline{V} = RT/P^{IG}$$

$P = P(T,\underline{V})$, input T, V in EOS model[61]

Figure 6-5 shows the partial pressure of HF at relatively low pressures as predicted by the free energy model and published vapor pressure measurements.[16] In this case the vapor phase was modeled as an ideal gas. The model predictions and published measurements correlate very well except at HF mole fractions less than 0.1. The model prediction does have the correct slope indicating temperature dependence is properly represented. One should expect a minimum of error at high mole fraction HF as the composition approaches pure HF. This is indeed the case. The error at low mole fraction HF is probably not coincidental with the fact that the transition of KHF_2 from α–phase to β–phase occurs at 470 K. At "free HF" mole fraction of 0.08 ($z_{HF} = 0.08$) the solid phase in equilibrium with the liquid phase transitions from α-KHF_2 to β-KHF_2. This transition is well represented in the model prediction of the liquidus. The impact of this transition on partial molar free energy of HF (and thus ideal partial pressure) may be substantially different than what is accounted for in the excess free energy model.

Figure 6-6 shows the partial pressure of HF at moderate pressures as predicted by the free energy model in conjunction with a Peng-Robinson equation of state. Experimental vapor pressure measurements at HF mole fractions of 0.98 and 0.818 are

included on this plot for comparison. The pressures predicted by the combined models compare favorably with the experimental values. The conclusion drawn from this data is that the free energy model adequately predicts the partial molar free energy of HF in the range 0.8 to 1.0 mole fraction HF.

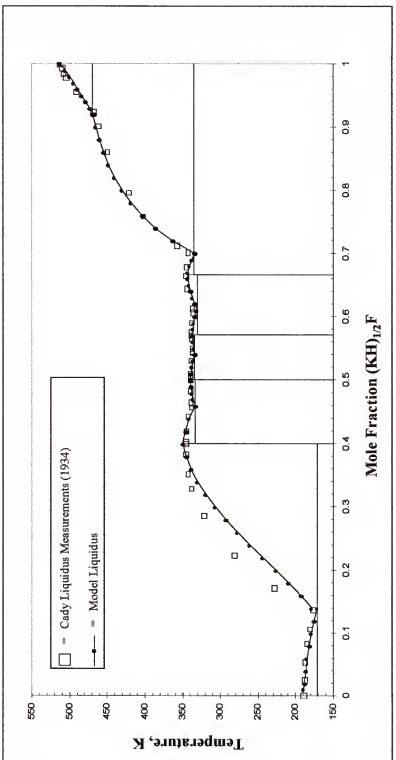

Figure 6-3. Temperature-composition phase diagram for $HF-(KH)_{1/2}F$

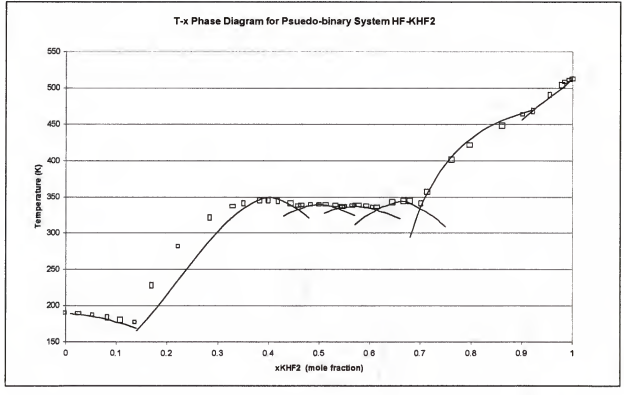

Figure 6-4. Liquidus predicted by adjusted model fit

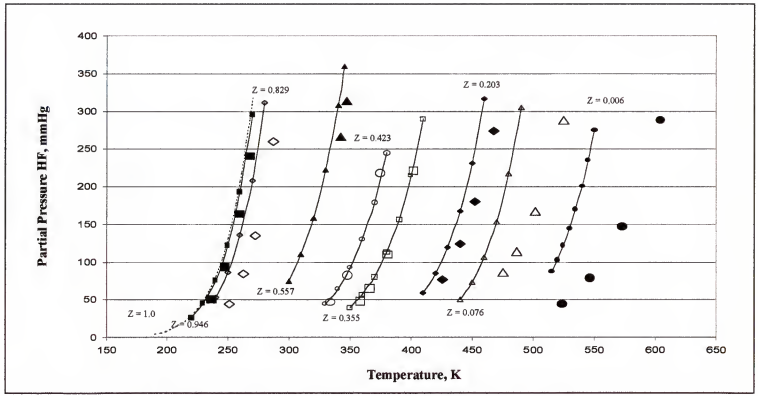

Figure 6-5. Partial pressure of HF as a function of temperature and composition near the liquidus

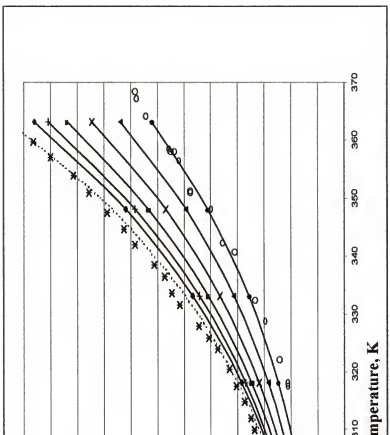

Figure 6-6. Partial pressure of HF as a function of temperature and composition at elevated temperatures away from the liquidus

REFERENCE LIST

1. A. J. Rudge, *The Manufacture and Use of Fluorine and Its Compounds*, Oxford University Press, 1962.

2. J. Ellis and G. May, *J. Fluorine Chem.*, **33**, 133 (1986).

3. W. C. Schumb, R. C. Young and K. J. Radimer, *Ind. Eng. Chem.*, **39**, 3 (1947).

4. G. H. Cady: "Preparation of Fluorine" in Fluorine Chemistry, Vol I, Ch. 8, Ed: J. H. Simons, Academic Press Inc., N.Y., 1950.

5. *Kirk-Othmer Encyclopedia of Chemical Technology*, 3rd ed., Vol. 10, Ed: H. Mark, D. Othmer, C. Overberger and G. Seaborg, John Wiley & Sons, N.Y., 1980.

6. D. Eames and J. Newman, *J. Electrochem. Soc.*, **142**, 3619 (1995).

7. R. Yeo and H. Yeager: "Structural and Transport Properties of Perfluorinated Ion-Exchange Membranes" in *Modern Aspects of Electrochemistry*; No. 16, Ed: E. Bockris, D. Conway, and R. White, Plenum Press, N.Y., 1985.

8. A. J. Rudge: "Production of Elemental Fluorine by Electrolysis" in *Industrial Electrochemical Processes*, Ed. A. T. Kuhn, Elsevier, N.Y., 1971.

9. *Asimov on Chemistry*, I. Asimov, Doubleday, N.Y., 1974.

10. L. Domange, Proc. Chem Soc., 172, June/July, (1959).

11. H. Moissan, *Compt. Rend.*, **102**, 1543, (1886).

12. O. Ruff, *Die Chemie des Fluors*, Julius Springer, Berlin, 1920.

13. W. Argo, F. Mathers, B. Humiston and C. Anderson, *Trans. Electrochem Soc.*, **35**, 335, (1919).

14. F. Mathers, *Trans. Electrochem. Soc.*, **36**, 207, (1919).

15. Several Authors, *Ind. Eng. Chem.*, **39**, 235 *et. seq.*, (1947).

16. G. Cady, *J. Am. Chem. Soc.*, 56, 1431, (1934).

17. G. Cady, D. Rodgers and C. Carlson, *Ind. Eng. Chem.*, **34**, 443, (1942).

18. "The Preparation, Propteries and Technologyof Fluorine and Organic Fluorine Compounds," C. Slesser and S. Schramm (Eds.), *Nat. Nucl. Energy Series., Div. VII*, Vol. I, McGraw-Hill Book Co., NewYork, Toronto, London, 1951.

19. W. Rudorff, U. Hofmann, G Rudorff, J. Endell and G. Ruess, *Z. Anorg. Allgem. Chem.*, **256**, 125, (1948).

20. J. Dykstra, S. Katz, C. Clifford, E. Powell and G. Montillon, *Ind. Eng. Chem.*, **47**, 883, (1955).

21. J. Jacobson, W. Henderson, T. Fleming, R. Levin and J. Marshall, *Ind. Eng. Chem.*, **47**, 878, (1955).

22. A Baines and A. Davies, *J. Appl. Chem.*, (London), **5**, 242, (1955).

23. J. Dykstra, B. Thompson and W. Paris, *Ind. Eng. Chem.*, **50**, 181, (1958).

24. W Kroll, *J. Elecrochem. Soc.*, **106**, 8C, (1959).

25. N. Watanabe, M. Ishii and S. Yoshizawa, *J. Electrochem. Soc. Japan*, **28**, E 180, (1961).

26. A. Rudge, *Chem. Ind. (London)*, 482, (1966).

27. J. Trainham, C. Law, J. Newman, K. Keating, and D. Eames, U.S. Patent No. 5,411,641, (1995)

28. D. Eames and J. Newman, *J. Electrochem. Soc.*, **142**(10), 3619 (1995).

29. T. Springer, M. Wilson, D. Eames, J. Newman, *J. Electrochem. Soc.*, **143**(5), 632, (1996).

30. S. Motupally, D. Mah, F. Freire, and J. Weidner, *Interface*, 7(3), 32 (1998).

31. S. Motupally, R. Rajenderan and R. White, *J. Electrochem. Soc.*, **145**(8), 2951 (1998).

32. S. Motupally, "The Mechanism of Proton Transport in a PEM Reactor for HCl Electrolysis", University of South Carolina, Ph.D. Dissertation, 1999.

33. M. Wilson and S. Gottesfeld, *J. Appl. Electrochem.*, **22**, 1 (1992).

34. T. Springer, T, Zawodzinski, M. Wilson, and S. Gottesfeld, *J. Electrochem. Soc.*, **143**(5), 587 (1996).

35. M. Pourbaix, *Atlas d'Equilibres Electrochemiques*, Gauthier-Villars, Paris, 1963.

36. W. Latimer, *J. Amer. Chem. Soc.*, **48**, 2868, (1926).

37. J. Newman, *Electrochemical Systems*, 2nd ed., Prentice Hall, Englewood Cliffs, N.J., 1991.

38. *CRC Handbook of Chemistry and Physics*, 70th ed., R. Weast, D. Lide, M. Astle, and W. Beyer, Eds., CRC Press Inc., Boca Raton, FL, 1989.

38. A. Guzmán-Garcia, P. Pintaro, M. Verbrugge, R. Hill, *AICHE Journal*, **36**(7), 1061 (1990).

40. Y. Chen and T. Chou, *Electrochimica Acta.*, **38**(15), 2171 (1993).

41. D. Hall, *J. Phys. Chem.*, **100**, 15599 (1996).

42. Z. Samec, A. Trojánek, and J. Langmaier, *J. Electrochem. Soc.*, **144**(12), 4236 (1997).

43. S. Basu and M. Sharma, *J. Memb. Sci.*, **124**, 77 (1997).

44. G. Cady, "Preparation of Fluorine" in *Fluorine Chemistry*, Vol. I, Ch. 8, J. Simons, Ed., Academic Press, Inc., N.Y., 1950.

45. M. Doyle, M. Lewittes, M. Roeloffs, S. Perusich, and R. Lowrey, submitted to *J. Membr. Sci.*

46. F. Huba, E. Yeager, and G. Olah, *Electrochim. Acta*, **24**, 489 (1979).

47. N. Hackerman, E. Snavely, and L. Fiel, *Corrosion Sci.*, **7**, 39 (1967).

48. T. Hoar in *Modern Aspects of Electrochemistry*, Vol. 2, J. Bockris, Ed., Butterworths, London (1959).

49. G. Cady, *XVII International Congress of Pure and Applied Chemistry*, Inorganic Chemistry, **1**, 205, Munich (1959).

50. *Handbook of Electrochemical Constants*, R. Parsons, Ed., Academic Press, New York (1959).

51. A. Doughty, M. Fleischmann, and D. Pletcher, *J. Electroanal. Chem.*, **51**, 329 (1974).

52. R. Lowrey, M. Doyle and T. Anderson, *Electrochemical and Solid State Letters*, **2** (10) (1999).

53. J. Thourey, G. Perachon, and P. Germain, *J. Fluorine Chem.*, **15**, 315 (1980).

54. G. Bottomley, J. Farrow, and F. Lincoln, *Aust. J. Chem.*, **36**, 649 (1983).

55. M. Davis and E. Westrum, *J. Phys. Chem.*, **65**, 338 (1961).

56. A. White and C. Pistorius, *J. Chem. Phys.*, **56(9)**, 4318 (1972).

57. C. Bale and A. Pelton, *Met. Trans. B*, **14(B)**, 77 (1983).

58. B. Diemer, Internal Company Document, Accession No. 17860, DuPont Engineering, Wilmington, DE, November 1992.

59. *Thermochemical Properties of Physical Substances*, I. Barin, O. Knacke, and O. Kubaschewski, Springer-Verlag, Berlin (1977).

60. *JANAF Thermochemical Tables*, 3rd ed., *J. Phys. Chem. Ref. Data*, **14(1)**, (1985).

61. G. Sweaney, Internal Company Document, PPD Report No. 90-E-46, DuPont Polymers Research and Development Division, Experimental Station, Wilmington, DE, June 1991.

BIOGRAPHICAL SKETCH

Robert Lowrey was born in Elgin, Illinois, on February 25, 1971. His parents, Haldor and Phyllis Lowrey, raised him. The family moved to Springfield, Illinois, in 1985 where he attended Rochester High School. In 1989 he enrolled at Northwestern University where he majored in chemical engineering. He remained in school while working on a co-op job at Argonne National Laboratory from 1991 through 1994. He received his bachelor's degree from Northwestern in 1994.

In 1995 Robert enrolled in the Graduate School of the University of Florida with the intention of pursuing a Ph.D. in chemical engineering. In 1996 he was awarded a research assistantship associated with a cooperative project between the University of Florida Chemical Engineering Department and DuPont deNemours Inc. The project required him to move to Wilmington, Delaware, in 1997 to work at DuPont Experimental Station with an R&D team developing a process for production of fluorine. In 1999 he was presented with the annual student achievement award of The Electrochemical Society in recognition of his unique research.

In January 2000 he completed the experimental work and returned to Gainesville to write his dissertation. He left school to pursue a job opportunity in California in 2001. The opportunity did not pan out and he returned to complete his dissertation in 2002. This manuscript is submitted as the final requirement toward his goal of earning a Ph.D. in chemical engineering from the University of Florida.

I certify that I have read this study and that in my opinion it conforms to acceptable standards of scholarly presentation and is fully adequate, in scope and quality, as a dissertation for the degree of Doctor of Philosophy.

Timothy J. Anderson, Chair
Professor of Chemical Engineering

I certify that I have read this study and that in my opinion it conforms to acceptable standards of scholarly presentation and is fully adequate, in scope and quality, as a dissertation for the degree of Doctor of Philosophy.

Mark Orazem
Professor of Chemical Engineering

I certify that I have read this study and that in my opinion it conforms to acceptable standards of scholarly presentation and is fully adequate, in scope and quality, as a dissertation for the degree of Doctor of Philosophy.

Eric Wachsman
Professor of Materials Science
and Engineering

I certify that I have read this study and that in my opinion it conforms to acceptable standards of scholarly presentation and is fully adequate, in scope and quality, as a dissertation for the degree of Doctor of Philosophy.

C. Marc Doyle
Senior Research Scientist
DuPont de Nemours & Co., Inc.

This dissertation was submitted to the Graduate Faculty of the College of Engineering and to the Graduate School and was accepted as partial fulfullment of the requirement for the degree of Doctor of Philosophy.

May 2003

Pramod P. Khargonekar
Dean, College of Engineering

Winfred M. Phillips
Dean, Graduate School